An early role for zebrafish hoxd4a and its cofactors in hematopoiesis

Zhang, Changqing

2017

Zhang, C. (2017). An early role for zebrafish hoxd4a and its cofactors in hematopoiesis. Doctoral thesis, Nanyang Technological University, Singapore.

http://hdl.handle.net/10356/73069

https://doi.org/10.32657/10356/73069

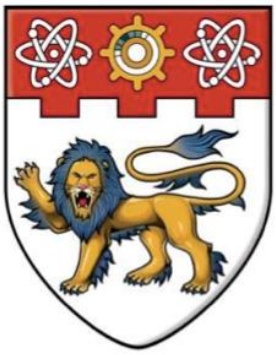

NANYANG TECHNOLOGICAL UNIVERSITY

AN EARLY ROLE FOR ZEBRAFISH HOXD4A AND ITS COFACTORS IN HEMATOPOIESIS

ZHANG CHANGQING

School of Biological Science

A thesis submitted to Nanyang Technological University in partial fulfillment of the requirement for the degree of Doctor of Philosophy

2017

ACKNOWLEDGEMENTS

First and foremost, I would like to express my sincere gratitude to my supervisor, Prof. Mark Featherstone, for his strong support, endless patience and keen guidance throughout the entire project. Without his supervision and encouragement, I could not have overcome the difficulties encountered in this project.

I am very much indebted to Assoc Prof. Li Hoi Yeung for taking over as my supervisor in the final stages of my dissertation. I am also very grateful to the members of my Thesis Advisory Committee, Prof. Klaus Erik and Prof. Vladimir Korzh for their valuable advice. I also wish to thank Prof. Ruedl Christiane for her great help with monoclonal antibody generation.

I thank all my lab members, Anusha, Lawrence, Ragini, Ana, Uthra, Ying, Reshma, Xiaolei and Sandeep for their help and encouragement throughout the course of my PhD. I also thank the Final Year Project student, Erica, for her great efforts with the BioID system.

This work would not have been possible without the financial support from NTU. I am extremely grateful for being awarded by NTU research scholarship.

Last but not least, I wish to take this opportunity to express my heartfelt thanks to my family and friends for their constant understanding and support. I am immensely blessed because of you all. Special thanks to my husband, Yao Kai, for his unwavering love. You have been a constant source of strength and motivation. To you all, I dedicate this thesis.

TABLES OF CONTENTS

LIST OF FIGURES

LIST OF TABLES

LIST OF ABBREVIATIONS

4-OHT	4-hydroxytamoxifen
abd-A	*abdominal-A*
abd-B	*abdominal-B*
AGM	aorta-gonad-mesonephros
ALM	anterior lateral mesoderm
ANT-C	antennapedia complex
AP	Anteroposterior
BioID	biotin identification
BMP	bone morphogenetic proteins
BX-C	bithorax complex
CBP	Creb binding protein
CDX	caudal type homeobox
ChIP-seq	chromatin immunoprecipitation sequencing
CHT	caudal hematopoietic tissue
Co-Smad	common Smad protein
CRISPR	clustered regularly interspaced palindromic repeat
DA	dorsal artery
Dfd	*Deformed*
DIG	Digoxigenin
DLAV	dorsal longitudinal anastomotic vessel
dpf	days post fertilization
DSB	double strand break
DV	Dorsoventral
EGFP	enhanced green fluorescent protein
ERT2	estrogen receptor variant
FGF	fibroblast growth factor
HD	Homeodomain
HDR	homologous directed repair
hpf	hours post fertilization
H293T	human embryonic kidney 293T
HSC	hematopoietic stem cells
ICM	intermediate cell mass
INDEL	insertions or deletions
I-Smad	inhibitory Smad
ISV	inter-segmental vessels
KI	Knockin
KLH	keyhole limpet hemocyanin
KO	Knockout
lab	*Labial*
MBT	mid-blastula transition

MGA	MAX gene-associated protein
MO	Morpholino
NCC	neural crest cell
NHEJ	non-homologous end joining
NMD	nonsense-mediated decay
NPB	neural plate border
NUP	Nucleoporins
PAM	proto-spacer adjacent motif
pb	*Proboscipedia*
PBX	pre-B cell leukemia
PcG	polycomb group
PLM	posterior lateral mesoderm
PTU	Phenylthiourea
RA	retinoic acid
RARE	retinoic acid response elements
RT-RCR	reverse transcription PCR
R-Smads	receptor-regulated Smad protein
RT-PCR	reverse transcription PCR
RXR	retinoid X receptors
scl	*stem cell leukemia*
Scr	*sexcombs reduced*
sgRNA	single guide RNA
SIV	subintestinal vessels
snRNPs	small nuclear ribonucleoproteins
T7EI	T7 Endonuclease I assay
TALE	three amino acid loop extension
TALEN	transcription activator like effector nucleases
TGF-β	transforming growth factor-β
trxG	trithorax group
VLM	ventral lateral mesoderm
VMM	ventral marginal mesoderm
WISH	Whole mount *in situ* hybridization
YSL	yolk syncytial layer
ZFN	zinc finger nucleases

ABSTRACT

Hox genes encode transcription factors which bind to DNA through a conserved domain called the homeodomain. A wealth of evidence shows that DNA-binding affinity and specificity of HOX proteins are highly enhanced by members of the TALE homeoprotein family, such as PBX and MEIS.

At shield stage, zebrafish *hoxd4a* and *meis1.1* are expressed in the whole embryo, while BMP is highly expressed at the ventral side. This temporal and spatial co-expression region includes the ventral marginal mesoderm from which blood and vasculature originate. More importantly, *hoxd4a*, along with *meis1.1* and BMPs, have been implicated in hematopoiesis and vasculogenesis in zebrafish. Additionally, loss of *hoxd4a* and *hoxc4a* causes specific defects of the NPB which is also specified at peri-gastrulation stage and arises from a region of the ectoderm specified by an intermediate level of BMP signaling. These results strongly suggest *hoxd4a* could act in cooperation with its cofactors at an early stage of embryonic development to direct different developmental programmes.

To study the time window of *hox4a* function, we exploited an inducible activation method based on the ligand binding domain of a variant human estrogen receptor, which can be activated by the estrogen antagonist tamoxifen, or 4-OHT. The role of *hoxd4a* in zebrafish hematopoiesis, vasculogenesis and NPB formation is shown to be required by 4 hpf, well before it takes up a more expected role in patterning the antero-posterior axis. Substitution of asparagine 51 of the homeodomain or the YPWM motif (required for interaction with PBX) impaired the ability of Hoxd4a to rescue the hematopoietic and vasculogenic defects, proving

that cooperative binding to DNA with PBX is essential for Hoxd4a in this process. The BMP signaling pathway is shown to synergize with *hoxd4a* to regulate hematopoiesis. In addition to the above partners, the BioID system specifically identified forty-five proteins proximate to Hoxd4a in mammalian cells, which could be validated in future for identification of novel Hox partners. The specificity of the hematopoietic phenotype induced by anti-*hoxd4a* morpholinos was validated in two ways: first, two non-overlapping morpholinos recapitulated the phenotype observed initially, while corresponding five-nucleotide mismatch morpholinos did not. Second, while *hoxd4a* null mutant embryos fail to recapitulate morphant phenotypes, they are much less sensitive to the effect of anti-*hoxd4a* morpholinos injection, indicating that the knockdown phenotype is specific but that complete loss of *hoxd4a* function from the onset of embryogenesis is compensated in such genetic mutants.

CHAPTER 1. INTRODUCTION

1.1. Zebrafish hematopoiesis

1.1.1. Mesoderm patterning

Although the primitive blood cells start to circulate from 24 hours post fertilization (hpf) in zebrafish, the process for hematopoietic stem cells (HSCs) formation is already underway from 5 hpf, the onset of gastrulation (Kimmel et al., 1990). At early gastrula stage, three germ layers are formed within the blastoderm. Among them, fate mapping studies demonstrate that zebrafish HSCs originate from the ventral marginal mesoderm (VMM), which also gives rise to endothelial lineages (Kimmel et al., 1990; Warga and Nusslein-Volhard, 1999).

Zebrafish mesoderm is induced as a ring in the marginal zone of early blastula-stage embryos by signals arising from the yolk syncytial layer (YSL) (Fig. 1.1). The study of zebrafish mesoderm comes from a classical transplantation experiment, in which the blastomere was mechanically removed from a zebrafish embryo and the remaining bottom part (mainly the YSL and yolk) was transplanted into the animal pole of another embryo called the host. The prospective ectodermal cells in the host embryo were found to be converted into mesoderm tissues, demonstrating that mesoderm is induced by signals from YSL (Mizuno et al., 1999). Among the mesoderm-inducing signals, *squint* (*sqt*) and *cyclops* (*cyc*), two members of the Nodal-related transforming growth factor-β (TGF-β) superfamily, are essential for mesoderm formation and induction (Schier, 2003). Zebrafish *squint;cyclops* double mutants lack all endoderm and mesoderm derivatives, including blood, heart, notochord, somites and

pronephros (Feldman et al., 1998). Additionally, other signaling factors have also been identified to be crucial for mesoderm induction. With Nodal family involved in mesoderm initiation as a main stimulus, Wnt and FGF signaling are important to maintain the mesoderm state and BMP signaling is primarily required for mesoderm dorsoventral (DV) patterning (Kimelman, 2006).

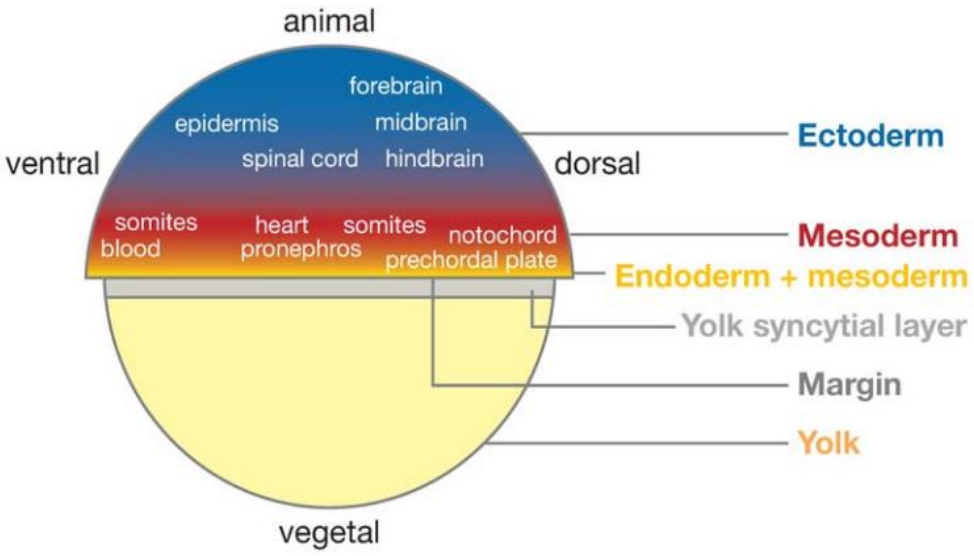

Figure 1.1: Zebrafish fate map at gastrula stage.

Three germ layers are formed at gastrula stage, endoderm, mesoderm and ectoderm. Mesoderm is formed as a ring at the equator of embryos and is further specified along the dorsoventral (DV) axis with ventral marginal mesoderm giving rises to blood and endothelial lineages. Picture adapted from (Schier and Talbot, 2005).

Once induced, mesoderm is further specified into different cell types along the DV axis. Unlike *Xenopus*, where the future DV axis is apparent at the two-cell stage through pigmentation differences (De Robertis et al., 2000), the zebrafish DV axis is not morphologically visible until the shield stage when a thickening of the blastoderm margin arises at the dorsal side, forming the embryonic shield which is equivalent to the Spemann

organizer in *Xenopus* (Saude et al., 2000). In fact, processes specifying the DV axis in zebrafish can be distinguished as early as the cleavage stage revealed by the accumulation of maternal dorsal determinants on the future dorsal side (Mizuno et al., 1999). One of the localized dorsal determinants is *β-catenin*, a downstream effector of the canonical Wnt signaling pathway (Schneider et al., 1996). After the mid-blastula transition (MBT), *β-catenin* activates the zygotic expression of some transcription factors including *sqt* and *boz* (Feldman et al., 2000; Yamanaka et al., 1998). Boz is a transcription repressor that can inhibit the expression of ventralizing genes like *vent* and *vox*, whereas Sqt can activate BMP inhibitors like *chordin* and *noggin* (Kimelman and Schier, 2002). Thus, a gradient of BMP activity is established along the future DV axis by the interplay between BMP ligands and their antagonists with an outcome that the future dorsal side secretes inhibitors of BMPs, diffusing from the organizer, whereas the future ventral side of the embryos highly expresses BMP signals (Fig. 1.2). Correspondingly, precursors of different mesodermal cells are arranged along the DV axis with axial mesoderm located most dorsally giving rise to notochord, paraxial mesoderm generating somites, intermediate mesoderm developing into pronephros and lateral plate mesoderm (LPM) becoming blood and vasculature. In addition to mesoderm specification, numerous studies demonstrate that the gradient of BMP signaling contributes to ectoderm patterning as well. The ectodermal cells with low BMP signals become neurectoderm, while the surrounding region with high BMP signals develops into epidermis. Between them is a region with an intermediate level of BMP activity which is required for the formation of the neural plate border (NPB) that gives rise to neural crest cells (NCCs) and Rohon-Beard cells (Rossi et al., 2009). Therefore, a high level of BMP signaling is critically

important for the production of all lineages derived from the ventral side in both mesoderm and ectoderm.

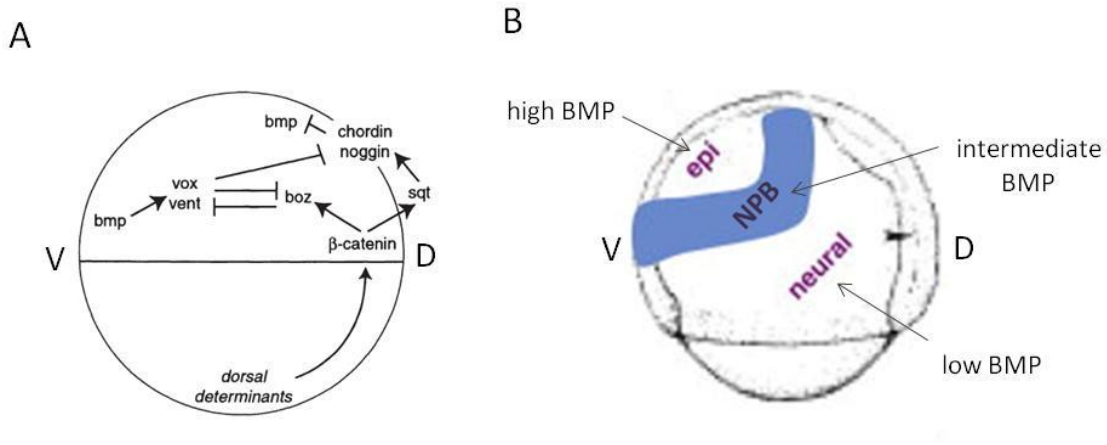

Figure 1.2: BMP gradient in zebrafish embryos at gastrula stage.

(A) Model for zebrafish mesoderm dorsoventral patterning. Dorsal determinants are moved to the future dorsal side after fertilization, which results in accumulation of *β-catenin*. Activation of its targets *boz* and *sqt*, inhibits the action of ventralizing factors, including BMP and its targets like *vox* and *vent*. Thus, a gradient of BMP is established along the DV axis. Picture adapted from (Kimelman and Schier, 2002)

(B) Schematic of the approximate location of the NPB between dorsal neurectoderm and ventral epidermal ectoderm in zebrafish embryos at 75% epiboly. Picture adapted from (Rossi et al., 2009).

1.1.2. Primitive hematopoiesis

Like other vertebrates, zebrafish also have two waves of hematopoiesis – primitive and definitive – occurring in an exact spatial and temporal manner (Ciau-Uitz et al., 2010; Paik and Zon, 2010). Primitive hematopoiesis produces transient erythrocytes and macrophages, which support the early embryonic development. The progenitor of HSCs and angioblasts, namely the hemangioblast, originates from the VMM located bilaterally in the ventral lateral

mesoderm (VLM) at the 2-somite stage (Fig. 1.3). Cells in the anterior lateral mesoderm (ALM) give rise to myeloid cells and endothelial cells, while cells in the posterior lateral mesoderm (PLM) generate vascular precursors and erythrocytes which start to circulate after 24 hpf (Detrich et al., 1995; Paik and Zon, 2010). Expression of *stem cell leukemia* (*scl*) starts at the 2-somite stage in the VLM (Porcher et al., 1996). Meanwhile, expression of the endothelial markers like *fli1* is also found in *scl* expressing cells (Chen and Zon, 2009), suggesting the existence of the bipotential precursors, namely the hemangioblast. Previous studies in zebrafish reveal that *scl* and *fli1* are crucial for hematopoietic development. Absence of *scl* results in loss of all hematopoietic lineages and severe defects in angiogenesis (Dooley et al., 2005). Knockdown of *fli1* leads to absence of hemangioblasts, while overexpression of a constitutively active form of Fli1 causes strong ectopic expression of hemangioblast markers such as *scl*, *gata2*, *lmo2* (Liu et al., 2008). From the 4-somite stage, the hemangioblast develops into either *gata1* expressing erythrocytes or *flk1* expressing endothelial precursor cells (Chen and Zon, 2009). The transcription factor Gata1 is a master regulator of erythrocyte development. Characterization of a "bloodless" mutant vlt^{m651} shows that nonsense mutation of *gata1* results in severe reduction of blood cell progenitors (Lyons et al., 2002). From the 12-somite stage, these bilateral hematopoietic stem cells (HSCs) and angioblasts in the PLM start to migrate toward the midline to become the intermediate cell mass (ICM) (Fig. 1.3), which is functionally equivalent to the yolk sac blood islands in mammals (Ciau-Uitz et al., 2010; Paik and Zon, 2010). With heartbeat starting at 24 hpf, the primitive blood cells begin to circulate. Within the first 4 days post fertilization (dpf), these primitive blood cells will be the only circulating erythrocytes in zebrafish (Weinstein et al.,

1996).

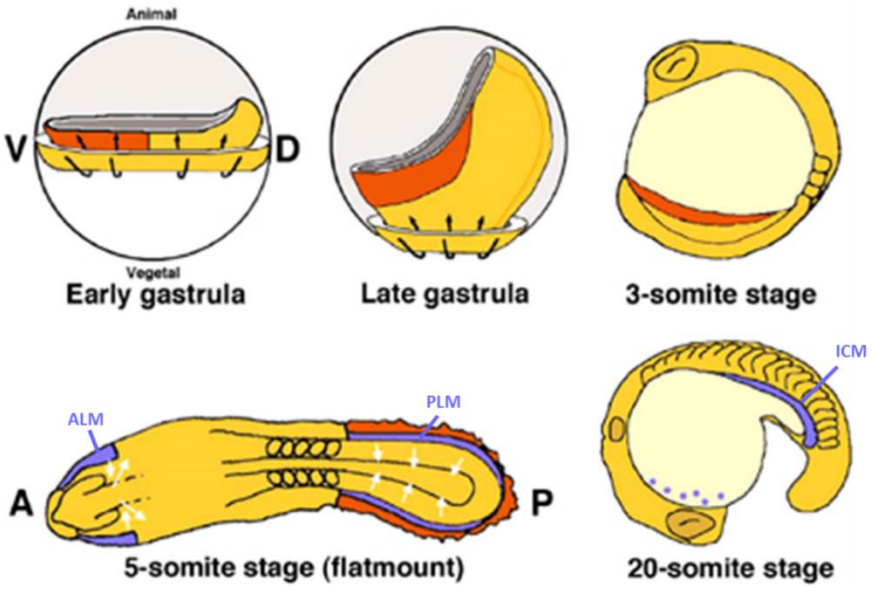

Figure 1.3: Schematic representation of zebrafish primitive hematopoiesis.

Hemangioblasts originate from the ventral marginal mesoderm (red) during gastrulation, which forms the anterior lateral mesoderm (ALM) and posterior lateral mesoderm (PLM) at the 5-somite stage. Then these bilateral hematopoietic stem cells (HSCs) and angioblasts in the PLM start to migrate toward the midline (white arrows) to become the intermediate cell mass (ICM) at the 20-somite stage. For the sake of clarity, only mesoderm is shown in gastrula-stage embryos. The 5-somite stage embryo is shown in a dorsal view after being flat-mounted. D: dorsal, V: ventral, A: anterior, P: posterior. Adapted from (Davidson and Zon, 2004).

1.1.3. Definitive hematopoiesis

Subsequent definitive hematopoiesis initiates at around 30 hpf (Fig. 1.4). The first definitive HSCs emerge from the ventral wall of the dorsal aorta (DA), a site analogous to the mammalian aorta-gonad-mesonephros (AGM) that is tightly associated with the first emergence of mammalian definitive HSCs (Ciau-Uitz et al., 2010; Paik and Zon, 2010). Like

in mammals, zebrafish definitive HSCs are capable of unlimited self-renewal and are able to give rise to all mature hematopoietic lineages. From 48 hpf, theses HSCs migrate to the posterior region to seed the caudal hematopoietic tissue (CHT) (Murayama et al., 2006), following which expansion and specification occurs. It is believed that zebrafish CHT is a site equivalent to mammalian fetal liver. By 4 dpf, HSCs seed the kidney marrow, which replaces the CHT as the region of definitive hematopoiesis. Almost all blood cell lineages can be found in kidney, making it functionally equivalent to bone marrow in mammals. The kidney marrow and thymus are the main hematopoietic organs responsible for lifelong hematopoiesis in zebrafish (Murayama et al., 2006).

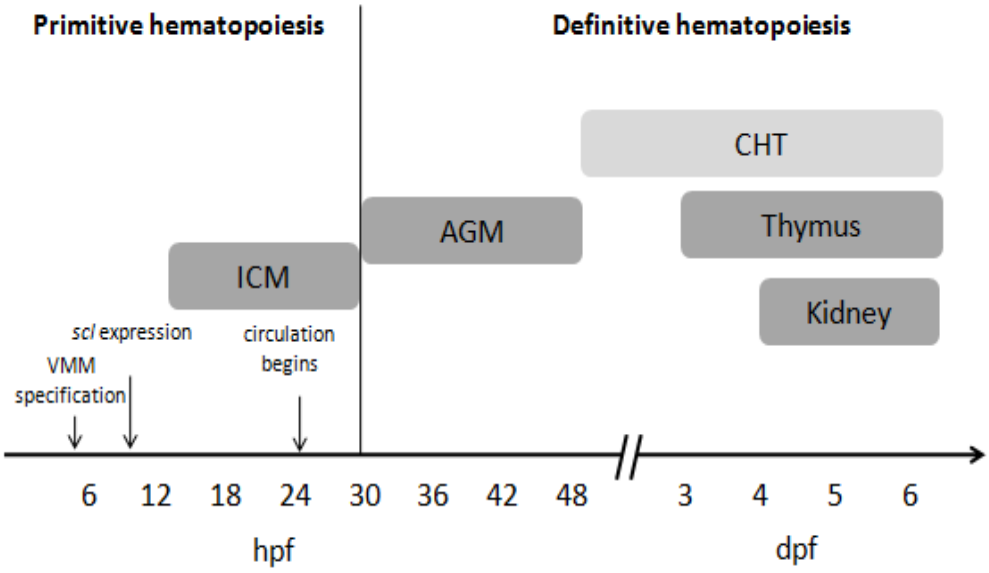

Figure 1.4: The timeline of major hematopoietic activities during zebrafish primitive and definitive hematopoiesis.

hpf, hours post fertilization; dpf, days post fertilization; VMM, ventral marginal mesoderm; ICM, intermediate cell mass; AGM, aorta-gonad-mesonephros. Adapted from (Paik and Zon, 2010).

1.2. *Hox* genes

1.2.1. Genomic organization and collinear expression of *Hox* genes

Hox genes encode homeodomain-containing transcription factors which were originally identified as major determinants of anteroposterior (AP) axis patterning in the fruit fly *Drosophila* (Krumlauf, 1994; Mallo and Alonso, 2013). *Drosophila* has eight *Hox* genes in a single cluster that is split into two groups: the bithorax complex (BX-C) containing *Ubx*, *abdominal-A* (*abd-A*), *abdominal-B* (*abd-B*) and the Antennapedia complex (ANT-C) containing *labial* (*lab*), *proboscipedia* (*pb*), *Deformed* (*Dfd*), *Sexcombs reduced* (*Scr*) and *Antp* (Fig. 1.6). By contrast, in mammals, there are 39 *Hox* genes distributed among 4 chromosomes. Due to genome duplication in teleosts, zebrafish has 47 *Hox* genes organized in 7 clusters (Koh et al., 2003). In each cluster, the order of *Hox* genes along the chromosome corresponds to the relative time at which they are activated and also to their expression domains along the body axis (Mallo and Alonso, 2013). In other words, *Hox* genes located at the 3' end are expressed earlier and more anteriorly than those located at the 5' end. The former correlation refers to “temporal collinearity” and the latter refers to “spatial collinearity”, phenomena that are conserved between vertebrates and invertebrates (Fig. 1.5).

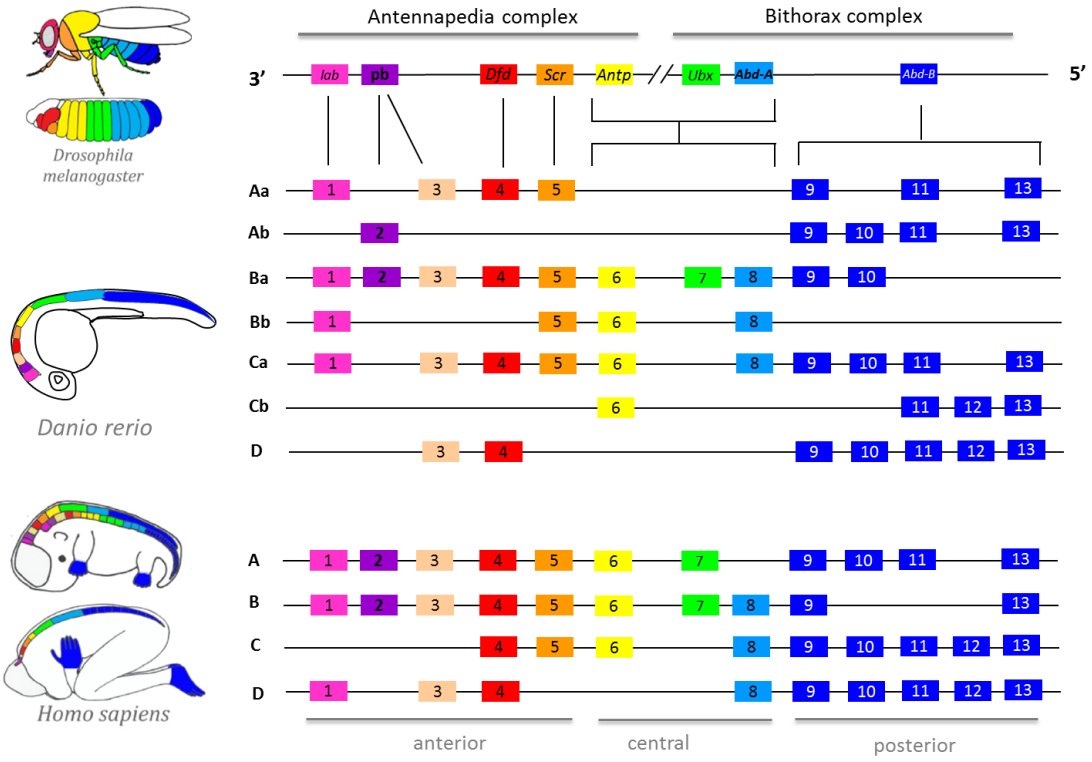

Figure 1.5: Genomic organization and collinearity of *Hox* genes in fruit fly, zebrafish and human.

During vertebrate development, the expression of *Hox* genes can be detected in various tissues including the developing nervous system. The development of the vertebrate nervous system starts during gastrulation and is marked by the appearance of a thickened sheet of epithelial cells derived from ectoderm, the neurectoderm, brought about by a process called neural induction. Subsequently, the lateral edges of the neural plate fuse together to form the neural tube through a process with slight differences between species. Meanwhile, the embryo trunk is extended along the AP axis by convergent extension driven by intercalation coupled with cell proliferation at the posterior end in the cells of neural tube and paraxial mesoderm, the latter of which gives rise to the somites. During this process, the anterior portion of the neural tube becomes partitioned into four distinct compartments: forebrain,

midbrain, hindbrain, and spinal cord. The hindbrain undergoes a transient segmentation process which subdivides the hindbrain into seven compartments called rhombomeres. The spinal cord can be further subdivided into cervical, thoracic, lumbar, and sacral domains (Fig. 1.6).

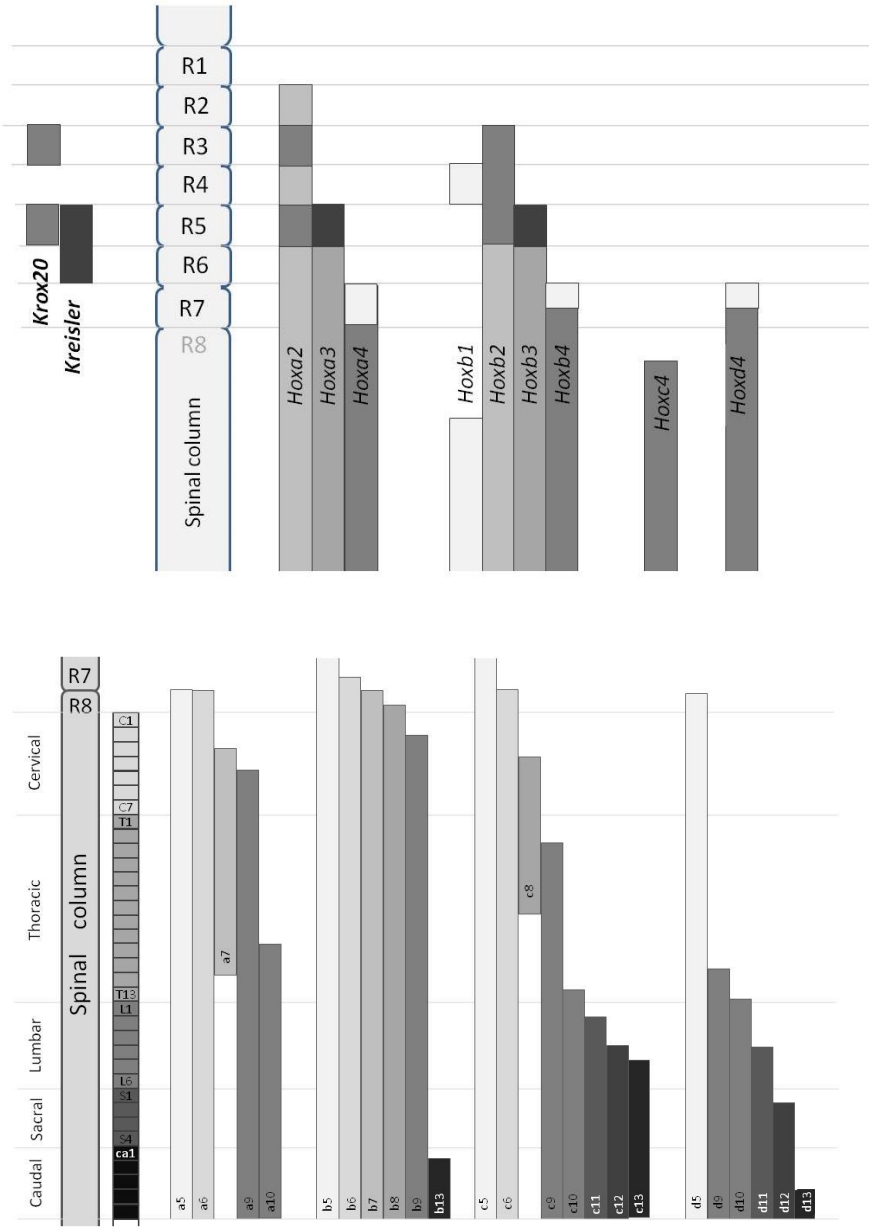

Figure 1.6: *Hox* gene expression in mouse hindbrain and spinal column during early embryonic development. Since the spinal cord lacks segmentation process, the adjacent somites (s) and pre-vertebrae are utilized to show the Hox gene expression in spinal column. Adapted from (Papageorgiou, 2007).

Hox gene expression in the nervous system exhibits a highly rhombomeric-restricted pattern. As a result of collinearity, *Hox* genes from paralog groups 1-4 are mainly expressed with an anterior boundary in the hindbrain, whereas those from groups 5-13 have an anterior border that maps to the spinal cord (Fig. 1.6) (Nolte and Krumlauf, 2007). In posterior segments where *Hox* gene expression is highly overlapped, the activity of more posterior Hox proteins is dominant over the function of more anterior genes, a property known as “posterior dominance” (Duboule and Morata, 1994). Unlike *Drosophila*, where individual *Hox* genes decide the identities of various embryonic domains, the morphology of a given segment in vertebrates is defined by the combinatorial expression of *Hox* genes, a regulatory program usually referred as the "Hox code" (Fig. 1.5).

1.2.2. Regulation of *Hox* gene expression

Given the crucial role of *Hox* genes in body patterning, transcriptional regulation of *Hox* genes must be tightly controlled during early embryonic development. The process of *Hox* gene expression can be divided into three phases: initiation, establishment and maintenance. In mouse, initial activation of *Hox* genes occurs in cells of the posterior primitive streak that do not directly contribute to embryonic tissues. Subsequently this early expression spreads anteriorly into cells of the lateral plate and paraxial mesoderm until it reaches the anterior limits, thereby establishing the *Hox* expression domains. After the definitive expression boundary is reached, polycomb group (PcG) and trithorax group (trxG) gene products act at the epigenetic level to maintain the appropriate transcriptional state (repressed vs activated, respectively) throughout embryonic development.

In the mouse, anterior progression of initial *Hox* gene expression is coupled to the progressive formation of axial structures in the node region. Therefore, the establishment of *Hox* gene expression is highly associated with several signaling pathways involved in axial elongation, such as Wnt, fibroblast growth factor (FGF) and retinoic acid (RA). Wnt signaling is involved in the anterior progression of *Hox* gene expression in the mouse as it regulates the primitive streak and mesoderm formation (Liu et al., 1999). Mouse *Wnt3a* mutants exhibit homeotic transformations in vertebrae along with a shift of *Hox* gene expression in somites (Ikeya and Takada, 2001). The involvement of FGF signaling in the control of *Hox* gene expression and body axis patterning has been reported in *Xenopus* and mouse (Partanen et al., 1998; Pownall et al., 1996). In *Xenopus*, overexpression of FGF from gastrula stage causes ectopic activation of genes that are posteriorly expressed, including *Hox* (Pownall et al., 1996). In the mouse, mutation of *FGFR1* results in homeotic transformation in the vertebral column and changes in *Hox* gene expression (Partanen et al., 1998). RA signaling is primarily transduced by two transcription factors, retinoic acid receptors (RARs) and retinoid X receptors (RXRs), which form heterodimers and bind to specific DNA motifs called Retinoic Acid Response Elements (RARE) (Mangelsdorf and Evans, 1995). Multiple RAREs have been identified near the promoter region of *Hox* genes from paralog groups 1 and 4 (Nolte and Krumlauf, 2007). Inactivation of *Hoxa1* 3' RARE leads to delayed establishment of the anterior expression boundary and abnormalities in hindbrain patterning at later stages, indicating that it directly controls the initiation expression of *Hox* genes (Dupe et al., 1997). On the contrary, treatment of mouse embryos with RA induces ectopic expression of 3' *Hox* genes, resulting in homeotic transformation of the rhombomeres 2/3 into

a 4/5 identity (Conlon and Rossant, 1992; Marshall et al., 1992). RA is also shown to induce *Hox* gene expression in a collinear sequence from 3' to 5' in human embryonic cell line (Simeone et al., 1990).

In addition to signaling molecules, several upstream regulators of *Hox* gene expression have been identified in vertebrates, such as *Krox20*, *Kreisler* and *Caudal type homeobox* (*CDX*). *Krox20* can directly regulate the expression of *Hoxa2* and *Hoxb2* in rhombomere 3 and 5, through a conserved enhancer in the 5'-flanking regions (Nonchev et al., 1996; Sham et al., 1993). Likewise, *Kreisler* is required for the activation of *Hoxa3* and *Hoxb3* in rhombomere 5 and 6 through an enhancer located between *Hoxa3* and *Hoxa4* (Fig. 1.5) (Manzanares et al., 1999). Cdx proteins modulate the expression of many *Hox* genes in both mesoderm and neural tissues (van den Akker et al., 2002). Mutation of *cdx1* in mouse leads to anterior homeotic transformation of vertebrae, which coincides with a posterior shift of *Hox* gene expression (Subramanian et al., 1995). Interestingly, *cdx* genes are also direct targets of RA, FGF and Wnt signaling, suggesting concerted effects on *Hox* gene expression (Mallo et al., 2010) .

1.2.3. Hox function

As key developmental regulators, *Hox* genes play an important role in specifying positional identities of each body segment along the AP axis. Genetic analysis of numerous *Drosophila* mutants demonstrates that single *Hox* gene mutation typically results in homeotic transformation, namely the morphology of a given body part is transformed into another. For example, loss of *Ubx* in developing halteres results in transformation of halteres into wings,

which gives rise to a four-winged fruit fly (Lewis, 1978). By contrast, *gain-of-function* mutations of *Ubx* in developing wings results in transformation of wings into halteres (Casanova et al., 1985). Like in *Drosophila*, mutation of individual *Hox* genes in vertebrates can also result in altered axial identity. However, because vertebrate *Hox* gene expression domains are highly overlapping, especially posteriorly, mutation of a single *Hox* gene often results in an incompletely penetrant phenotype due to functional redundancy. In this case, mutations affecting a set of *Hox* genes have proved to be more informative. A good example is the mutant studies for three *Hox* genes of group 4 which show that the number of transformed vertebrae in mutants of *hoxa4*, *hoxb4* and *hoxd4* is remarkably dose-dependent (Horan et al., 1995). In more detail, single mutants exhibit incompletely penetrant phenotypes with changes only in the second or third cervical vertebra, whereas triple mutants display more complete transformations in vertebral morphology with C2 through C5 transformed to a C1 phenotype. With extensive evidence showing that *Hox* genes within the same cluster often share the same functions (Greer et al., 2000; Tvrdik and Capecchi, 2006), further studies demonstrate that functional redundancy is not limited to paralogous genes, but also exists between neighboring genes within one cluster (de la Cruz et al., 1999; Rancourt et al., 1995) and even between *Hox* genes from different clusters (Soshnikova et al., 2013).

Hox genes are also required for the proper development of the vertebrate limb along the AP axis and proximodistal axis. *Hoxa* and *Hoxd* genes play an important role in this process as lacking of both *Hoxa* and *Hoxd* clusters results in an early developmental arrest of limb growth and severe truncations of distal elements (Fig. 1.7) (Kmita et al., 2005). By contrast, *Hoxb* and *Hoxc* clusters are dispensable for limb development in mouse as deletion of both

Hoxb and *Hoxc* clusters does not cause obvious abnormalities in limbs (Medina-Martinez et al., 2000; Suemori and Noguchi, 2000). Corresponding to limb patterning, *Hox* gene expression in limb development follows two phases (Nelson et al., 1996; Tarchini and Duboule, 2006). In the first phase, genes within the *Hoxa* and *Hoxd* clusters are expressed in a temporally and spatially collinear fashion in the early limb bud, with 3' located genes being expressed earlier and more proximally than 5' genes. This results in a nested expression pattern in which 3' genes are expressed in a more antero-proximal region, followed by the expression of subsequent 5' genes at a more postero-distal region (Fig. 1.7). Subsequently, in the distal region of the limb bud, the expression of 5’ genes extends to the distal extremity which will generate the digits.

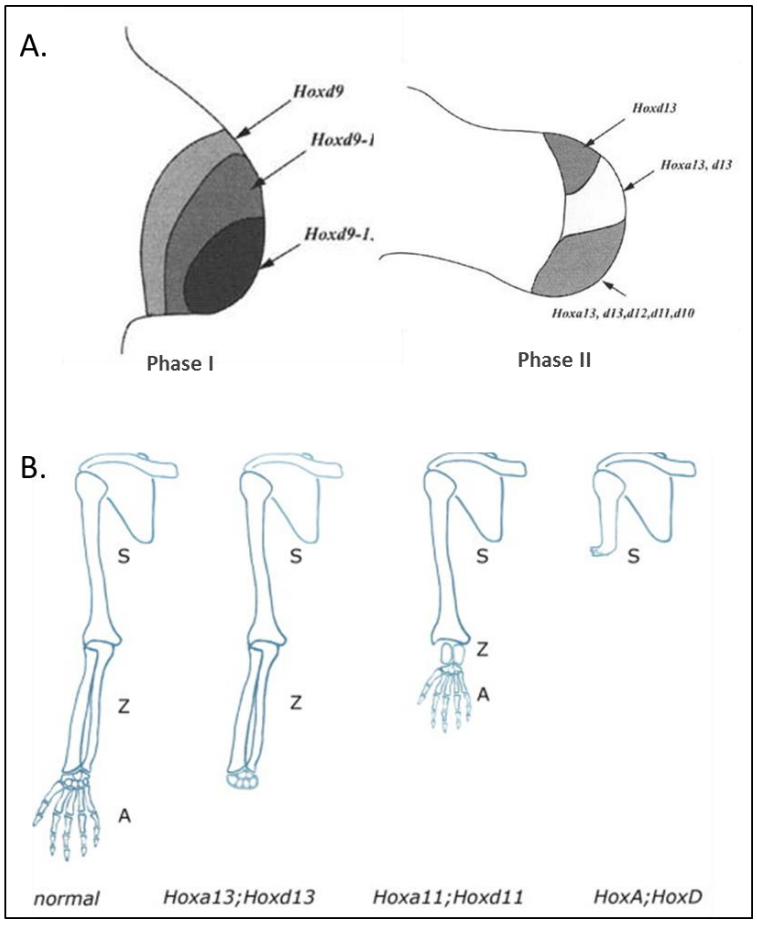

Figure 1.7: *Hox* gene expression and mutant phenotypes in mouse limb.

(A) Two phases of *Hox* gene expression during limb development.

(B) Forelimb phenotypes of compound mutant mice. S, stylopods; Z, zeugopods; A, autopods. Adapted from (Zakany and Duboule, 2007).

Loss-of-function studies in the mouse find that loss of either single or multiple *Hox* genes strongly affects limb development, especially genes located at 5' positions within a cluster. Unlike the typical homeotic transformation in trunk patterning, mutation of *Hox* genes in the limb bud often results in loss of skeletal elements (Fig. 1.7). For example, disruption of paralog 11 *Hox* genes leads to truncated zeugopods with normal stylopods and autopods (Davis et al., 1995; Fromental-Ramain et al., 1996). In contrast, absence of *Hoxa13* and *Hoxd13* leads to the loss of digits in the autopods whereas the stylopods and zeugopods are normal (Davis et al., 1995).

The patterning functions of *Hox* genes in trunk and limb occur during a relatively late phase beginning at and after the onset of gastrulation. On the contrary, mouse, chick, *Xenopus*, and zebrafish have a distinct early phase of *Hox* gene expression prior to gastrulation (Fig. 1.8) (Alexandre et al., 1996; Forlani et al., 2003; Iimura and Pourquie, 2006, 2007; Wacker et al., 2004a; Wacker et al., 2004b). In the mouse, *Hoxb1* is found as the earliest expressed *Hox* gene in the caudal part of the primitive streak at the onset of gastrulation, which is 12 hours earlier than the time when the majority of *Hox* genes start to be expressed (Forlani et al., 2003). In *Xenopus*, temporally collinear initiation of *Hox* genes in mesoderm during early gastrulation is translated into a spatial AP pattern that depends on a sequential interaction between the non-organizer mesoderm with the Spemann organizer (Wacker et al., 2004b). In

more detail, early *Hox* gene expression is found in the non-organizer mesoderm during early gastrulation, which is only transient and by itself insufficient to pattern the AP axis. Their later expression pattern in the presumptive neurectoderm depends on convergence and extension which continuously bring the cells from the non-organizer mesoderm to the Spemann organizer, thus, establishing the Hox code by sequential stabilization in both involuted mesoderm and overlying neurectoderm. Studies in the chick demonstrate that *Hox* genes control the timing of cell ingression from the epiblast to the primitive streak by sequentially activating their own expression at the gastrula stage, which further contributes to the establishment of the spatial collinearity at later stage (Iimura and Pourquie, 2006). Taken together, similar kinetics of *Hox* gene activation observed in different organisms implies a conserved role across vertebrates, which depends on its early expression at gastrula stage.

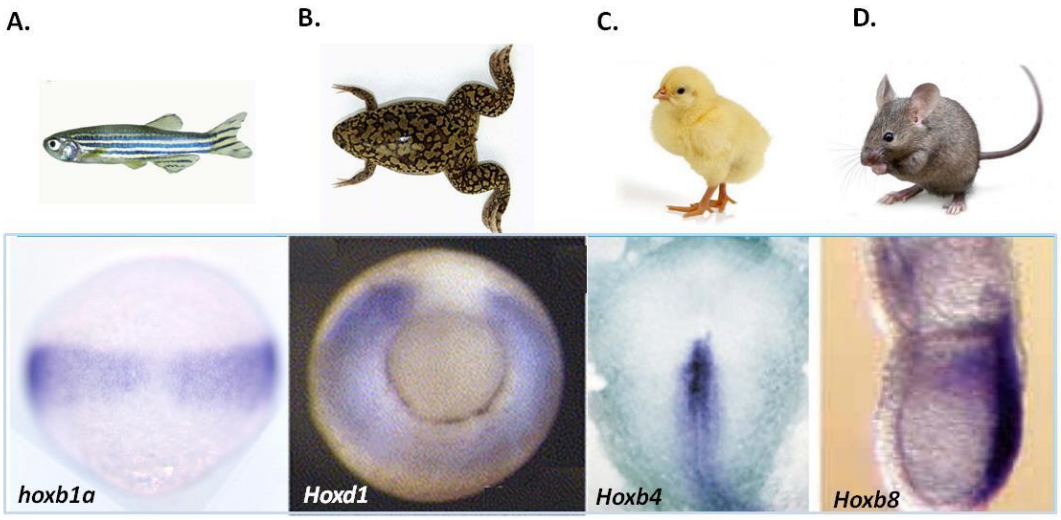

Figure 1.8: *Hox* gene expression at pre-gastrulation in different organisms.

(A) The expression of zebrafish *hoxb1a* at shield stage in a dorsal view. (Kudoh et al., 2001)

(B) The expression of *Xenopus Hoxd1* in the non-Spemann organizer mesoderm at mid-gastrula stage in a vegetal view, organizer to the up. (Wacker et al., 2004a)

(C) The expression of chick *Hoxb4* in the epiblast of the primitive streak at 5HH stage in a dorsal view,

anterior to the top. (Iimura and Pourquie, 2006)

(D) The expression of mouse *Hoxb8* in the caudal part of the primitive streak at E8 stage. (Forlani et al., 2003)

1.2.4. Hox protein

Mammalian HOX proteins are relatively small, generally encoded by two exons with the second exon containing the homeobox. The homeodomain (HD) is composed of three alpha helices and a variable N-terminal arm. Although they are highly conserved, HOX proteins have been shown to bind DNA with poor affinity and specificity, with most HOX proteins binding to AT-rich recognition sequences. The core DNA motif for HOX protein binding is 'TAAT', with the first two base pairs specified by the N-terminal arm in the minor groove and the last two base pairs specified by the third helix of the HD in the major groove of DNA (Featherstone, 2003). Asparagine at position 51 in the third helix of the homeodomain is very conserved and plays a key role in the affinity of DNA binding (Kissinger et al., 1990). Mutation of this asparagine to serine (N51→S51) in HOXD4 results in complete loss of DNA binding in both monomeric and heterodimeric complexes with PBX1A (Shanmugam et al., 1999b; Vershon et al., 1995). Specificity is conferred in part by glutamine 50 (Q50) which restricts base identity 3' to the 'TAAT' core sequence (Treisman et al., 1989). Additionally, HOX proteins from paralog groups 1 to 8 share a very conserved short motif with the consensus YPWM located N-terminal to the homeodomain, and which is required for the interaction between HOX and the PBX homeoproteins (Chang et al., 1996a). In HOX proteins from paralogs 9 and 10, the YPWM motif is functionally replaced by a similar tryptophan-containing motif, ANW (Chang et al., 1996b). More recently, binding by HOX

and PBX to bonafide enhancers has been shown to be mediated by multiple low-affinity sites, a strategy that may, paradoxically, confer heightened discrimination between different HOX-PBX complexes (Crocker et al., 2014).

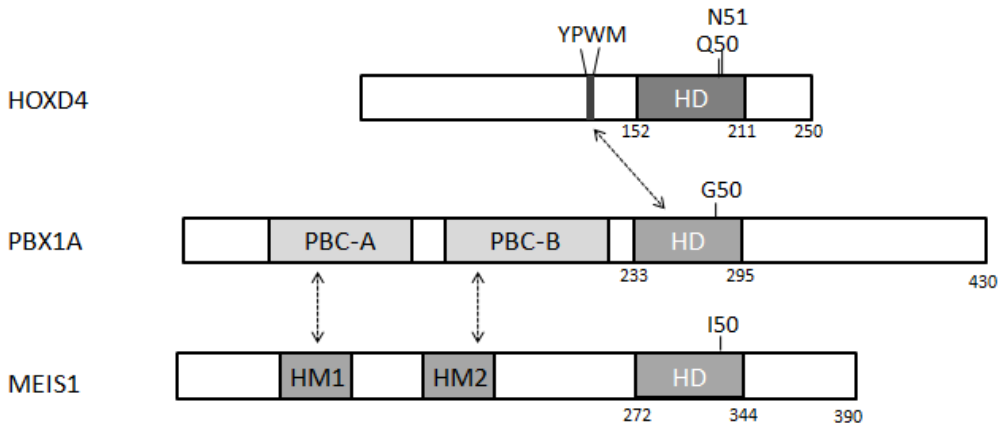

Figure 1.9: Structure of HOX, PBX and MEIS proteins.

Domains of murine HOXD4A, PBX1 splicing isoform a and MEIS1 are shown here. HOX-PBX interaction is mediated by the YPWM motif and the homeodomain of PBX. PBX binds to MEIS through the PBC and HM domains, respectively.

1.3. Hox cofactors

Much evidence shows that the DNA-binding affinity and specificity of HOX proteins are markedly enhanced by other proteins known as Hox co-factors, among which the most intensively studied are PBX and MEIS/PREP (Moens and Selleri, 2006). PBX and MEIS/PREP belong to the three amino acid loop extension (TALE) homeodomain proteins that typically contain a three-amino acid insertion between helices 1 and 2. The HOX homeodomain has a glutamine at position (Q50) as mentioned above, whereas, PBX has G50, and MEIS has I50 (Featherstone, 2003; Moens and Selleri, 2006).

HOX proteins from paralog groups 1 to 10 are able to bind PBX (Chang et al., 1996a). The cooperative DNA-binding site of HOX-PBX consists of the core sequence 'TGAT' for PBX binding and 'TAAT' for HOX binding, in which the core DNA motifs of PBX and HOX must immediately juxtapose (Chang et al., 1996a; Passner et al., 1999; Piper et al., 1999; Shen et al., 1997). Even one base pair insertion between the core recognition sites will abrogate the cooperative DNA binding (Knoepfler et al., 1996). The interaction between HOX and PBX occurs through the homeodomain of PBX and the YPWM motif of HOX (Lu and Kamps, 1996; Passner et al., 1999; Piper et al., 1999). Site-directed mutation studies show that the YPWM to YPAA mutation prevents cooperative binding of HOX and PBX to DNA (Joshi et al., 2010; Prince et al., 2008). Furthermore, mice with the WM to AA point mutation of *Hoxa1* exhibit hindbrain and skeletal defects reminiscent of *Hoxa1* mutant mice, demonstrating the importance of this hexapeptide for *Hox* gene function (Remacle et al., 2004). In addition to the increased affinity and specificity of DNA binding, PBX proteins can modulate HOX functions by recruiting other factors to regulate the activity of HOX transcription complexes (Abramovich et al., 2000; Saleh et al., 2000).

MEIS/PREP proteins are able to form heterodimers with HOX proteins from paralog group 9 to 13 through the C-terminal domain of MEIS (Shen et al., 1997). Unlike PBX, MEIS proteins are likely to affect HOX functions in a different way. They exert their effects indirectly by regulating the availability of PBX proteins (Abu-Shaar et al., 1999; Berthelsen et al., 1998; Waskiewicz et al., 2001). Evidence shows that the interaction between PBX and MEIS affects the nuclear localization (Abu-Shaar et al., 1999) and stability of PBX proteins (Waskiewicz et al., 2001). Additionally, in some contexts, MEIS fulfill its functions by

modulating the interaction between HOX and PBX (Ladam and Sagerstrom, 2014).

In addition to PBX and MEIS, another class of transcription factors without DNA-binding domain has been found in HOX transcription complexes as well. These so-called general factors are recruited by protein-protein interactions and are able to modify HOX functions as some of them are chromatin modifying enzymes, like CREB-binding protein (CBP) (Ladam and Sagerstrom, 2014).

1.4. The role of Hox and its cofactors in hematopoiesis

The expression of *Hox* genes in hematopoietic cells exhibits a stage-restricted pattern with highest expression in HSCs and lowest in differentiated hematopoietic cells (Sauvageau et al., 1994). The function of *Hox* genes and their cofactors in hematopoiesis has been extensively studied in murine models and human hematopoietic cell lines using antisense knockdown and enforced overexpression (Alharbi et al., 2013). Generally, overexpression of *Hox* genes often results in an increase of hematopoietic progenitor expansion together with an inhibition of its differentiation (Thorsteinsdottir et al., 1997; Thorsteinsdottir et al., 2002). However, due to functional redundancy, knockdown or deletion of different *Hox* genes often has no significant effects on the lineage commitment, which seems very confusing in consideration of the overexpression studies (Alharbi et al., 2013). For example, ectopic expression of *Hoxb6* in murine bone marrow results in an expansion of HSCs and myeloid precursors concomitant with a block of erythropoiesis and lymphopoiesis (Fischbach et al., 2005). However, in *Hoxb6* knockout mice, the differentiation of major lineages is unaffected (Kappen, 2000).

In contrast to some *Hox* genes whose ectopic expression causes hematopoietic malignancies,

HOXB4 overexpression enhances the expansion of the HSCs, but fails to induce leukemia (Antonchuk et al., 2001; Sauvageau et al., 1995; Thorsteinsdottir et al., 1999). *Hoxb4* knockout mice display significant reduction of cellularity in spleen and bone marrow and mild reduction of primitive progenitors, whereas the hematopoietic cell commitment is unaffected (Brun et al., 2004). Further studies of *Hox* paralog group 4 members (*Hoxa4*, *Hoxb4*, *Hoxc4* and *Hoxd4*) show that they have broadly similar effects on the self-renewal ability of HSCs (Iacovino et al., 2009). Taken together, this suggests that the function of *Hox* genes from paralog group 4 in hematopoiesis could be distinct from other *Hox* genes.

In zebrafish, extensive studies have established a genetic hierarchy in which homeobox genes *cdx1*/*cdx4* act as master regulators of *Hox* genes in both AP axis patterning and hematopoiesis (Davidson et al., 2003; Lengerke and Daley, 2012; Subramanian et al., 1995). *Cdx4* single null mutants exhibit severe hematopoietic defects including down-regulation of hemangioblast makers and a severe reduction in the number of erythroid cells, accompanied by aberrant expression of some *Hox* genes. These defects of *cdx4* mutants can be rescued by overexpressing *hoxb6b*, *hoxb7a* or *hoxa9a*, demonstrating that the function of *cdx4* is mediated by *Hox* genes (Davidson et al., 2003). Further analysis using chromatin immunoprecipitation sequencing (ChIP-seq) identified the transcription factor *spalt-like 4* (*sall4*) as a direct downstream target gene of Cdx4 (Paik et al., 2013). Gene expression profiling finds that *cdx4* and *sall4* can directly activate genes that are critical for hematopoiesis initiation, such as *Hox* genes, *scl* and *lmo2* (Paik et al., 2013). Another direct evidence for the role of *Hox* genes in zebrafish hematopoiesis comes from studies using a transgenic line stably overexpressing EGFP-tagged Hoxb4a under the control of *lmo2*

promoter, which results in considerable increase of primitive hematopoietic progenitors (Shu et al., 2015). In support of this, our lab has demonstrated that its paralog *hoxd4a* plays an important role in zebrafish hematopoiesis and vasculo/angiogenesis (Amali et al., 2013). Knockdown of *hoxd4a* leads to severe defects in blood and endothelial development. The expression of hemangioblast markers like *scl* and *lmo2* is highly down-regulated, suggesting it has an early role in the primitive hematopoiesis (Amali et al., 2013).

As key partners of Hox, Pbx and Meis are also implicated in hematopoiesis. In the mouse, *Meis1* is expressed in HSCs and some definitive hematopoietic sites during murine embryonic development. Loss of *Meis1* results in embryonic lethality due to defects in fetal hematopoiesis (Azcoitia et al., 2005; Hisa et al., 2004). Similarly, *Pbx1* mutant mice die at the early mid-gestation stage showing severe anemia (DiMartino et al., 2001). In zebrafish, five *Meis* genes (*meis1.1, meis2.1, meis3.1, meis3 and meis4*) and four *Pbx* genes (*pbx1, pbx2, pbx3 and pbx4*) have been identified. Knockdown of *meis1.1* causes severe reduction of blood cells (Cvejic et al., 2011b). The differentiation of endothelial cells is also impaired in *meis1.1* morphants (Minehata et al., 2008). *Pbx*-depleted embryos exhibit phenotypes reminiscent of those in *meis1* morphants (Pillay et al., 2010). This could result from the fact that PBX and MEIS reciprocally stabilize each other. Strongly supporting this, in *pbx*-depleted embryos, the nuclear translocation of Meis is blocked. Furthermore, simultaneous absence of *meis* and *pbx* leads to much more severe hematopoietic defects in zebrafish (Pillay et al., 2010).

1.5. BMP signaling pathway

Bone morphogenetic proteins (BMPs) belong to the TGF-β superfamily, which is crucial for early embryonic development. In canonical BMP signaling pathway, BMP ligands bind to type I and type II receptor complex which are serine/threonine kinases. Upon ligand binding, type II receptor activates type I receptor by phosphorylation, which promotes activated type I receptor to phosphorylate receptor-regulated Smad protein (R-Smads, Smad1, 2, 3, 5, 8). Phosphorylated R-Smad subsequently forms a complex with the common mediator (Co-Smad, Smad4) and then translocates to the nucleus to regulate gene expression. R-Smad proteins can be further divided into two classes: R-Smad 2 and 3 specifically mediate signals from TGF-β/Activin/Nodal receptors, whereas R-Smad 1, 5, 8 primarily mediate signals from BMP receptors. Another class of Smad protein is inhibitory Smad (I-Smad, Smad6, 7), which inhibits TGF-β and BMP signaling by a negative feedback loop .

1.5.1. BMP in hematopoiesis

As mentioned above, during gastrulation, a gradient of BMP activity is established along the DV axis with low expression at the dorsal side and high expression at the ventral side. Inhibition of BMP signaling at early stages results in dorsalization of zebrafish embryos that lacks blood and vasculature (Kondo, 2007). This implies that BMP signaling is crucial for the development of ventrally derived structures. Indeed, zebrafish mutants defective in *bmp2b* (*swirl*), *bmp7* (*snailhouse*) and BMP type I receptor *Alk8* (*lost-a-fin*), are all severely dorsalized with an expansion of dorsal cell fates at the expense of ventrally derived structures, including blood, vasculature and tail tissue (Dick et al., 2000; Hild et al., 1999; Kishimoto et

al., 1997). Overexpression of *bmp4* is able to rescue *bmp2b* (*swirl*), *bmp7* (*snailhouse*) mutants (Hammerschmidt et al., 1996; Schmid et al., 2000). Reciprocally, ectopic expression of *bmp4* in wild-type embryos results in an expansion of ventral derivatives (Dale et al., 1992). Studies using zebrafish embryos and murine embryonic stem cells suggest a conserved *BMP-Wnt-Cdx-Hox* linear pathway during blood formation, in which *BMP4* induces ventral posterior mesoderm formation and afterwards cooperates with *Wnt3a* to enhance blood formation by the activation of the *Cdx-Hox* pathway (Lengerke et al., 2008). Further investigation using inducible methods to attenuate BMP signaling at different stages reveals that its function in patterning ventral mesoderm is stage-specific (Pyati et al., 2005; Schmerer and Evans, 2003). By ectopic expression of a dominant-negative BMP receptor in zebrafish using a heat-shock promoter, it has been shown that the development of ventral mesoderm derivatives requires high BMP signals at early gastrulation (Pyati et al., 2005). In *Xenopus*, inhibition of BMP signaling after gastrulation leads to specific defects in primitive hematopoiesis without apparent effects on axial patterning, which indicates that BMP signaling is required for the differentiation of primitive erythrocytes during and after gastrulation (Schmerer and Evans, 2003). By contrast, disruption of BMP signaling in lateral mesoderm during the segmentation stage results in an expansion of hematopoietic and endothelial cells in zebrafish, which suggests BMP could restrict hematopoietic and vascular development during somitogenesis (Gupta et al., 2006). Taken together, these results suggest BMP signaling could act differentially and even exert opposite effects on hematopoietic development during different phases of early embryonic development.

Effector molecules R-Smads are also involved in zebrafish hematopoiesis. *Smad5* mutant

somitabun^{tc24}*(sb)* is severely dorsalized as shown by the absence of most ventral tissues, similar to zebrafish *bmp2* mutants (Hild et al., 1999). Gene function studies by morpholino mediated knockdown finds that *Smad1* and *Smad5* differentially regulate zebrafish hematopoiesis (McReynolds et al., 2007). While both *Smad1* and *Smad5* are required to initiate definitive hematopoiesis, *Smad1* is specifically essential for the differentiation of macrophages and *Smad5* is mainly required for erythropoiesis. In these processes, *Smad1* can functionally replace *Smad5*, whereas *Smad5* cannot replace *Smad1*. A further study shows that *Smad1* and *Smad9* act redundantly to regulate the DV patterning and myelopoiesis as direct transcriptional targets of Smad5 (Wei et al., 2014).

1.5.2. Hox and BMP

Hox genes and BMPs are closely related in many common developmental processes. In *Xenopus*, BMP4 cooperates with mesoderm inducing factor Xbra to control the early initiation of *Hox* gene expression during gastrulation (Wacker et al., 2004a). Ectopic activation of BMP signaling results in an expansion of *Hox* gene expression in the organizer mesoderm which normally excludes *Hox* gene expression. Correspondingly, blocking BMP signaling represses *Hox* expression, which can be restored by injection of BMP4 protein. In chick, ectopic expression of BMP2 at the margin of the early limb bud activates the expression of *Hoxd11* and *Hoxd13*, suggesting BMP2 is involved in regulating *HoxD* gene expression in limb axis patterning (Duprez et al., 1996). All the evidence implies that BMP signaling could regulate *Hox* gene expression in different developmental programmes.

Additionally, the transcriptional activity could also be affected mutually between *Hox* genes

and BMP signaling. Several studies reveal that Smad1 can interact with Hoxc8 and prevent its repression in *osteopontin* (OPN) and *osteoprotegerin* (OPG) transcription by dislodging it from the promoter binding site (Shi et al., 1999a; Yang et al., 2000). On the other hand, Smad6 can interact with Hoxc8 and Hoxa9 as a co-repressor and prevent Smad1 to interact with Hoxc8 and thus inhibit Smad1-mediated transcription activation (Bai et al., 2000). Another study in *Xenopus* using an animal cap explant assay shows that Smad1 inhibits Hoxb4 transcriptional activity during early development (Li et al., 2006b). In support of these studies, extensive evidence shows that the Hox-Smad interaction could be a general property (Li et al., 2006b; Wang et al., 2006; Zhou et al., 2008). In strongly supporting evidence, *Hox* group 13 proteins have been shown to be capable of interacting with R-Smads and modulating Smad-induced transcriptional activation. Interestingly, this function is independent of the DNA-binding capability of the Hox protein (Williams et al., 2005a). Another study tested 12 Hox proteins representative of different paralogs and revealed that most of the tested Hox are able to interact with Smad1, Smad4, and Smad6 in a similar way, which further suggests that Hox proteins could act downstream in BMP signaling pathway (Li et al., 2006a). Furthermore, the Hox-Smad interaction could be dependent on the MH domain (MH1 and MH2) of Smad and the homeodomain of Hox proteins (Li et al., 2006b; Wang et al., 2006; Williams et al., 2005b; Zhou et al., 2008).

1.6. Gene function study in zebrafish: knockdown and knockout

1.6.1. Knockdown

Morpholinos (MOs) are synthetic oligonucleotides typically 25 nucleotides (nt) in length (25

mers). Their molecular structure differs from DNA and RNA in that the nucleotide base is linked to a morpholine ring through a nonionic phosphorodiamidate backbone. This feature allows MOs to bind to the targeted RNA via complementary base pairing with several important advantages. First, as they are composed of a neutrally charged backbone, they are less likely to interact electrostatically to charged macromolecules, which may result in decreased toxicity. Second, they are resistant to nuclease degradation, making them more stable in developing embryos.

There are two types of morpholinos used in zebrafish: translational blockers and splicing blockers. Translation blocking MOs are targeted to the translational start site or the 5'-untranslated region (5'-UTR) of the mRNA so as to interfere with the assembly of the ribosome initiation complex and thereby inhibit the translation of targeted transcripts whether maternally or zygotically derived. Generally, translation blocking morpholinos do not cause degradation of mRNA transcripts, which means their efficacy cannot be assessed by reverse transcription PCR (RT-PCR). Instead, if an antibody against the targeted protein is available, the targeting efficiency can be assessed by the level of protein through western blot. Splice blocking MOs are designed to interfere with the processing of pre-mRNA by binding to either the splice donor or splice acceptor site. Base pairing to the MO precludes the binding of small nuclear ribonucleoproteins (snRNPs), and thereby inhibits the formation of the splice lariat structure, which could result in partial intron inclusion, exon deletion and activation of cryptic splice site. All the above could lead to the creation of premature stop codons and nonsense-mediated decay (NMD). The resultant truncated gene product are usually reduced and nonfunctional. Therefore, the efficacy of a splice blocking MO can sometimes be

assessed by RT-PCR to quantify wild-type and abnormal transcripts resulting from aberrant splicing. Unlike translational blockers, splice blocking MOs can only target zygotic transcripts (Bill et al., 2009).

With all the successful implementation of MOs in deciphering gene function, problems about the potential off-target effects with its application in zebrafish soon emerged; that is, MOs could interfere with the function of a completely irrelevant gene, as well as, or rather than the gene of interest. Problematically, it is difficult to identify if there are any non-specific effects caused by binding to unintended RNAs. The mechanism(s) of the off-target effect is not fully understood. One well-described mechanism is mediated by *p53* activation and the induction of apoptosis (Robu et al., 2007). In several cases, concurrent knockdown of *p53* can alleviate the non-specific neural cell death. However, it should always be borne in mind that not all MOs have off-target effects, and not all off-target effects can be attenuated by *p53* knockdown.

Therefore, it has become increasingly important for MO users to establish a direct causal link between a morphant phenotype and the attenuated function of the gene of interest. This can be done in different ways. One commonly used validation method is to restore the observed phenotype by co-injection of synthetic mRNAs encoding the protein of interest. Fully restored phenotype by mRNA rescue provides strong evidence for the specificity of a morpholino. With respect to translation blocking morpholinos that target the coding sequence around ATG, the mRNA used for rescue could be modified by recombinant DNA technology without changing the encoded protein. However, mRNA rescue cannot be applied to every gene; for example, some open reading frames are too long to be cloned and transcribed in the

lab. And there is also evidence showing that the injected mRNA itself could cause a strong overexpression phenotype (Eisen and Smith, 2008).

Morpholino specificity can also be validated if the same phenotype is observed by using a second non-overlapping MO against the same gene of interest. This has become standard practice when it comes to MO usage. Specificity could be further proved by simultaneous application of two non-overlapping MOs at a threshold dose at which each alone only causes a slight effect. If both are specific to the same targeted RNA, co-injection of two MOs should synergize to generate a much more severe phenotype than obtained with either MO alone. Furthermore, appropriate controls should always be included in each experiments. GeneTools LLC provides a standard control morpholino against the human *β-globin* that is not present in the zebrafish genome, and thus normally does not cause any changes. While this control is commonly used, it is not necessarily a good approach as it does not rule out the possibility of sequence-specific off-target effects. In other words, the experimental MOs could bind to a closely related sequence in a different and unintended target. Therefore, a more specific control would be a mismatch morpholino that differs from the experimental MO at four or five nucleotides. Ideally mismatch morpholino should not evoke a phenotype, or only produce much weaker effects when injected at the same dose as the experimental MO. The same phenotype could be observed when a higher dose of mismatch morpholinos is injected. Last but not least, as every zebrafish researcher knows, it's very difficult to inject the exactly same volume or amount of morpholinos during different injections. So knockdown experiments should be conducted very carefully and repeated independently at least three times. Variations of each experiment should be recorded in detail with a careful statistical

evaluation.

Despite all approaches mentioned above to prove the specificity of a morpholino-induced phenotype, it is still preferred to validate the phenotype by comparison with a genetic mutant. Problems and concerns emerge when a genetic mutant fails to recapitulate the phenotype observed in morphants, which will be discussed in detail in the following section.

1.6.2. Knockout

The last two decades have witnessed a rapid development of programmable site-specific nucleases, including zinc finger nucleases (ZFNs), transcription activator like effector nucleases (TALENs), and the clustered regularly interspaced palindromic repeat CRISPR/Cas9 system. Compared with ZFN and TALEN, CRISPR/Cas9 is the most straightforward due to the relatively easy recombinant DNA technology involved. The system is composed of a Cas9 endonuclease and two small RNA molecules, tracrRNA and crRNA which have been fused into a fully functional single guide RNA (sgRNA) (Jinek et al., 2012). The engineered sgRNA starts with a 20-nucleotide "seed" sequence complementary to the targeted genomic site which is followed by a proto-spacer adjacent motif (PAM). The 3' end sequences of sgRNA can form a secondary structure that is able to interact with Cas9 protein and direct it to the targeted site. Then Cas9 endonuclease cleaves the genome within the targeted sequences to generate a double strand break (DBS), which is subsequently repaired by different mechanisms. Since the non-homologous end joining (NHEJ) is much more active than homologous directed repair (HDR) in zebrafish, the resulting DSB is most likely to be repaired by the NHEJ, which will introduce short insertions or deletions (INDELs). When

this occurs in coding sequences, the INDEL mutations may cause frame shift or a premature stop codon resulting in non-functional proteins. However, if a template with homologous sequences is introduced, HDR will lead to the incorporation of the exogenous DNA; the target sites can thus be modified in a more flexible way.

While the CRISPR/Cas9 approach was initially reported as a genome editing technology (Hwang *et al*., 2013), subsequently continuous development of different variants of CRISPR/Cas9 system has highly expanded their applications in gene function study. Among these, the most extensively used is the CRISPRi system, in which the catalytically inactive Cas9 (called 'dead' Cas9) is still capable of binding to the target site with sgRNA, but not able to cleave it (Qi et al., 2013). As a result, complex with the dead Cas9 remains stalled at the genomic site and blocks the binding or progress of other proteins such as RNA polymerase, thus silencing the gene of interest without altering its sequence. Beyond this, the dead Cas9 protein can be attached to an activator to stimulate gene expression. Similarly, it can also be utilized to alter the epigenetic marks of histone proteins by coupling the dead Cas9 with histone modifying enzymes (Hilton et al., 2015). In addition to refining Cas9 protein, great efforts are also made to minimize the off-target effect of CRISPR/Cas9 system, which is mainly achieved by different websites and softwares for target site design, such as sgRNAcas9, CRISPRdirect and CRISPy-web (Blin et al., 2016; Naito et al., 2015; Xie et al., 2014). Previous studies showed that the specificity of CRISPR/Cas9 system is determined by the 20-nucleotide seed sequence and the PAM motif. Many studies show that the 3' end of the target site sequence is particularly important for its specificity (Cong et al., 2013). In contrast, the system can tolerate up to 5 bp mismatches in the 5' region or 1-2 bp mismatch in other

regions of the target sequence (Fu et al., 2014; Hsu et al., 2013; Moreno-Mateos et al., 2015), which means it could bind to other unintended sites within the genome thus causing some nonspecific effects. However, like other techniques, characterization of potential off-target effects is quite challenging. Whole genome sequencing in human pluripotent stem cells reveals that the off-target mutation is very rare and is thus not a significant concern for its application (Veres et al., 2014). By contrast, whole genome sequencing performed in a CRISPR/Cas9 edited mouse finds a very high number of single nucleotide variants, which is at odds with the widely shared assumption of high precision (Schaefer et al., 2017). In zebrafish, little is known about the off-target effects *in vivo* since unbiased assessment has not been performed in any mutants. Therefore, it is highly recommended to minimize the undesirable effects by other methods, such as deletion of large genomic fragments.

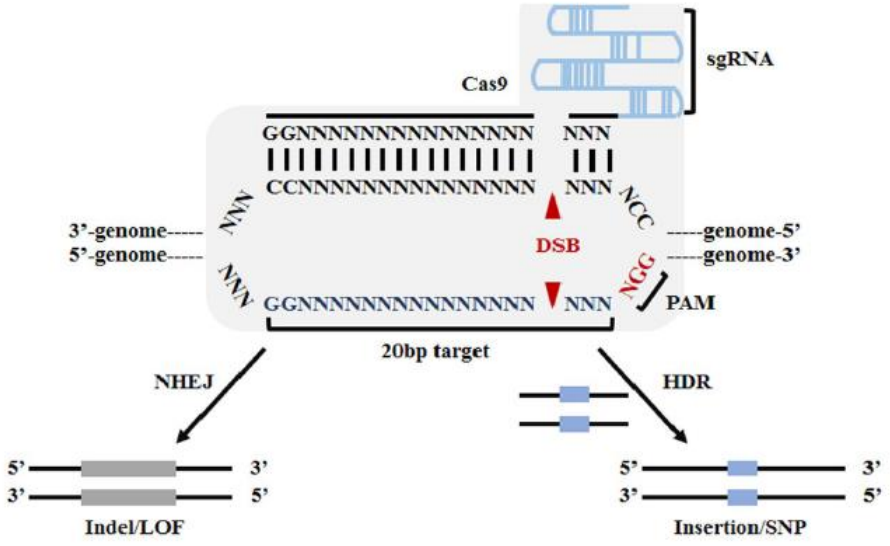

Figure 1.10 : Schematic illustration of the CRISPR/Cas9 system.

The sgRNA binds to the complementary strand of the genome target site neighboring the PAM sequence. Cas9 endonuclease introduces double strand breaks within the targeted genomic site which will be repaired by the NHEJ or HDR. Adapted from (Liu et al., 2017).

1.6.3. Knockdown and knockout

Along with the widespread application of genome engineering tools, serious concerns have been raised about the discrepancies between morphant and mutant phenotypes in zebrafish studies. An increasing number of studies in zebrafish find that mutants often fail to exhibit the same phenotype observed in morphants. Moreover, many researchers attribute this to the off-target effect of MOs. One of the recent examples came from the work of Nathan Lawson and his colleagues (Kok et al., 2015) in which they generated and analyzed 32 mutant lines for 24 genes involved in zebrafish vascular development. Among these mutants, only 3 mutant lines recapitulated the phenotype of morphants. A further integrative comparison of covert morphant phenotypes with the Sanger Zebrafish Mutation Project revealed 80% of MO-induced phenotypes failed to be recapitulated in the corresponding mutants (Kok et al., 2015). Based on these, the authors recommended that MO-mediated phenotypes should always be validated by genetic mutants to define a gene function. In support of this, Stainier et al., discussed the same issues and concluded that if a phenotype is reported for the first time and solely based on morpholino injection without a comparison of genetic mutants, it should be viewed very critically (Vidal et al., 2005).

While researchers were still arguing over the use of MOs within zebrafish community, Rossi et al., (Rossi et al., 2015) found that induction of a compensatory pathway could explain the phenotypic differences caused by knockouts and knockdowns. In this paper, they first found that an *egfl7* mutant hardly showed any changes in morphology while the embryos injected with *egfl7* MO exhibited severe vascular defects. Interestingly, *egfl7* mutant embryos were

less sensitive than wild type to the effect of *egfl7* MO injection, which confirmed the specificity of *egfl7* MO action and implied different but specific responses to gene knockdown vs knockout. Next, they found that this differential response was due to the up-regulation of a set of proteins that only occurs in mutants but not morphants. Among these were some proteins which contain the same functional domain as Egfl7 and which turned out to be able to rescue the vascular defects of *egfl7* morphants. This result indicated that the up-regulation of other genes could compensate for the loss of *egfl7* in the mutant. However, the underlying mechanism by which such genetic compensation takes place in mutants but not morphants is still unclear. *Rossi et al*. also showed that titrating the MO to a dose that did not induce *p53* expression is very critical for the use of MOs in gene function studies as we know MOs are likely to induce off-target effects at high doses.

To conclude, although there seems to be a high demand for genetic support for a morpholino-induced phenotype in zebrafish, we should always bear in mind that these two techniques are not mutually exclusive, but in fact complementary to each other. Much work remains to be done to investigate the reason behind the discrepancy between morphants and mutants. Meanwhile, it is still highly recommended to provide enough documentation to prove the reliability of a morpholino action such as stringent controls and optimized doses.

1.7. Hypothesis and Rationale

As opposed to late stage functions, our lab observed that loss of zebrafish *hoxd4a* results in significant down-regulation of the hemangioblast marker *scl* in the PLM at 13 hpf despite the fact that, at this stage, the expression of *hoxd4a* in PLM is only detected at background levels. This surprising result, along with its early expression, suggests that *hoxd4a* could act at an early stage of embryonic development, long before it takes up a more expected role in patterning the AP axis.

In addition, embryos simultaneously depleted for the function of *hoxd4a* and *hoxc4a* by morpholino injection show major disruption of two lineages derived from the neural plate border (NPB), namely neural crest cells (NCC) and Rohon-Beard (RB) primary sensory neurons. Like the VMM, the NPB is also specified at peri-gastrulation stages of development, arising at a region of intermediate levels of BMP signaling. In contrast, the adjacent placodes, which are not derived from the NPB develop normally. The specific impairment of NPB derivatives without changes in the adjacent placodes strongly implicates a function for *Hox* genes and BMP signaling during early embryonic development. Moreover, in both cases, co-injection of *meis1.1* mRNA was able to rescue the hematopoietic defects in *hoxd4a* morphants and the formation of NPB derivatives in *hoxc4a*/*hoxd4a* double morphants. Again, this suggests that the function of *Hox* genes in these different developmental programmes could depend on their cofactors.

In situ hybridization shows that *hoxd4a*, *hoxc4a* and *meis1.1* are all ubiquitously expressed throughout the embryonic epiblast at pre-gastrulation stages, while BMP is highly expressed

at the ventral side by shield stage. This temporal and spatial co-expression of *hoxd4a*, *hoxc4a* and BMP signaling is notable at the VMM from which the blood and vasculature are derived. In short, all of these genes are co-expressed at the 'right' time and 'right' place – when and where the hemangioblast is specified. More importantly, physical interactions between HOX and either of these factors (Pbx, Meis and Smads) have been reported. Notably, all of them are associated with hematopoietic and vascular development.

Based on these findings, we hypothesize that zebrafish *hoxd4a* acts prior to gastrulation to specify the hemangioblast in the VMM, a function which could be mediated by cooperative interactions with cofactors like Pbx, Meis, and the BMP signaling pathway. Excitingly, this novel function of *hoxd4a* in the control of two major lineages occurs at a time earlier than, and distinct from, its function in AP patterning, and have clear implications for the functions of *Hox* genes in mammals.

CHAPTER 2 : MATERIALS AND METHODS

2.1. Animals and ethics statements

2.1.1. Zebrafish

Wild type zebrafish from a commercial supplier were used in this study. Zebrafish were maintained under a 14 hours light/10 hours dark cycle at 28°C as described (Westerfield, 2000). Staging of zebrafish embryos was performed according to (Kimmel et al., 1995).

2.1.2. Mice

C57BL/6 mice were used for monoclonal antibody production and were purchased from the Centre for Animal Resources (CARE) in Singapore and housed under a 12 hours light/12 hours dark cycle in the animal facility of Nanyang Technological University.

2.1.3. Ethics statements

All animal work was performed in accordance with the Institutional Animal Care and Use Committee (IACUC) guidelines at Nanyang Technological University and were approved under protocol number ARF SBS/NIE-A 0144 AZ.

2.2. Plasmid construction

2.2.1. Plasmids used for *in situ* hybridization

DNA plasmids for synthesizing *scl*, *fli1*, *gata1*, *prdm1*, *islet1* RNA probes were generous gifts from Bernard Thisse and Christine Thisse. The plasmid used for *sox10* RNA probe synthesis

was a kind gift from Vincent Cunliffe.

2.2.2. Plasmids used for mRNA rescue experiments

Full-length cDNA for zebrafish *hoxd4a* was cloned in the pSP64 vector between HindIII and XbaI sites (Amali et al., 2013). All other plasmids containing *hoxd4a* in the pSP64 vector were constructed based on this plasmid. pSP64-*hoxd4a*-ERT2 was generated by overlap-extension PCR with primers indicated in Table 2.1. The coding sequence of the ligand-binding domain (LBD) of a human estrogen receptor variant (ERT2) was amplified using plasmid pMB80 (Addgene, plasmid ID 12168) and inserted in frame 3' to *hoxd4a* using a SacI restriction site. Point mutations of *hoxd4a* were made using the Quick Change Lightning Site-Directed Mutagenesis Kit (Agilent Technologies, Cat. no. 210518).

2.2.3. Plasmids used for the BioID system

A plasmid containing the coding sequence of BirA* was a kind gift from Dr. Brian Burke (Roux et al., 2012). The plasmid encoding Hoxd4a-BirA*-FLAG was created by overlap-extension PCR with primers indicated in Table 2.1. BirA*-FLAG was inserted in frame 3' to *hoxd4a* using a SmaI restriction site. The *hoxd4a*-BirA*-FLAG fragment was excised from the pSP64 vector and inserted in the pcDNA3.1 (+) vector between HindIII and EcoRV sites. To add the FLAG tag to Hoxd4a, the coding sequence of the FLAG tag was included in the reverse primer used for amplification of *hoxd4a* (Table 2.1). The *hoxd4a*-FLAG fragment was then cloned into the pSP64 vector and pcDNA3.1 (+) vector between HindIII and XbaI sites.

2.2.4. Plasmids used for BMP signaling studies

Plasmid encoding MH1-c was a kind gift from Dr. Stefan Karlsson and Ronan Quéré (Quere et al., 2011). MH1-c was amplified with primers indicated in Table 2.1 and cloned into the pSP64 vector between PstI and BamHI sites. The coding sequences of s*mad1*, s*mad4*, s*mad5* and *smad9* were amplified form 6 hpf zebrafish cDNA using primers indicated in Table 2.1. All amplified fragments were subsequently inserted into HindIII and EcoRV sites of the pcDNA3.1 (+) vector. pCS2+PCAB plasmid used for *in vitro* transcription was kindly requested from Prof. Sagerstrom (Choe, 2002).

2.2.5. Plasmids used for CRISPR/Cas9 mediated knockout and knockin

Plasmid DR274 (Addgene, plasmid ID 42250) was used for sgRNA construction. A pair of oligonucleotides (Table 2.1) containing the target site was annealed and ligated into BsaI-digested DR274 vector. The donor plasmid *hoxd4a*-P2A-EGFP used for attempts to create a knockin transgenic line was constructed based on the plasmid *th*-P2A-EGFP (Addgene, PlasmidID 65562). The left arm between KpnI and BamHI sites was replaced with *hoxd4a* sequences spanning the intron and exon 2 that had been amplified with primers indicated in Table 2.1. The right arm between AgeI and PstI sites was replaced with the 3' UTR sequence of *hoxd4a* that had been amplified with primers indicated in Table 2.1.

All above constructs were validated by restriction enzyme digestion and direct sequencing analysis.

Table 2.1: List of primers used for plasmid construction.

Name of gene	Primers (Forward and Reverse)
hox4a	5’-AACAAGACGGCGTCGCATCGAGATC 5’-CTCATGTCTCCAGCAGATAAAGTTGTGATCTCTG-3’
ERT2 (*hox4a*)	5’-CAGAGATCACAACTTTATCTGCTGGAGACATGAG-3’ 5’-GATCGAGCTCTCAGACCGTGGCAGGGAAAC-3’
hox4a N51S mutation	5’-AAAATCTGGTTTCAGtcCAGGAGAATGAAATGG-3’ 5’-CCATTTCATTCTCCTGGACTGAAACCAGATTTT-3’
hox4a YPAA mutation	5’-GCTGTAGTTTACCCGgcGgcGAAGAAAGTGCACGTT-3’ 5’-AACGTGCACTTTCTTCGCCGCCGGGTAAACTACAGC-3’
smad 1	5’-CCCCAAGCTTATAATGAATGTCACCTCACTCTTTTCC-3’ 5’-CCGGAATTCGCGGACACTGAAGAAATGGGGTTGTG-3’
smad 4	5’ -CCCCAAGCTTATAATGTCCATCACAAACACTCCCAC-3’ 5’-CCGGAATTCGCGTCTAACGGTGTGGGGTCTGCGAT-3’
smad 5	5’-CCCCAAGCTTATAATGACCTCCATGTCTAGTCTGTTT-3’ 5’-GGGGGGATATCCGAGACAGAAGAGATGGGGTTCAG-3’
smad 9	5’-CCCCAAGCTTATAATGCACTCCTCTACCTCCATCAC-3’ 5’-TTTAAGATATCGGACACCGAGGAAATGGGGTTGTG-3’
hoxd4a (BirA*)	5’-TATGTGGATCCCAAATTTCCTCCTTGC-3' 5'-GGCACGGTGTTGTCCTTTAAAGTTGTGATCTCTG-3'
BirA*(*hoxd4a*)	5'-CAGAGATCACAACTTTAAAGGACAACACCGTGCC-3' 5'-TTCCCCCGGGTTACTTGTCGTCATCGTCCT-3'
BirA*	5'-CCCCAAGCTTATAATGAAGGACAACACCGTGCCCC-3' 5'-GCTCTAGATTACTTGTCGTCATCGTCCT-3'
MH1-c	5'- AAACTGCAGCTCGGATCTCACGTGG -3' 5'-AGGGAGAGGGGCACGGATC-3'
hoxd4a target site used for knockout	5'-TAGGCTCGTCGGTGCAGCCGCG-3' 5'-AAACCGCGGCTGCACCGACGAG-3'
hoxd4a target site 5 used for knockin	5'-TAGGAGTGGCCAACACAGCTAG-3' 5'-AAACCTAGCTGTGTTGGCCACT-3'
hoxd4a intron and exon2 (left arm of KI plasmid)	5’-CGGGGTACCGCCAATTACACCAGCCATA-3’ 5’-CCGCGGATCCTAAAGTTGTGATCTCTGTCTGGCT-3'
hoxd4a 3'UTR (right arm of KI plasmid)	5’-CCGACCGGTTAAGTGGATATCTCTCCCTCCCTT-3’ 5’-AAACTGCAGTGTGAACCATCATTCGATGCCTC-3’

2.3. Microinjection of morpholinos and mRNA

Morpholinos were ordered from Gene Tools and diluted with nuclease-free water to the desired concentration. At the 1-2 cell stage, 1 nl of morpholino was injected into the yolk. Morpholino targeting the splice acceptor site of *hoxd4a* was used for the majority of experiments in this study (Amali et al., 2013). All statements about 'anti-*hoxd4a* morpholino' refers to this morpholino unless otherwise specified. Morpholino targeting the splice donor site of *hoxd4a* was also used in this study to investigate the specificity of the morphant phenotype. Morpholinos containing a five-nucleotide mismatch were designed by Gene Tools and injected at different doses as indicated. All morpholinos were designated as follows:

splicing acceptor MO (*hoxd4a*-MO^{SA}): 5'-GTTCACTGTGAAGGACAAAATCACA-3'

5-nt mismatch MO1 (*hoxd4a*-mis-MO^{SA}): 5’-GTTCAgTcTcAAGcACAAAATgACA-3'

splicing donor MO (*hoxd4a*-MO^{SD}): 5'-GCAAAGAGAGTGGATCTTACCCGTA-3'

5-nt mismatch MO2 (*hoxd4a*-mis-MO^{SD}): 5’-GCAtAcAGAcTGcATCTTACCCcTA-3' .

As suggested by our previous study (Amali et al., 2013), all mRNAs used for the rescue experiments were injected at a dose of 50 pg.

2.4. Drug treatment

4-hydroxytamoxifen (4-OHT; Sigma, Cat. no. H7904) was dissolved at 10 mM in 100% ethanol and stored in foil-wrapped tubes at -20°C. Before use, a working solution of 10 µM 4-OHT was prepared by dilution in standard fish water. Controls were treated with the same amount of ethanol. BMP inhibitor LDN193189 hydrochloride (Sigma, Cat. no. SML0559) was dissolved at 10 mM in water and stored at -20°C. Embryos were treated with

LDN193189 from 4 hpf until the desired stages. For o-dianisidine and alkaline phosphatase staining, zebrafish embryos/larvae were treated with 200 μM phenylthiourea (PTU; Sigma, Cat. no. P7629) in fish water from 24 hpf to inhibit melanization.

2.5. Whole mount *in situ* hybridization (WISH) and imaging

2.5.1. Antisense DIG-labeled RNA probe synthesis

Plasmids used for RNA probe synthesis were linearized with corresponding restriction enzymes and purified by phenol/chloroform extraction. Digoxigenin (DIG)-labeled antisense RNA probes were synthesized from linearized plasmids using SP6/T7/T3 RNA polymerases (Roche) according to the manufacturer's instructions.

2.5.2. Embryos fixation and storage

Embryos at different developmental stages were collected and fixed in 4% paraformaldehyde (PFA; Sigma, Cat. no. 441244) in phosphate buffered saline (PBS) at 4°C overnight. Embryos older than 24 hpf were dechorionated before fixation. Fixed embryos were either used immediately for *in situ* hybridization or dehydrated in methanol and stored at -20°C for a few months.

2.5.3. *in situ* hybridization (ISH)

Whole-mount *in situ* hybridization was performed by following the protocol as previously described (Thisse and Thisse, 2008). Dehydrated embryos were washed by successive dilutions of methanol in PBS with 0.05% Tween-20 (PBST) at 75% (v/v), 50% (v/v) and 25%

(v/v) for 5 min each. Embryos were washed with PBST and then permeabilized with Proteinase K (10 μg/ml in PBST) at room temperature for the time depending on the developmental stages as indicated in Table 2.2. Permeabilized embryos were fixed again in 4% PFA at room temperature for 20 min and then washed for four times in PBST, 5 min for each wash. Embryos were pre-hybridized in 200 μl of hybridization plus buffer (Hyb(+); 50% formamide, 5×saline sodium citrate (SSC) buffer, 0.1% Tween-20, 50 μg/ml heparin and 500 μg/ml yeast tRNA in DEPC water) at 65°C for 2 hours. The hybridization buffer was then replaced with 200 μL of Hyb(+) containing 50 ng of RNA probes and incubated at 65°C for overnight.

Table 2.2: Proteinase K digestion times for different developmental stages.

Developmental stage	Duration of Proteinase K treatment
< 13 hpf	Not required
14 hpf -20 hpf	5 min
24 hpf	10 min

On the second day, Hyb(+) was discarded and embryos were washed by a serial dilutions of hybridization minus buffer (Hyb(-); 50% formamide, 5×SSC buffer, 0.1% Tween-20 in DEPC water) in 2×SSC: 75% (v/v), 50% (v/v) and 25% (v/v) at 65°C, 10 min for each wash. Embryos were next incubated in pre-heated 2×SSC at 65°C for another 10 min and then changed into 0.2×SSC at 70°C for 30 min. Incubation in 0.2×SSC was repeated one more time. Embryos were then successively washed by a serial dilutions of 0.2×SSC in PBST: 75% (v/v), 50% (v/v) and 25% (v/v) at room temperature, 5 min for each incubation. After

equilibration in PBST for another 5 min at room temperature, embryos were incubated in 200-500μL of blocking buffer (2 mg/ml bovine serum albumin and 2% sheep serum in PBST) at room temperature for 2 hours. The blocking buffer was then replaced with fresh blocking buffer containing anti-DIG antibody conjugated with alkaline phosphatase (Roche,1:3,000) and incubated at 4°C overnight.

On the next day, the blocking solution was discarded and embryos were transferred into 24-well plates. Unbound antibody was thoroughly removed by six 10-min washes with PBST at room temperature. Embryos were next incubated with freshly prepared NTMT buffer (100 mM Tris·HCl pH 9.5, 50 mM $MgCl_2$, 100 mM NaCl, 0.1% Tween-20) for 3 times, 5 min for each wash. Color was developed in darkness with staining buffer containing 337 μg/ml NBT and 175 μg/ml BCIP (Roche, Cat. no. 11383221001). The staining reaction was stopped when the appropriate intensity was reached. Embryos were washed 3 times with PBST, 5 min for each wash. Background signal was removed by incubating embryos in 100% methanol for a few minutes and then rehydrated through serial dilutions of methanol in PBST: 75% (v/v), 50% (v/v) and 25% (v/v). Embryos were equilibrated in PBST for 5 min and stored in glycerol at 4°C without light.

Flat mounting of stained embryos at segmentation stages was performed as previously described (Cheng et al., 2014). A Zeiss lumar V.12 stereo microscope with Axio Vision software was used for imaging.

2.6. Embryo staining

2.6.1. Alkaline phosphatase staining

Alkaline phosphatase staining was carried out as previously described (Amali et al., 2013). Embryos at 72 hpf were fixed in 4% PFA in PBS at 4°C overnight. Fixed embryos were washed with PBS twice and then treated with pre-cooled acetone for 30 min at -20°C. After washing with NTMT buffer for three times at room temperature, embryos were stained in NTMT buffer containing NBT/BCIP for 30-50 min without light. To aid visualization of the vasculature, embryos were treated with graded methanol/PBST and were finally equilibrated in PBST. Embryos were stored in glycerol at 4°C for imaging.

2.6.2. O-dianisidine staining

O-dianisidine (Sigma. Cat. no. D9143) staining of red blood cells was done as previously described (Amali et al., 2013). Embryos at 72 hpf were fixed in 4% PFA in PBS at 4°C overnight. Fixed embryos were washed with PBS for three times at room temperature and then stained in freshly prepared staining solution (0.6 mg/ml o-dianisidine, 10 mM sodium acetate, 0.65% hydrogen peroxide and 40% ethanol) for 10 min in darkness. The staining reaction was stopped by washing the embryos in PBST.

2.7. Real-time qPCR and semi-quantitative RT-PCR

2.7.1. Total RNA extraction

Total RNA was extracted from 20-30 embryos using 500 µl of Trizol reagent (Invitrogen, Cat.

no. 15596-026) according to the manufacturer's instructions.

2.7.2. cDNA synthesis

Extracted RNA was digested by DNaseI (Thermo Scientific, Cat. no. EN0521) at 37℃ for 30 min to remove genomic DNA contamination. The digestion reaction was terminated by heating at 65°C for 10 min with 50 mM EDTA. RNA was purified by phenol/chloroform extraction. First strand cDNA was synthesized with SuperScript III First-Strand cDNA Synthesis Kit (Invitrogen, Cat. no. 18080051) according to the manufacturer's instructions.

2.7.3. Real-time qPCR

Real time qPCR was performed by using SYBR Green qPCR SuperMix (Life technologies, Cat. no. kk4608) on BioRad iCycler iQ5 or SYBR StepOnePlus™ 7500 Fast according to the manufacturer's instructions with primers indicated in Table 2.3.

Table 2.3: List of primers used for real-time qPCR.

Name of gene	Forward (5' to 3')	Reverse (5' to 3')
β-actin	TTCCTTCCTGGGTATGGAATC	GCACTGTGTTGGCATACAGG
Scl	CTATTAACCGTGGTTTTGCTGG	CCATCGTTGATTTCAACCTCAT
fli1	CAACGGATCCAGAGAGTCG	CCATGTAGGCCAGTATAGTTCATCTG
gata1	AAGATGGGACAGGCCACTAC	TGCTGACAATCAGCCTCTTTT
prdm1	GGATACTCACCAGCAGGCTC	CAGGGTAGTGGTGCATGAGG
sox10	TCCATGTCCCCTGGTCACTC	CTTCCTCGTCGGACTTCACC
islet1	GGTGCTGTGACCCATTAAG	GGAGCTGTTTTCGTTGAGG
hoxb4a	CTGCGGTCAGACTCCCACTA	GTTCGGGCTCACGATGTTTA
hoxc4a	TCCACTATAATCGCTACTTAACACG	GGAGGACGAGGATCTGACTTTG
hoxd4a	ACCCCTAGCCCTTTCCCTG	GGTCTTTGTGTTTTGTTGTTGTCC
hoxb6b	AGGACAGGAGTCTTTCTTGGGTC	GAGCGGTCAGCGGTTCG
hoxb7b	CTTCATCATCTTCTGTCTCCCTG	TAGCCCCTCTGCTCTTCCTT
hoxa9a	CCCAACGCACTTCTCCACT	GTATTCCGTGCCGTCATCAT
meis1.1	GAGGACACACATCGCACAGT	GAGCCATGCCCTCATAATGT

2.7.4. Statistical analysis

All statistical analysis to determine the significant difference of two samples/conditions were performed using the one-tailed unpaired t-test. The definition for N (or number of measurements) is described in each figure.

2.7.5. Semi-quantitative RT-PCR

Semi-quantitative RT-PCR was done using *Taq* DNA polymerase (Thermo Scientific, Cat. no. EP0401) according to the manufacturer's instructions. To avoid saturation of PCR amplification, the cycle number was adjusted for each gene individually by checking PCR products at different cycles. For *hoxd4a*, PCR amplification was performed with a cycle number between 27-29. β-actin was amplified for 19-22 cycles.

2.8. Genome editing by the CRISPR/Cas9 system

2.8.1. Target site design

The target site was designed through the ZiFiT Targeter website (http://zifit.partners.org/) which requires 5’-GG-N18-NGG-3’ as default. For the target site used for *hoxd4a* knockout, no off-target sites were identified by the website. Putative off-target sites were further checked by BLAST for mismatch of the 3' thirteen bases of the N_{20} target site sequence. Target sequences used for *hoxd4a* knockout (KO) and knockin (KI) are listed below.

hoxd4a KO ts: 5'-GGCTCGTCGGTGCAGCCGCG-3'

hoxd4a KI ts1: 5'-GGAAATAGGCCGCTAGCTGTGT-3'

hoxd4a KI ts2: 5'-GACTCTCAATACTGCAAGAG-3'

hoxd4a KI ts3: 5'-GCCATAAATTTTTATTGCTT-3'

hoxd4a KI ts4: 5'-GGCTAAAACAGCAGAATAGGGA-3'

hoxd4a KI ts5: 5'-GAGTGGCCAACACAGCTAG-3'

2.8.2. *in vitro* transcription of sgRNA and Cas9 mRNA

Plasmid pCS2-nzcas9n (Addgene, Plasmid ID 47929) was used for *in vitro* transcription of capped mRNA using the SP6 mMESSAGE mMACHINE kit (Ambion, Cat. no. AM1340). Synthesized mRNA was purified by ammonium acetate precipitation following the manufacturer's guidelines. The template used for *in vitro* transcription of sgRNA was obtained by PCR with primers spanning the T7 promoter, target sequence and guide RNA sequences using High Fidelity DNA Polymerase (Thermo Scientific, Cat. no. EP0501) and purified using QIA quick PCR purification kit (QIAGEN, Cat. no. 28106). sgRNA was transcribed using MAXIscript T7 kit (Life Technologies, Cat. no. AM1312) and purified by phenol/chloroform extraction.

2.8.3. Microinjection of sgRNA and Cas9 protein

Purified Cas9 protein (NEB, Cat. no. M0386M) was used to generate knockout mutants. A mixture containing 200 ng/μL of Cas9 nuclease, 1×Cas9 nuclease reaction buffer (provided by NEB with Cas9 nuclease), 70-120 ng/μL of sgRNA was prepared and incubated at room temperature for 5 min before injection. Each embryo was injected with 1 nL of the mixture at the one-cell stage. Single-stranded stop codon oligonucleotide was designed as previously

described (Gagnon et al., 2014), and contained stop codons in all three reading frames. This stop-codon cassette was flanked by two 20 nt homologous arms spanning the predicted double strand breakpoints introduced by CRISPR/Cas9. The sequence of the relevant portion of the donor oligonucleotide is 5'-CAGGGCTCGTCGGTGCAGCCGTCATGGCTAATTAA TTAAGCTGTTGTAGGCGGGGTCATGTGCAGGATC-3'. It was ordered from Integrated DNA Technologies (IDT), diluted with nuclease-free water and injected at a concentration of 3 μM with the Cas9/sgRNA mixture. Constructed donor plasmid *hoxd4a*-P2A-EGFP was co-injected with Cas9/sgRNA at a concentration of 20 ng/μl. The concentration of donor plasmid was adjusted from 5 ng/μl to 50 ng/μl.

2.9. Genotyping

2.9.1. Genomic DNA extraction

Embryos at 24 hpf were digested with DNA extraction buffer (10 mM Tris·HCl pH 8.2, 10 mM EDTA, 200 mM NaCl, 0.5% SDS, 200 μg/ml proteinase K) at 55°C for 2-3 hours until tissues were completely digested. The reaction was stopped by heating at 95°C for 5 min to inactivate proteinase K. Two volumes of pre-cooled 100% ethanol were added to precipitate genomic DNA on ice for 30 min. The DNA precipitate was collected by centrifugation at 10,000 g for 15 min, followed by a wash with 70% ethanol. The final DNA extracts were resuspended in TE buffer (10 mM Tris·HCl pH 8.0, 0.1 mM EDTA).

2.9.2. Fin clips

Zebrafish larvae were anesthetized in tricaine (Sigma, Cat. no. E10521) at 50-300 μg/ml in

egg water. The tail fin was clipped using a micro scalpel (FEATHER, 200200715, Plastic 15° P-715) at the pigment gap as described (Wilkinson et al., 2013). Clipped fin tissue was transferred to a PCR tube containing 20 µL of 50 mM NaOH and subsequently heated in a thermal cycler at 95°C for 3-5 min. The reaction was neutralized with 1/10 volume of 1 M Tris·HCl (pH 8.0). One microlitre of the solution was used as template in a 15 µl PCR reaction. Zebrafish larvae were transferred to egg water in 12-well plates for recovery.

2.9.3. T7 Endonuclease I assay

The target site was amplified with primers named P1-P4 as indicated in Table 2.4. PCR products were denatured and re-annealed slowly to form the presumptive heteroduplex structure. The reannealing process consists of a 5 min denaturing step at 95°C, followed by a temperature decrease to 85°C at −2°C/sec and further to 25 °C at −0.1°C/sec. Reannealed PCR products were digested with T7 endonuclease I at 37°C for 60 min. The reaction was stopped with 25 mM EDTA. Digested samples and a DNA ladder (GeneRuler, Cat. no. SM0241 and SM0311) were resolved by 1.5-2.5% agarose gel electrophoresis and visualized by ethidium bromide staining.

2.9.4. SacII digestion assay

PCR products bearing the target site were directly digested with 0.2-0.5 units of SacII (NEB, Cat. no. R0157S) at 37°C for 1 hour. The reaction was inactivated by heating at 65°C for 20 min. Sample was resolved by 2% agarose gel electrophoresis and visualized by ethidium bromide staining. Positive PCR products were cloned into pCR4-TOPO®TA vector

(Invitrogen, Cat. no. K457502) for sequencing.

2.9.5. Genotyping

Genotyping of presumptive *hoxd4a* mutations was also analyzed by PCR amplification. First-round PCR products amplified with primers P1 and P4 (Table 2.4) were used as templates for a second round of nested PCR using locus specific screening primers (Table 2.4). Screening primers (wtFWd and mFwd) were designed such that only wild type or mutated alleles can be amplified, respectively.

Table 2.4: List of primers used for screening of CRISPR/Cas9 mutants.

Name of primers	Sequences
P1	5'-GATGAAGTCCCTCCACCTCG-3'
P2	5’-TATGTGGATCCCAAATTTCCTCC-3"
P3	5'-AATCAAGCTTCGGGCCAAAGG-3'
P4	5'-GCGTGTTGTGCATGCTGATT-3'
hoxd4a exon1 Fwd	5’-CACAAAGACCCAGAACGGGA-3’
hoxd4a exon2 Fwd	5'-AATCAGCATGCACAACACGC-3'
EGFP Rev	5'-CTTGTAGTTGCCGTCGTCCT-3'
hoxd4a 3'UTR Rev	5'-ATGGTGTGTGCTTCAGCTTCT-3'
wtFwd	5'-AGGGCTCGTCGGTGCAGCCG-3'
mFwd (#24)	5'- AGGGCTCGTCGGAGCAGGTC-3'
mFwd (#25)	5'-AGGGCTCGTCGGTCCGAGTC-3'

2.10. Cell culture, transfection and BioID

HEK293T (H293T) cells were cultured in high glucose Dulbecco's Modified Eagle Medium (DMEM) (Gibco, Cat. no. 12100-046) supplemented with 10% fetal bovine serum (FBS) and 1% of penicillin and streptomycin antibiotics. H293T cells were transiently transfected using Lipofectamine®2000 (Invitrogen, Cat. no. 11668-019) according to the manufacturer's instructions. Biotinylation was enhanced by the addition of 50 µM biotin (Sigma, Cat. no.

B4501-5G) for 18 hours starting from 6 hours post-transfection.

To prepare samples for mass spectrometry analysis, five 10-cm plates of H293T cells were transfected as described above. To ensure complete lysis, cell lysates were incubated on ice for 30 min, followed by dounce homogenization for 20 strokes. The viscosity was reduced by sonication at 30% AMPL for 3 cycles. One cycle consists of a 20 sec sonication followed by a 20 sec pause on ice. Biotinylated proteins were captured using streptavidin-agarose beads (Thermo Scientific, Cat. no. 20347) following the manufacturer's instructions. Proteins were finally eluted by boiling in 2× Laemmli buffer at 95°C for 5 min.

2.11. Immunoblotting

2.11.1. Sample preparation from cultured cells

Transfected cells were harvested from 6-well plates with 0.25% Trypsin-EDTA (Gibco, Cat No. 25200056). Cell lysates were prepared in lysis buffer containing 50 mM Tris·HCl pH 8.0, 150 mM NaCl, 0.5% Triton-100, 0.1% NP-40, 1×protease inhibitor cocktail. Mechanical disruption with a 21G needle was used to ensure efficient lysis of nuclei. Cellular debris were pelleted by centrifugation at 13,000 rpm for 10 min and the supernatant was subjected to SDS-polyacrylamide (SDS-PAGE) fractionation and immunoblotting.

2.11.2. Sample preparation from zebrafish embryos

Zebrafish embryos were carefully dechorionated under a stereoscopic microscope. After two washes with PBS, dechorionated embryos were transferred into deyolking buffer (1/2 Ginzburg Fish Ringer: 55 mM NaCl, 1.8 mM KCl, 1.25 mM $NaHCO_3$). The yolk was

disrupted by pipetting up and down for 5-6 times using a yellow tip. Embryos were collected by centrifugation at 1,000 g for 3 min. The embryos bodies was resuspended in washing buffer (10 mM Tris·HCl pH 8.5, 110 mM NaCl, 3.5 mM KCl, 2.7 mM $CaCl_2$). Total protein extract was prepared by dissolving the cell pellet in lysis buffer (50 mM Tris·HCl pH 8.0, 150 mM KCl, 0.5% Triton X-100, 0.5% NP-40 and 1×protease inhibitor).

2.11.3. Immunoblotting

Cell lysates were mixed with an equal volume of 2×Laemmli buffer with 5% β-mercaptoethanol and boiled at 95°C for 5 min. Protein samples and a pre-stained dual color protein ladder (BioRad, Cat. no. 1610374) were resolved on 12% SDS-PAGE gel and transferred to PVDF membrane (Thermo Scientific, Cat. no. 88518). The membrane was subsequently blocked with 5% nonfat milk in tris-buffered saline (TBS) with 0.05% Tween-20 (TBST) at room temperature for 1 hour and probed with appropriate primary antibody at 4°C overnight. The membrane was washed four times 10 min with TBST and incubated with HRP-conjugated secondary antibody at room temperature for 1 hour. The blot was washed 6 times 10 min with TBST. Proteins were visualized using the chemiluminescence kit (Immobilon, Millipore, Cat. no. WBKLS0500) using Image Quant™ LAS 4000 (GE Healthcare Life Sciences).

For the detection of another protein on the same blot, the membrane was stripped with stripping buffer (Thermo Scientific, Cat. no. 21059) for 20-40 min at room temperature. After briefly washing with TBST, the blot was blocked again in 5% non-fat milk and subjected to the same procedure described above.

Biotinylated proteins were detected similarly but with slight modifications to the procedure. After proteins were transferred to the PVDF membrane, the blot was blocked in 2.5% bovine serum albumin (BSA) in TBST at room temperature for 1 hour. The blot was subsequently incubated with a 1:10,000 dilution of streptavidin-HRP conjugate in 2.5% BSA at room temperature for 1 hour. After washing with TBST for 4 times 10 min, the blot was developed with the chemiluminescence kit.

2.11.4. Antibodies

The following antibodies were used for analysis: monoclonal ANTI-FLAG®M2 antibody produced in mouse (Sigma, Cat. no. A2220), monoclonal anti-β-Actin antibody produced in mouse (Sigma, Cat. no. A1978), monoclonal anti-HA antibody produced in rat (Roche, Cat. no. 3F10), polyclonal anti-Pbx1/2/3 antibody produced in rabbit (Santa Cruz, Cat. no. SC-888), anti-mouse IgG produced in rabbit (Sigma, Cat. no. A9044), Streptavidin HRP conjugate (Invitrogen, Cat. no. 43-4323), monoclonal anti-Rat IgG1 (heavy chain) produced in mouse (Abcam, Cat. no. ab99655), anti-Rabbit IgG (whole molecule) produced in goat (Sigma, Cat. no. A0545).

For immunoblotting, primary antibodies were used at a concentration of 1:2,000-1:5,000 diluted in 5% nonfat milk and secondary antibodies were used at a concentration of 1: 5,000-1:10,000 in 5% nonfat milk in all experiments unless specifically stated.

2.12. Co-immunoprecipitation

Following preparation of cell lysates, 10% was kept as input control while the remainder was

used for immunoprecipitation (IP) with either anti-FLAG M2 affinity agarose beads (Sigma, Cat. no. A2220) or anti-HA magnetic beads (Pierce, Cat. no. 88836) following the manufacturer's instructions. The protein extracts were incubated with the beads at 4°C overnight with gentle mixing followed by three washes with the lysis buffer to remove the non-specific binding proteins. The bound protein was eluted by boiling in 2×Laemmli buffer at 95°C for 5 min.

2.13. Monoclonal antibody production

2.13.1 Antibody production

Cysteine-tagged peptide corresponding to the zebrafish Hoxd4a C-terminus (CSVGNQHAQHAQKDSQTE-OH) was ordered for monoclonal antibody production. To increase immunogenicity, the peptide was coupled with Keyhole Limpet Haemocyanin (KLH) using Imject® Maleimide Activated mcKLH kit (Thermo Scientific, Cat. no. 77605). KLH-coupled peptide in complete Freund's adjuvant (Sigma) was injected subcutaneously in mice, followed by a second subcutaneous injection in incomplete Freund's adjuvant. After two weeks, the final booster was given in PBS. Mice were sacrificed three days later. Isolated popliteal lymph node cells were fused with SP2/0 myeloma cells (ATCC® CRL-1581™) by polyethylene glycol (Sigma, Cat. no. P7181) following a standard protocol (Harlow and Jane, 1988). Upon colony formation, culture supernatant from different wells was screened by ELISA using biotinylated peptides with the same sequence (Bio-Ahx-GNQHAQHAQKDSQTE-OH). Cells from the positive wells were subjected to limiting dilution to isolate a single clone, which was further screened by ELISA. A final

positive hybridoma was expanded in roller bottles. Monoclonal antibody was purified using Gamma Bind Plus Sepharose (GE Healthcare, Cat. no. 17-0886-01).

2.13.2. ELISA

ELISA was performed using Reacti-Bind TM Streptavidin Coated Clear 96-well plates (Thermo Scientific, Cat. no. 15124). Plates were quickly washed three times with PBST at room temperature and then coated with 20 μg/ml biotinylated peptides in PBST at 4°C overnight. Each well was quickly washed three times with 200 μL of PBST. Mouse serum or purified monoclonal antibody was diluted in PBST and added into each well. After incubation at room temperature for 1 hour, plates were quickly washed 3 times with PBST. Anti-mouse HRP secondary antibody (Biolegend, Cat. no. 405306) was diluted at 1:3,000 in PBST and incubated at room temperature for 1 hour. Unbound antibody was removed with 5 washes of PBST. Color development was performed by adding 50 μl of TMB High Sensitivity Substrate Solution (Biolegend, Cat no. 421501) into each well and incubated in the dark. The reaction was stopped with 2N H_2SO_4 and signals were measured at 450 nm.

2.13.3. Peptide competition assay

Purified monoclonal antibody was incubated with different concentrations of free peptide (CSVGNQHAQHAQKDSQTE-OH) at room temperature for 1 hour. Control peptide used in this study is another short fragment of Hoxd4a (CSTVQGSSVQPRGHVQDQ). After incubation, the peptide-antibody mixture was added to the streptavidin-coated plates bound with biotinylated peptides at 4°C overnight. Reactivity was then measured at 450 nm.

CHAPTER 3 : RESULTS

3.1. Timing of *hoxd4a* function in hematopoiesis and NPB formation

3.1.1. In hematopoiesis

An inducible activation method was used to study the time window during which *hoxd4a* exerts its function. As done for many other studies, the coding sequence of *hoxd4a* was fused with the ligand binding domain of a human estrogen receptor (ERT2) variant which has a high affinity for the estrogen antagonist tamoxifen, but little for estrogen itself. In this way, the activity of *hoxd4a* can be controlled by the addition or withdrawal of the bio-active tamoxifen metabolite 4-hydroxy-tamoxifen (4-OHT). *In vitro* transcribed chimeric mRNA and anti-*hoxd4a* morpholino (MO) were co-injected into the one-cell stage embryos. At the time points indicated in Figure 3.1.1, a final concentration of 10 μM 4-OHT was added to the injected embryos. Controls were treated with the same amount of vehicle (ethanol).

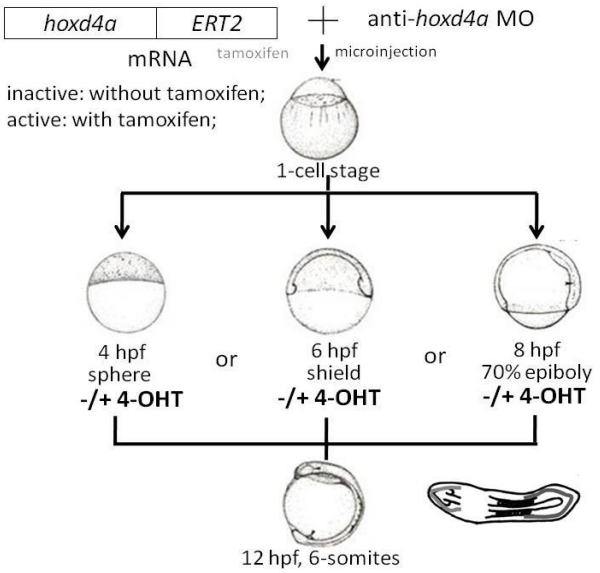

Figure 3.1.1: Schematic representation of 4-OHT treatment.

First, the expression of the hemangioblast marker *scl* was analyzed by *in situ* hybridization at 12 hpf (Fig. 3.1.2). Consistent with our previous findings (Amali et al., 2013), *scl* transcripts were significantly diminished in the PLM of *hoxd4a* morphants (Figure 3.1.2, EtOH treated embryos). Compared with controls, *scl* expression was rescued to wild type levels in the group treated with tamoxifen at 4 hpf. Rescue was moderately reduced in 6 hpf treated embryos. But for the 8 hpf group, the expression of *scl* was still severely down-regulated. Similarly, the expression of the endothelial differentiation marker *fli1* and the erythroid marker *gata1* were both rescued by activation of Hoxd4a at 4 hpf, but not 8 hpf (Fig. 3.1.3), suggesting that the role of *hoxd4a* in primitive hematopoiesis and vasculogenesis is required by 4 hpf.

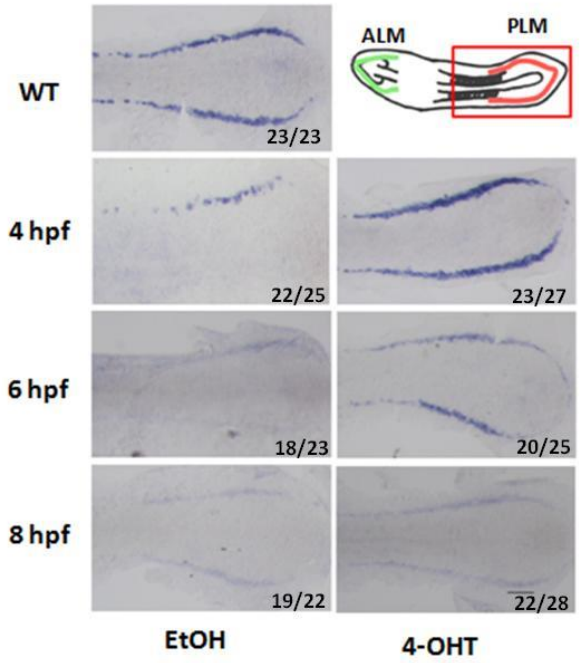

Figure 3.1.2: *scl* expression at 12 hpf with the addition of ethanol/4-OHT at 4 hpf, 6 hpf and 8 hpf. In ethanol (EtOH) treated embryos (*hoxd4a* morphants), the expression of the hemangioblast marker *scl* was highly down-regulated in the PLM. Addition of 4-OHT resulted in full rescue of *scl* expression. By contrast, addition of 4-OHT failed to provide any detectable rescue. Expression indicated in the red box is shown in dorsal views of flat-mounted embryos, anterior to the left.

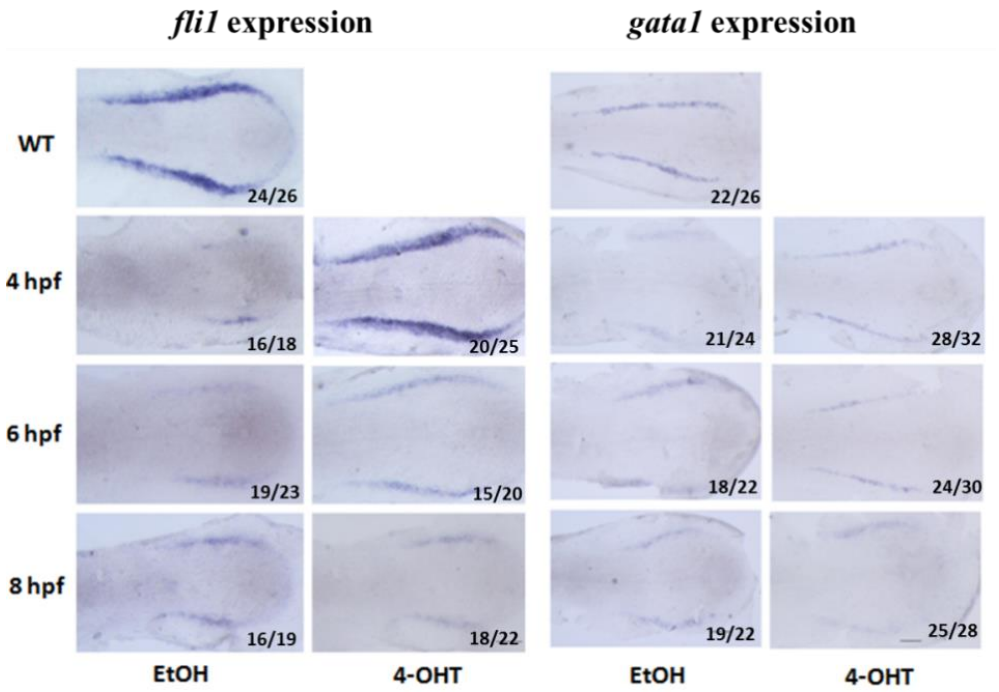

Figure 3.1.3: *fli1* and *gata1* expression at 12 hpf with the addition of ethanol/4-OHT at 4 hpf, 6 hpf and 8 hpf. In ethanol (EtOH) treated embryos (*hoxd4a* morphants), the expression of the endothelial differentiation marker *fli1* and the erythroid marker *gata1*was highly reduced, which was rescued by activation of Hoxd4a-ERT_2 at 4 hpf, but not 8 hpf. Expression in the PLM is shown in dorsal views of flat-mounted embryos, anterior to the left.

To quantify this striking result, qRT-PCR was performed at 12 hpf. In support of the *in situ* hybridization results, qRT-PCR showed that the expression of *scl*, *fli1* and *gata1* were completely rescued by 4 hpf, but not 6 or 8 hpf (Fig. 3.1.4).

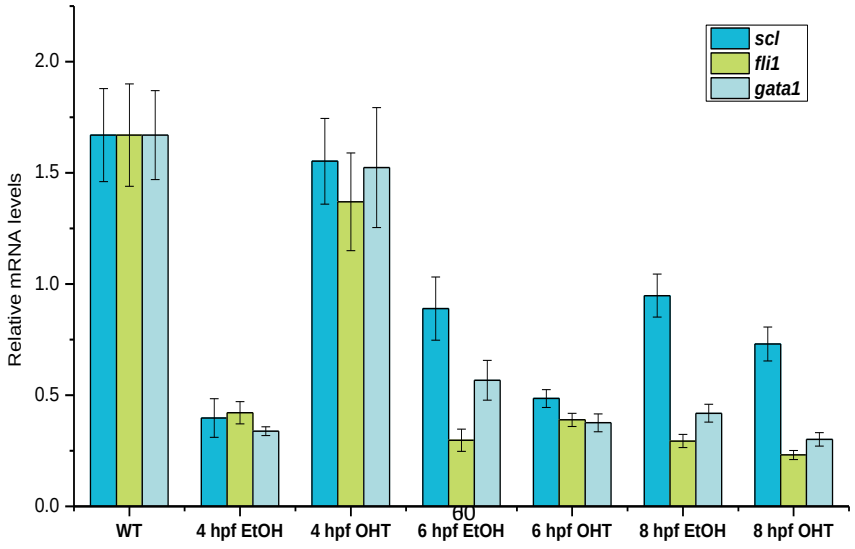

Figure 3.1.4: Real-time qPCR analysis of *scl*, *fli1* and *gata1* expression in 12 hpf embryos treated with ethanol/4-OHT. Samples were normalized to *β-actin*. Error bars indicate standard error of three technical replicates.

To study the effect of activating Hoxd4a at different time points on erythroid development, o-dianisidine staining of hemoglobin within red blood cells was conducted at 72 hpf. Consistent with previous data, in the *hoxd4a* knockdown groups (4 hpf EtOH, 6 hpf EtOH, 8 hpf EtOH), the number of blood cells was considerably reduced (Fig. 3.1.5). However, this can be rescued by the addition of tamoxifen at 4 hpf and 6 hpf. By contrast, no changes were observed between the knockdown groups and embryos treated with 4-OHT at 8 hpf. In combination with *gata1* expression, this result implies that the action of *hoxd4a* in hematopoiesis is required by 4 or 6 hpf.

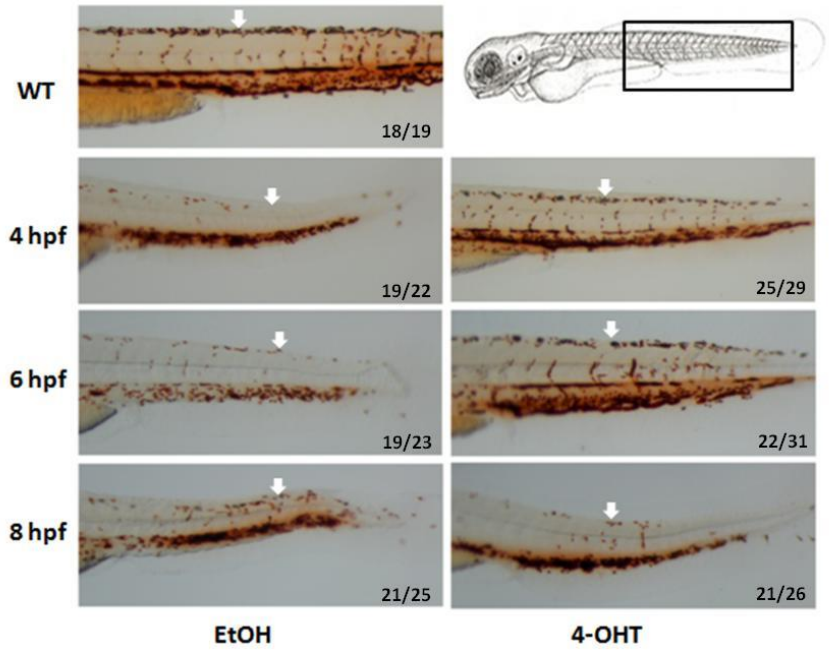

Figure 3.1.5: O-dianisidine staining of the red blood cells in 72 hpf embryos treated with ethanol/4-OHT. Consistent with our previous findings, the number of red blood cells was obviously

reduced in the EtOH-treated embryos (*hoxd4a* morphants). It was fully rescued by the addition of 4-OHT at 4 hpf and 6 hpf, but not 8 hpf. The tail region indicated in the black box is shown in lateral views.

To visualize the vasculature, endogenous alkaline phosphatase in endothelial cells was stained at 72 hpf. Likewise, when Hoxd4a is inactive (4 hpf EtOH, 6 hpf EtOH, 8 hpf EtOH), vessel formation such as for the subintestinal vessels (SIV) and intersegmental vessels (ISV) was severely impaired; however, it was successfully rescued by activation of Hoxd4a at 4 hpf and 6 hpf, but not 8 hpf (Fig. 3.1.6).

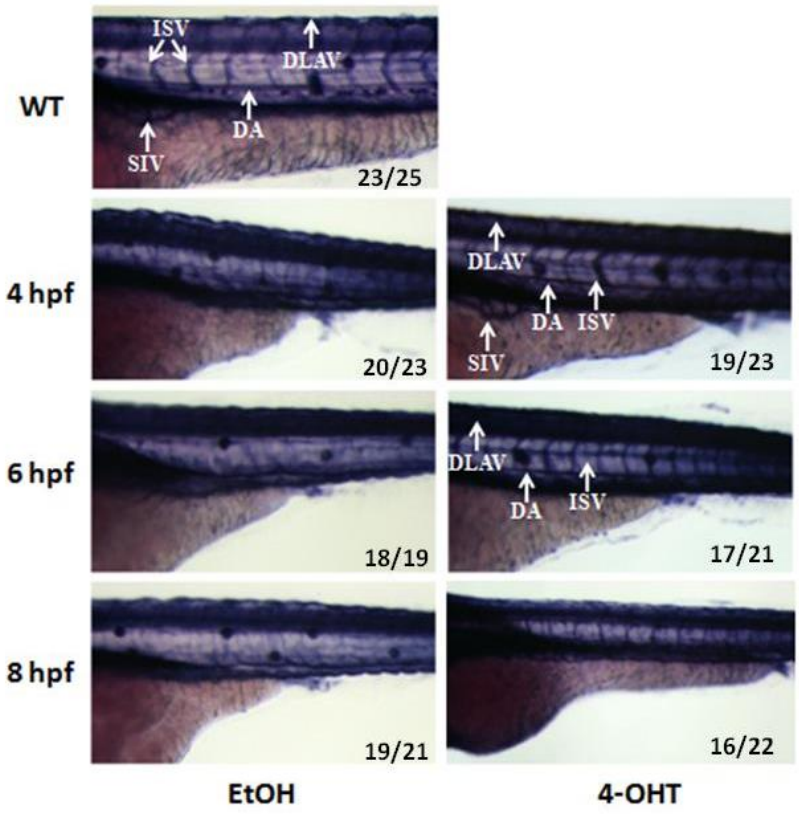

Figure 3.1.6: Alkaline phosphatase staining of endothelial cells in 72 hpf embryos treated with ethanol/4-OHT. Impaired endothelial development in *hoxd4a* morphants (EtOH-treated embryos) was only rescued by the addition of 4-OHT at 4 hpf and 6 hpf. Tail region is shown in lateral views. ISV, inter-segmental vessels; DA, dorsal artery; DLAV, dorsal longitudinal anastomotic vessels; SIV, subintestinal vessels.

Together, these results suggest that the action of *hoxd4a* in directing hematopoiesis and

vasculogenesis is required by 4 hpf, consisting with the findings described above.

3.1.2. In NPB formation

In addition to hematopoiesis and vasculogenesis, our lab also observed a second major disruption in a different developmental process following loss of *Hox* gene function. While the phenotype is apparent in single morphants of *hoxd4a* or *hoxc4a*, it is much more obvious in double morphants (despite using lower doses of morpholinos) which exhibit dramatic defects in the development of lineages derived from the neural plate border (NPB). Briefly, the phenotypes include decreased pigmentation, reduced RB sensory neurons and trigeminal ganglia, and malformation of branchial cartilages. In support of the phenotypic defects, the expression of *prdm1*, a key regulator of the NPB, is significantly reduced as early as 90% epiboly. This coincides with a down-regulation of *sox10* and *islet1*, which are required for the specification of neural crest cells (NCCs) and neurons, respectively. By contrast, the development of adjacent placode derivatives, such as the lens and otic vesicle, is quite normal. Based on these, we hypothesize that *hoxd4a* and *hoxc4a* could act in cooperation with BMP signaling to direct NPB induction or formation at an early developmental stage.

To test this hypothesis, the function of *hoxd4a* in NPB formation was investigated using the same strategy described above. *Hoxd4a-ERT2* mRNA was co-injected with lower doses of *hoxd4a* and *hoxc4a* morpholinos, followed by the addition of 4-OHT at different time points. In wild type embryos, *prdm1* was expressed in the boundary of neural and non-neural ectoderm at 12 hpf (Fig. 3.1.7). High expression was also found in the prechordal plate, adaxial cells and branchial arch progenitor cells. Consistent with our previous results, in

ethanol treated embryos, namely *hoxd4a* and *hoxc4a* double morphants, *prdm1* expression in the NPB and branchial arch precursor cells was highly reduced. This was moderately rescued in embryos treated with tamoxifen at 4 hpf and 6 hpf. By contrast, activation of Hoxd4a by 8 hpf failed to restore *prdm1* expression.

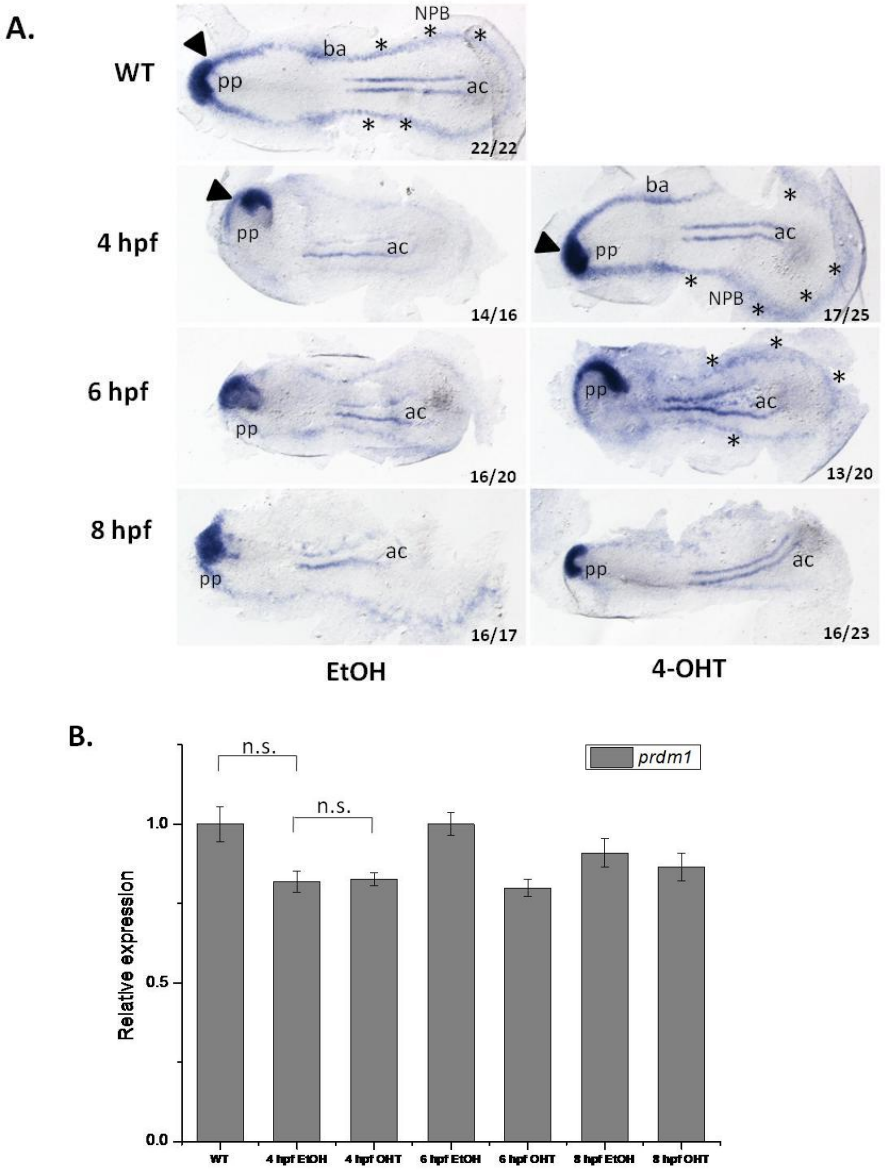

Figure 3.1.7: *prdm1* expression in *hoxd4a* and *hoxc4a* double morphants at 12 hpf with the addition of ethanol/4-OHT.

(A) *in situ* hybridization of *prdm1* at 12 hpf in dorsal views of flat-mounted embryos. In WT embryos, *prdm1* was highly expressed in prechordal plate (pp), the boundary of neural and non-neural ectoderm (the

NPB), slow muscle precursors (adaxial cells) and branchial arch (ba) progenitors. In *hoxd4a*/*hoxc4a* double morphants, its expression in the NPB was obviously reduced (marked by asterisk marks). Arrowheads indicate its expression in the prechordal plate.

(B) qPCR analysis of *prdm1* expression in *hoxd4a* and *hoxc4a* double morphants at 12 hpf. Data are shown as mean of fold changes ± standard error (s.e.m) from three independent experiments. n.s. means not significant.

Similarly, the expression of the neuronal marker *islet1* and the NCC marker *sox10* were also determined. Both were rescued by the addition of 4-OHT at 4 hpf, but not 8 hpf (Fig. 3.1.8 and 3.1.9). However, these changes revealed by *in situ* hybridization were only reflected in the expression of *sox10* when measured by qPCR (Fig. 3.1.9). It was not obvious for *prdm1* and *islet1*, possibly because high *prdm1* and *islet1* expression in the anterior polster of double morphants may mask decreases in the NPB (Fig. 3.1.7 and 3.1.8).

Taken together, these results strongly confirmed that *hoxd4a*, and likely its paralog *hoxc4a*, are required for different developmental programmes at an early developmental stage, long before the late-phase of *Hox* expression.

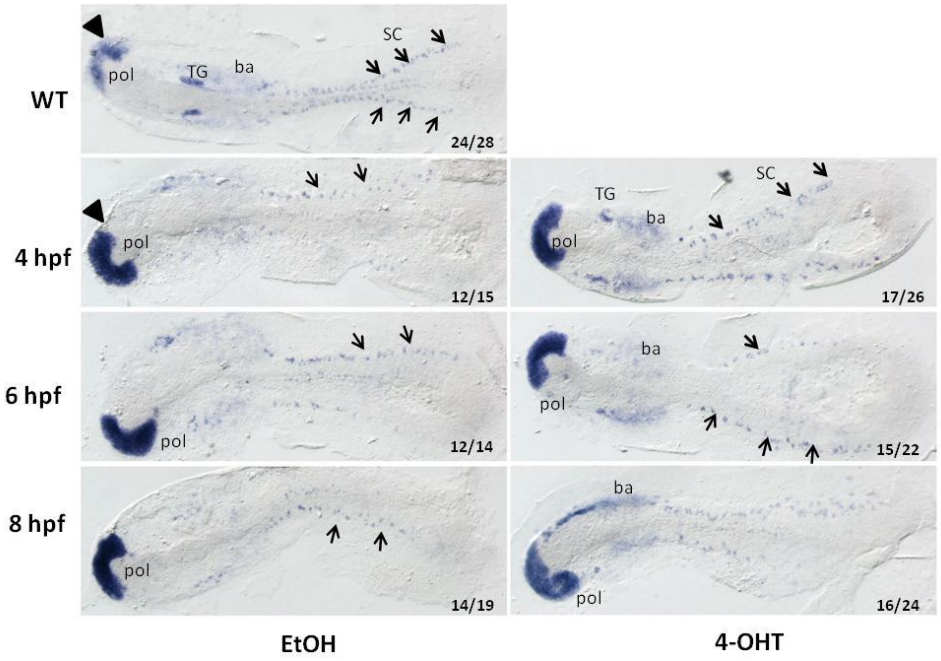

Figure 3.1.8: *islet1* expression in *hoxd4a*/*hoxc4a* double morphants at 12 hpf with the addition of ethanol/4-OHT.

In WT embryos, the expression of *islet1* was found in the anterior polster (pol; a part of prechordal mesoderm), trigeminal ganglia (TG), ventral and dorsal spinal cord (SC) neurons (black arrows). When *hoxd4a* and *hoxc4a* were depleted by morpholino injection, the expression of *islet1* was highly reduced in neuron cells. It was only rescued by the addition of 4-OHT at 4 hpf. Images are shown in dorsal views of flat-mounted embryos.

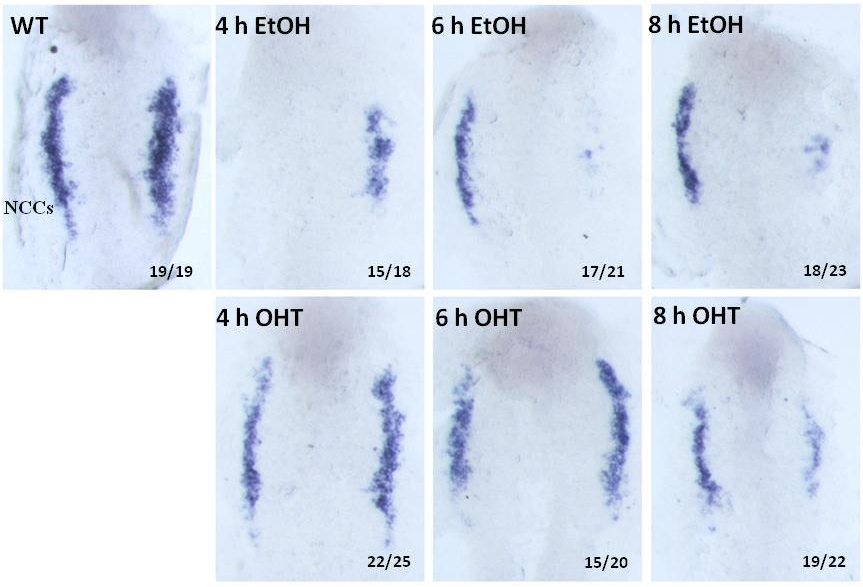

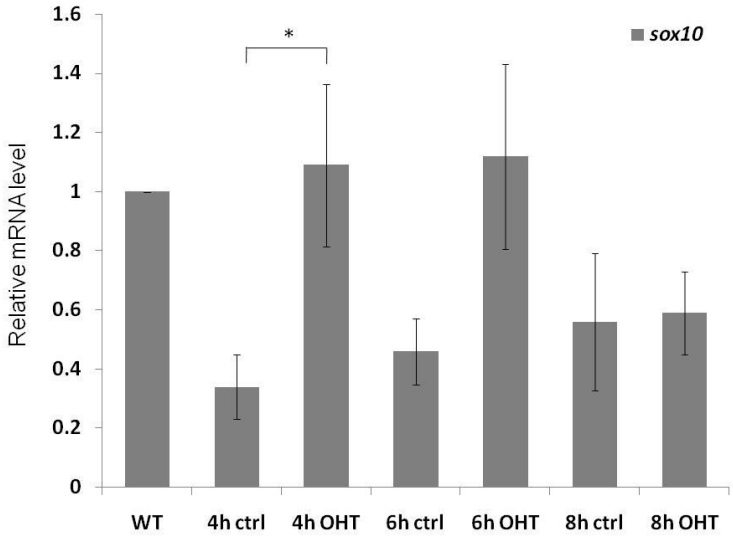

Figure 3.1.9: *sox10* expression in *hoxd4a* and *hoxc4a* double morphants at 12 hpf with the addition of ethanol/4-OHT.

(A) *in situ* hybridization of *sox10* in 12 hpf embryos shown in dorsal views. NCCs, neural crest cells.
(B) qPCR analysis of *sox10* expression in *hoxd4a* and *hoxc4a* double morphants at 12 hpf. Data are shown as mean of fold changes ± standard error (s.e.m) from three independent experiments (n=3). * denotes $p \leq 0.05$.

3.2. Implication of Hox cofactors in the control of hematopoiesis by Hoxd4a

3.2.1. Functional domains of Hoxd4a in hematopoiesis

The defects provoked by knockdown of *hoxd4a* with anti-sense morpholinos can be rescued by co-injection of *hoxd4a* mRNA. This provides an approach by which I can assess the importance of different functional domains of the Hoxd4a protein. In order to investigate how *hoxd4a* regulates hematopoiesis and vasculogenesis, asparagine 51 in the homeodomain (N51) and/or the YPWM motif was mutated (Fig. 3.2.1), thus impairing the ability of Hoxd4a to bind to DNA and/or PBX, respectively. Then, by co-injecting the mutated mRNA with anti-*hoxd4a* morpholino, the ability of these mutated mRNAs to rescue the defects provoked

by loss of *hoxd4a* was assessed, for example, the reduced expression of *scl*, *fli1* and *gata1*. Note that numerous studies suggest that neither of these mutations affects protein stability or nuclear localization (Rambaldi et al., 1994).

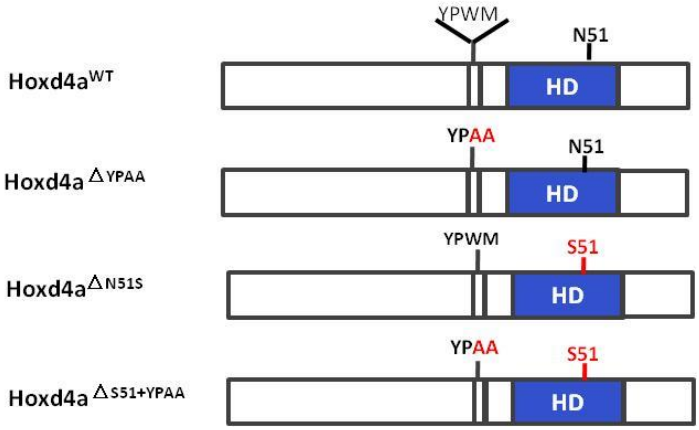

Figure 3.2.1: Schematic representation of the wild-type Hoxd4a (Hoxd4a^{WT}) and different mutants (Hoxd4a$^{\Delta N51S}$, Hoxd4a$^{\Delta YPAA}$, Hoxd4a$^{\Delta S51+YPAA}$).

As illustrated in Fig. 3.2.2, co-injection of *hox4a*^{WT} mRNA with anti-*hoxd4a* morpholino yielded the expected rescue of *scl* and *fli1* expression. While the rescue by Hoxd4a mutants (*hoxd4a*$^{\Delta N51S}$, *hoxd4a*$^{\Delta YPAA}$, *hoxd4a*$^{\Delta S51+YPAA}$) was obviously less efficient than *hox4a*^{WT}, marker gene expression nonetheless remained higher than in *hoxd4a* morphants. This suggests that both the homeodomain (HD) and the YPWM motif are required for the function of Hoxd4a in regulating the expression of *scl*, *fli1 and gata1*. It could be true especially for the YPWM motif as shown by qRT-PCR, where *hoxd4a*$^{\Delta YPAA}$ significantly lost the ability to rescue the expression of *scl* and *fli1* (Fig. 3.2.2). Surprisingly, none of the mutants was able to rescue the expression of *gata1*, implying a different mechanism by which it is regulated by Hoxd4a. In support of the gene expression at an early stage, defects of blood and endothelial cell formation caused by loss of *hoxd4a* were only partially rescued by the different mutated

mRNAs (Fig. 3.2.3).

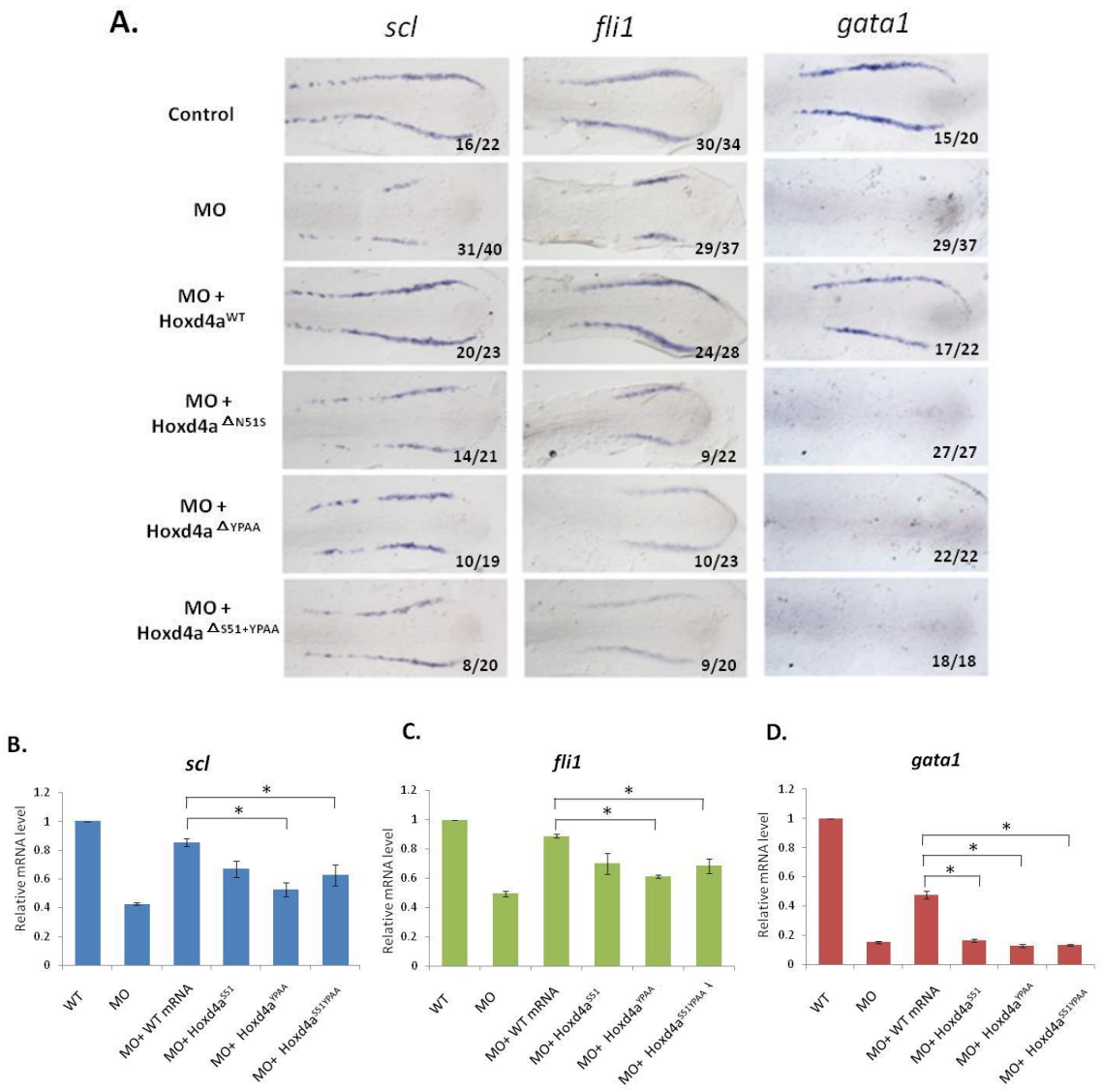

Figure 3.2.2: *scl, fli1* and *gata1* expression at 12 hpf in *hoxd4a* morphants rescued by different *hoxd4a* mutated mRNAs.

(A) *scl*, *fli1* and *gata1* expression in PLM shown in dorsal views of flat-mounted embryos, anterior to the left. MO embryos were injected with 4 ng of anti-*hoxd4a* morpholinos.

(B-D) qPCR analysis of *scl*, *fli1* and *gata1* expression. Data are shown as mean of fold changes ± standard error (s.e.m) from three independent experiments (n=3). Statistical analysis was performed between different mutated mRNA and WT mRNA. * denotes $p \leq 0.05$.

Figure 3.2.3: O-dianisidine staining and alkaline phosphatase staining of *hoxd4a* morphants rescued by different mutated mRNAs. Blood cells in the tail region (left panel, lateral views) and around the yolk (middle panel, ventral views) are shown at 72 hpf. The inter-segmental vessel sprouts (right panel, lateral views) are marked by white dots.

3.2.2. Establishment of methods to detect endogenous Hoxd4a

3.2.2.1. Monoclonal antibody production

To better understand how *hoxd4a* regulates hematopoiesis, it would be useful to identify the interacting partners of Hoxd4a at early developmental stages. Also, identification of the downstream targets that are directly bound and regulated by Hoxd4a would be also helpful

for our understanding. Both of these aims require a means to physically detect the Hoxd4a protein *in vivo*. To this end, we first attempted to generate a monoclonal antibody against zebrafish Hoxd4a following a standard protocol (Harlow and Lane, 1988).

A specific peptide derived from zebrafish Hoxd4a was conjugated to the keyhole limpet hemocyanin (KLH) carrier protein, which was subsequently used to immunize mice. During the immunization process, the immune response was analyzed by ELISA and western blot. Serum collected before immunization was used as a negative control. As shown in Figure 3.2.4, all immunized mice showed a strong response to the antigen in ELISA by serial dilutions. To determine the specificity of the antibody, peptide competition assay was performed. Excess free peptides were able to specifically block the binding between the antibody and biotinylated peptides (Fig. 3.2.4, C), indicating the generated antibody is specific to the hapten peptide of Hoxd4a.

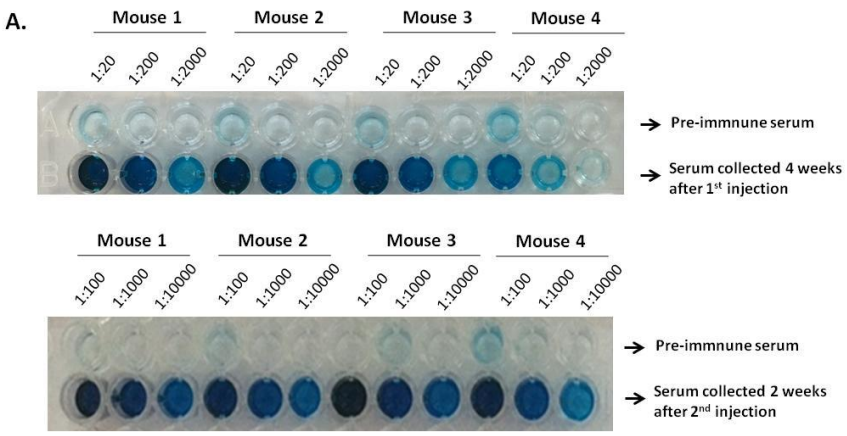

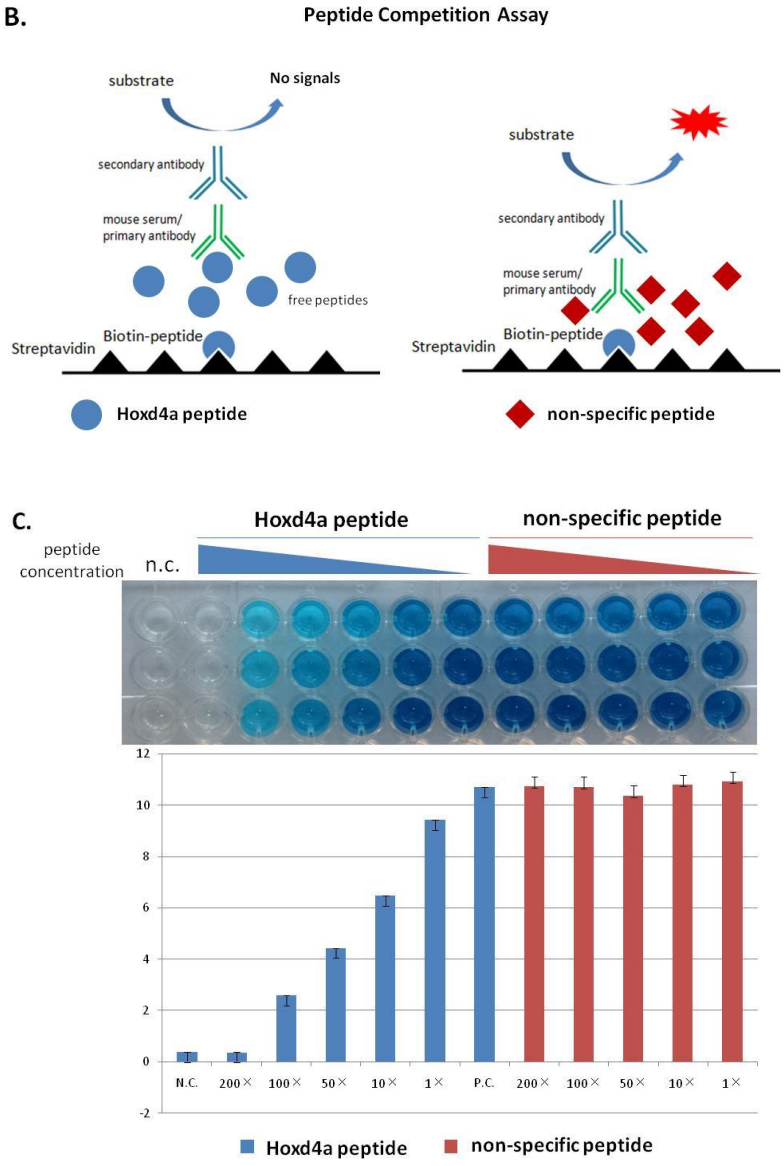

Figure 3.2.4: ELISA analysis of the mouse serum and purified monoclonal antibody.

(A) ELISA for serial dilutions of mouse serum isolated from four different immunized mice. Biotinylated hapten peptides were pre-incubated with the streptavidin-coated plates before the serum was added.

(B) Schematic presentation of peptide competition assay. If the antibody is specific to the biotinylated hapten peptide of Hoxd4a, pre-incubation of excessive free peptides (non-biotinylated same peptides) would prevent the antibody from binding to the biotinylated peptides bound to the plates. Non-specific control peptide is another short fragment of Hoxd4a which is completely unrelated to this antibody production.

(C) Peptide competition assays against the purified monoclonal antibody. n.c. means negative controls without antibody incubation.

Next, the antibody was analyzed by immunoblotting using different lysates with overexpressed Hoxd4a proteins. It was found that the antibody can recognize different epitope-tagged Hoxd4a proteins that were overexpressed in either mammalian cells or *E.coli*. However, endogenously expressed Hoxd4a in zebrafish cell lysates was hardly detected by the antibody (Fig. 3.2.5, D). All together, these results showed that the immunized mice were able to produce an antibody that is specific to Hoxd4a, however, it is not be suitable for the detection of Hoxd4a at an endogenous level in zebrafish.

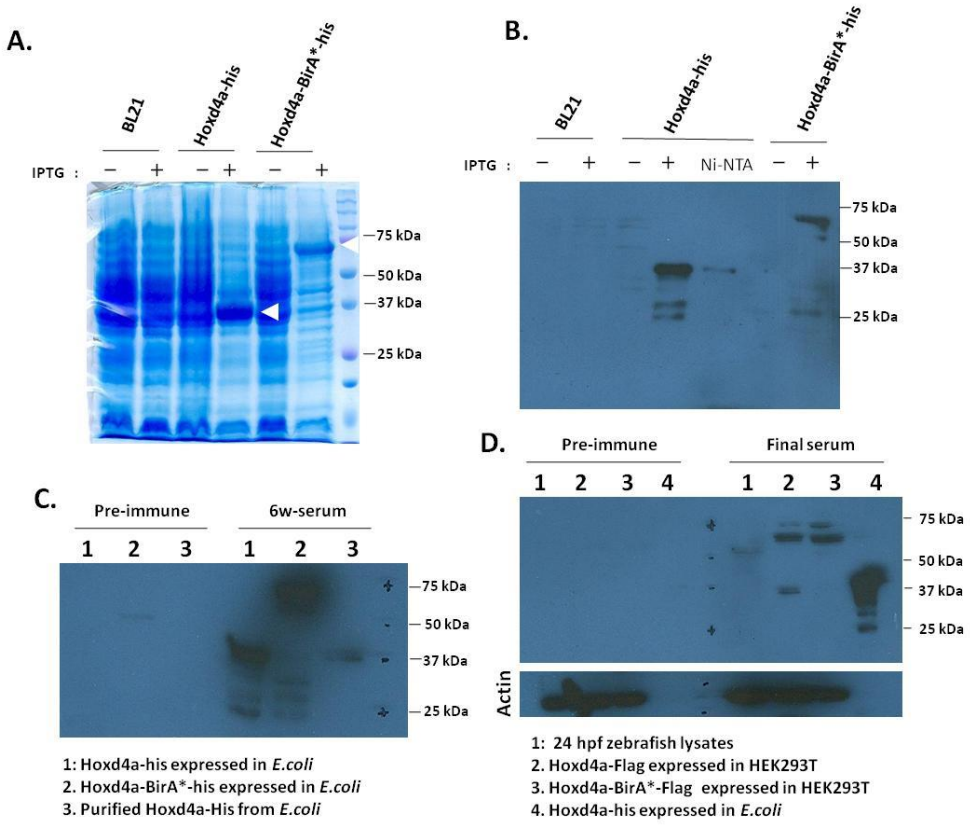

Figure 3.2.5: Immunoblotting analysis of the mouse serum.

(A) IPTG-induced expression of Hoxd4a proteins in *E.coli* BL21 (DE3) analyzed by 15% SDS-PAGE. (B-D) Western blot analysis of the mouse serum. Hoxd4a-his and Hoxd4a-BirA*-his overexpressed in *E.coli* were used for immunoblotting analysis (B-C). Hoxd4a-his was purified by Ni-NTA column in (B). Hoxd4a-Flag and Hoxd4a-BirA*-Flag were overexpressed in HEK293T cells. Final serum in panel D was collected before sacrificing the mice for lymph nodes harvest.

3.2.2.1. Generation of knock-in transgenic lines using CRISPR-Cas9 system

Meanwhile, we also attempted to establish a knock-in transgenic zebrafish line to tag endogenous Hoxd4a with a fluorescent protein. An intron-based knock-in method mediated by CRISPR/Cas9 system is shown to be very efficient in zebrafish (Li et al., 2015). In this system, the donor plasmid is provided for knock-in integration, which is composed of three parts: a left arm, a P2A-eGFP for multicistronic expression, and a right arm (Fig. 3.2.6). The left arm retains the full coding frame, starting from upstream of the target site designed in the intron and terminating at the last base before stop codon. The right arm contains a stop codon and the 3' intergenic region which was shown to be critical for gene expression (Li et al., 2015). When the donor plasmid is co-injected with Cas9/sgRNA, concurrent cleavage of the genomic *hoxd4a* locus and donor plasmid could result in an integration of the linearized donor plasmid into the opened chromosomal locus by non-homologous end joining (NHEJ). As the target site is designed in the intron, INDEL mutations introduced by NHEJ will not change the reading frame in exons, which highly increases the rate of successful protein expression.

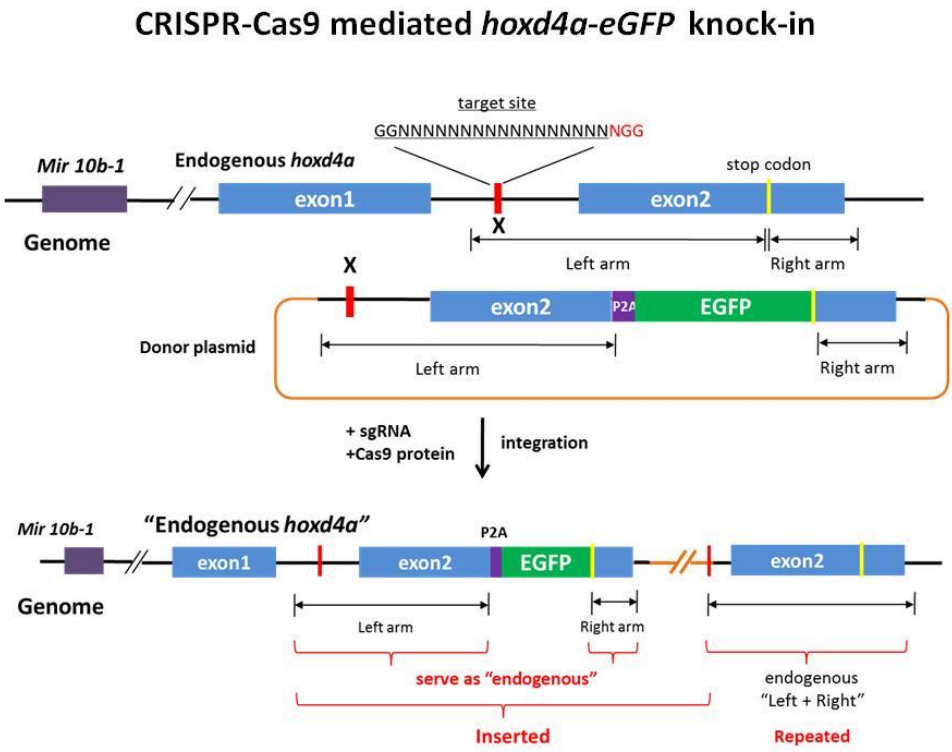

Figure 3.2.6: Schematic representation of the intron targeting-mediated strategy for *hoxd4a-eGFP* knockin by CRISPR/Cas9 system. *hoxd4a* has two coding exons with the second exon encoding the homeodomain. The target site is shown in red and the stop codon in yellow. The donor plasmid backbone is shown in orange. The left and right arms of the donor plasmid are indicated by double arrows.

The first step of this approach is to identify a highly efficient target site which is critical for the integration of the donor plasmid. Five different sgRNA sites targeting the intron of *hoxd4a* were designed and their efficiency of mutation was estimated by the T7 endonuclease I (T7EI) assay. Of these, only *hoxd4a* target site 5 was shown to be efficient and used for the following work (Fig. 3.2.7).

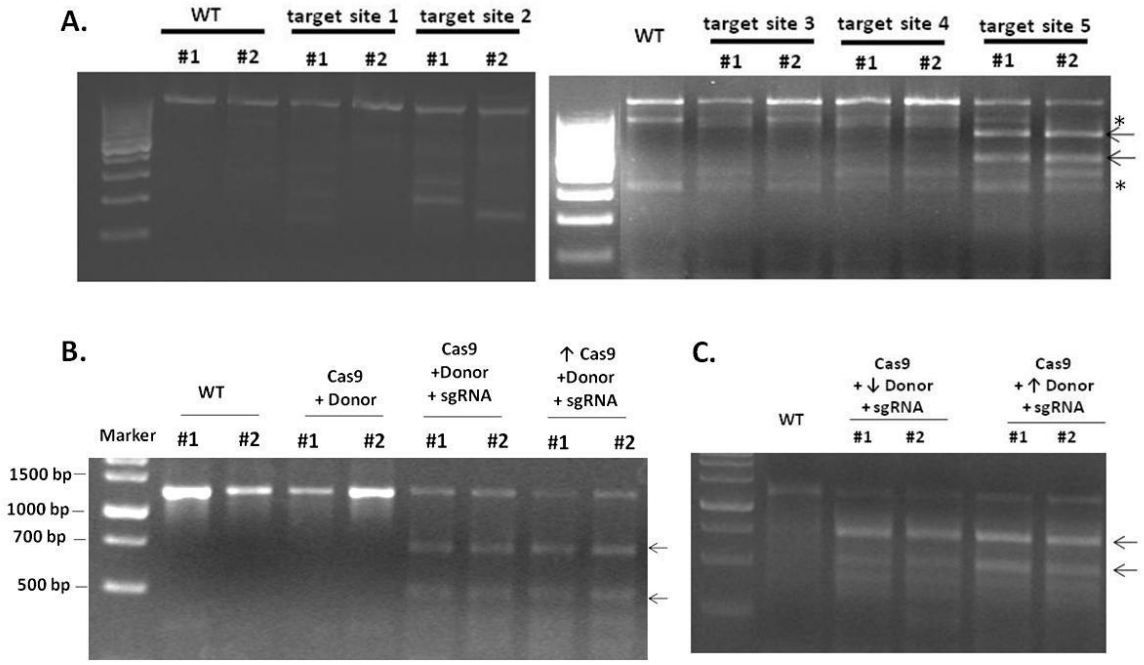

Figure 3.2.7: Activity analysis of different CRISPR/Cas9 target sites in the *hoxd4a* intron by the T7EI assay.

(A) Activity analysis of five CRISPR/CAS9 target sites in the *hoxd4a* intron by the T7EI assay. Black arrows indicates the expected DNA bands cleaved by T7 endonuclease I. White asterisk (*) marks non-specific cleaved bands which were also observed in WT controls.

(B-C) Analysis of the cleavage efficiency under different concentrations of Cas9 protein and the donor plasmid. As suggested by (Gagnon et al., 2014), 20 pg of the donor plasmid and 200 pg of Cas9 protein were injected into each embryos. Different amounts of Cas9 protein (400 pg) and donor plasmid (5-50 pg) were tested.

Based on the strategy, successful integration of the donor plasmid will result in eGFP expression in Hoxd4a expressing cells, which are expected in the hindbrain and some neural crest cells at 24 hpf (Amali et al., 2013). Therefore, injected embryos were screened based on eGFP expression after 24 hpf. Unfortunately, we failed to observe any eGFP signals in the injected embryos up to five days old. To rule out of the possibility that endogenous Hoxd4a expression is too low to be visualized by eGFP expression, locus-specific PCR amplification

was performed to detect the potential integration events (Fig. 3.2.8). While the T7EI assay showed that mutations were successfully introduced at the targeted locus, no PCR products were amplified using the genome and insert specific primers. Moreover, reverse transcription PCR (RT-PCR) analysis only identified endogenous transcripts of *hoxd4a*, but not fused transcripts (Fig. 3.2.8, D), which further confirmed a failure of donor plasmid integration. Since both of the donor plasmid and genomic DNA contain the target site, the donor plasmid could compete with the genome for sgRNA directed Cas9 protein binding. Thus, the concentration of the donor plasmid was optimized. With slight effects on the mutation efficiency (Fig. 3.2.7, C), it failed to lead to detectable integrations (Fig. 3.2.8, panel C).

In summary, we failed to establish a knock-in transgenic zebrafish line for *hoxd4a* due to unsuccessful integration of the donor plasmid.

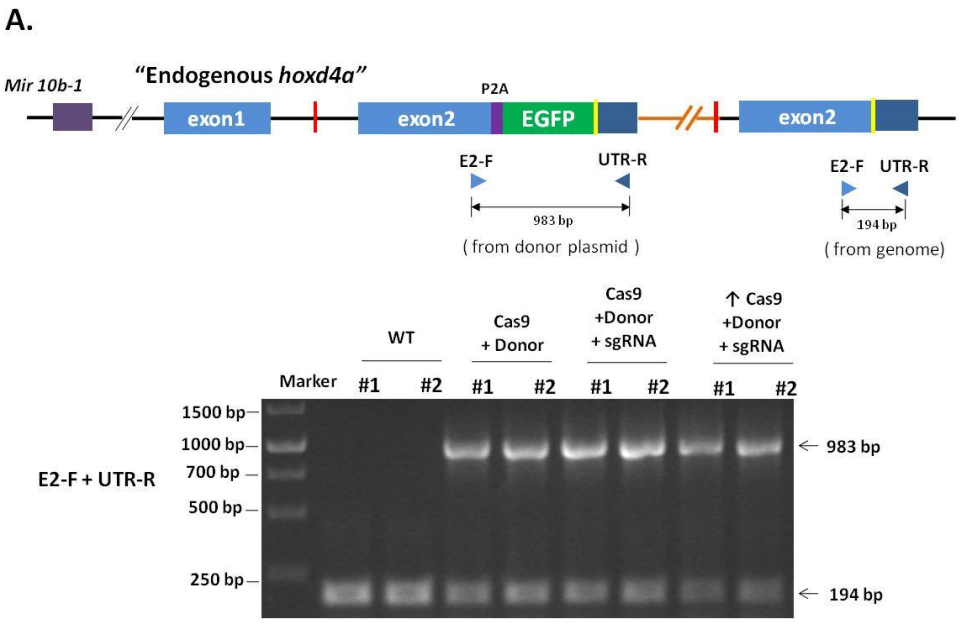

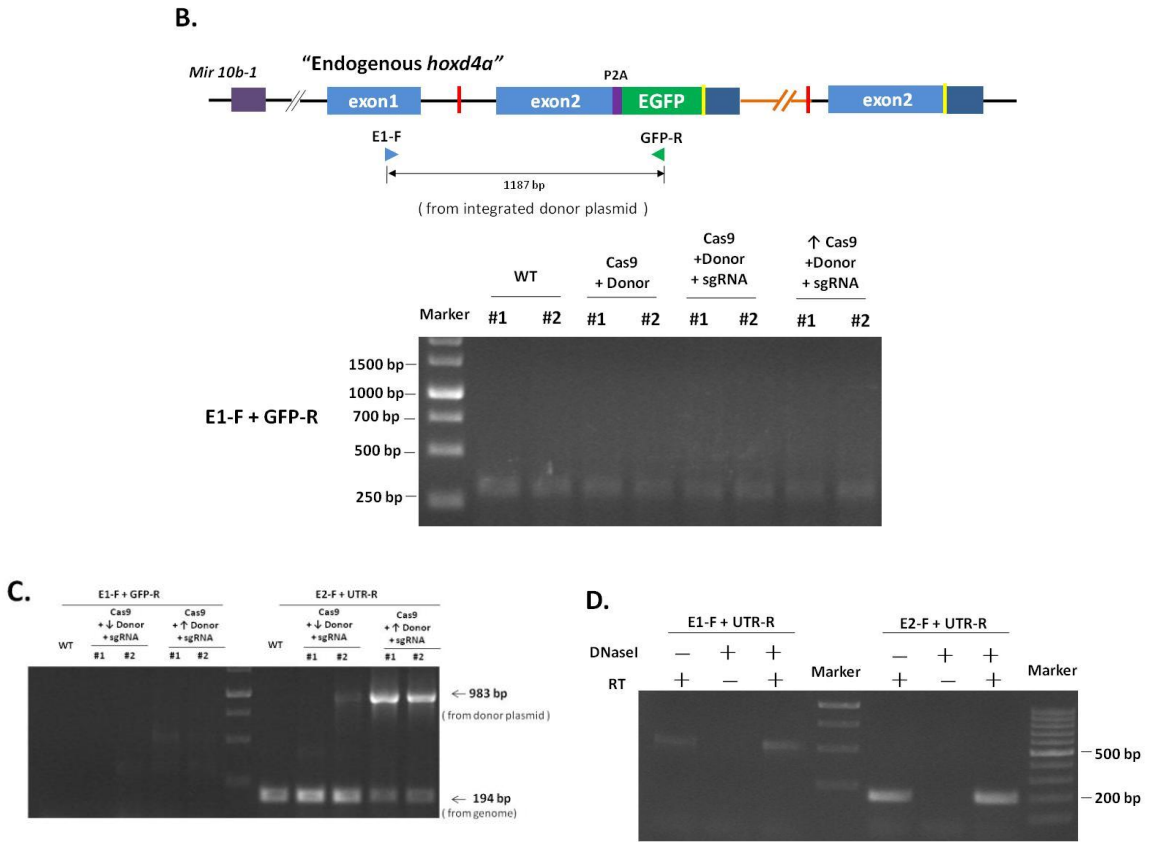

Figure 3.2.8: PCR analysis of the donor plasmid integration.

(A-B) Schematic representation of the locus specific primers used for the detection of integration. Donor plasmid failed to integrate in the zebrafish genome as evidenced by the absence of PCR band using the genome and insert-specific primers: E1-F and GFP-R (B). Each group (#1 and #2) represents 10 pooled embryos at 24 hpf.

(C) Optimization of the dose of donor plasmid. Neither increased (5 pg) nor decreased (50 pg) amounts leads to detectable integration.

(D). Reverse transcription PCR (RT-PCR) analysis of the transcripts in injected embryos at 24 hpf.

3.2.3. Identification of Hoxd4a interacting proteins using the BioID system

3.2.3.1. Application of the BioID system in zebrafish

To identify potential interacting partners of Hoxd4a, we adopted a newly developed technique, namely the proximity-dependent biotin identification (BioID) system. It is based

on a mutant of *E.coli* biotin protein ligase, BirA*, which is broadly promiscuous in biotinylating proximally located primary amines, typically of lysine, regardless of sequence (Kim et al., 2014; Roux et al., 2013). In this method, a protein of interest is fused to BirA* in the expectation that both remain functional. Biotinylated vicinal neighbors can be isolated through streptavidin-biotin affinity purification and identified by liquid chromatography-mass spectrometry (LC-MS) (Fig. 3.2.9).

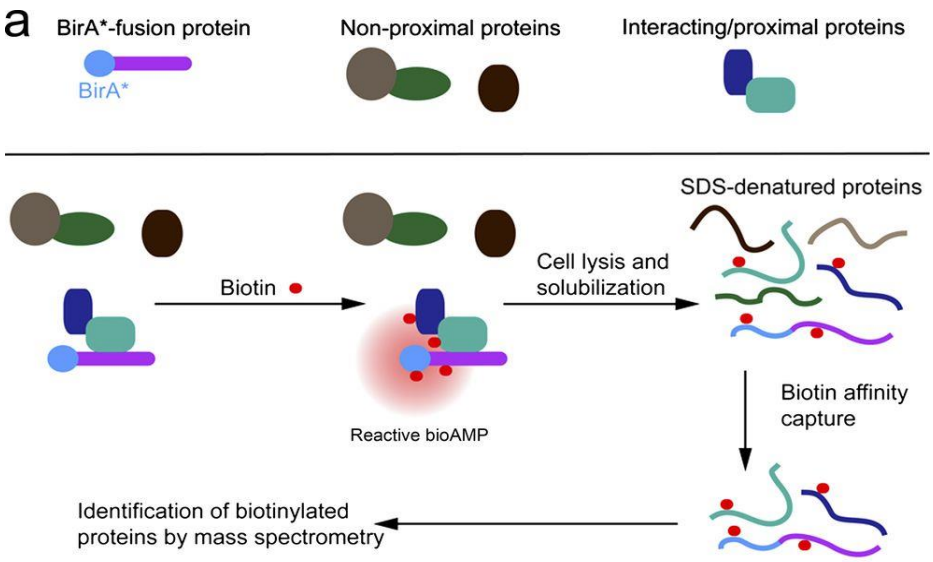

Figure 3.2.9: Schematic presentation of the BioID system. The protein of interest, in our case Hoxd4a, is indicated in purple and BirA* in blue. Biotinylated proximal proteins are most likely to interact with the BirA*-fusion protein. Picture adapted from (Roux et al., 2012).

As the affinity between biotin and streptavidin is one of the strongest non-covalent interactions, issues about protein solubility and maintenance of weak protein complexes are overcome. Harsh lysis buffer and stringent washes can be applied to efficiently solubilize the "prey" proteins and minimize false positives. To date, the BioID system has been successfully applied to identify interacting partners of insoluble proteins, like nuclear Lamin A (Roux et

al., 2012) and highly labile proteins, like MYC (Dingar et al., 2015). It has also been used to characterize the constituent proteins of different complexes, such as the trypanosome bilobe (Morriswood et al., 2013), the tight junction complex (Van Itallie et al., 2013) and human centrosomes (Comartin et al., 2013). In zebrafish, this method has been successfully implemented to study specific translational profiling in skeletal muscle cells (Housley et al., 2014).

First, we sought to determine if this system works for Hoxd4a in zebrafish. *In-vitro* transcribed mRNA encoding Hoxd4a-BirA*-Flag (HBF) was injected at the one-cell stage. Embryos were collected and lysed at different developmental stages and the fusion protein was immunodetected with an anti-Flag antibody. Hoxd4a-Flag was used as a positive control and was stably expressed from 4 hpf till 12 hpf. Strikingly, Hoxd4a-BirA*-Flag was only detected at 8 hpf at a very low level (Fig. 3.2.10, A). Supplementation with exogenous biotin did not obviously increase the level of protein biotinylation, including at least two endogenous biotinylated proteins with molecular weights of 75 kDa and 130 kDa (Fig. 3.2.10, C). As expected, injection of HBF mRNA failed to rescue the hematopoietic defects caused by loss of *hoxd4a* (Fig Fig. 3.2.10, B), which further confirmed that this system did not work for Hoxd4a in zebrafish.

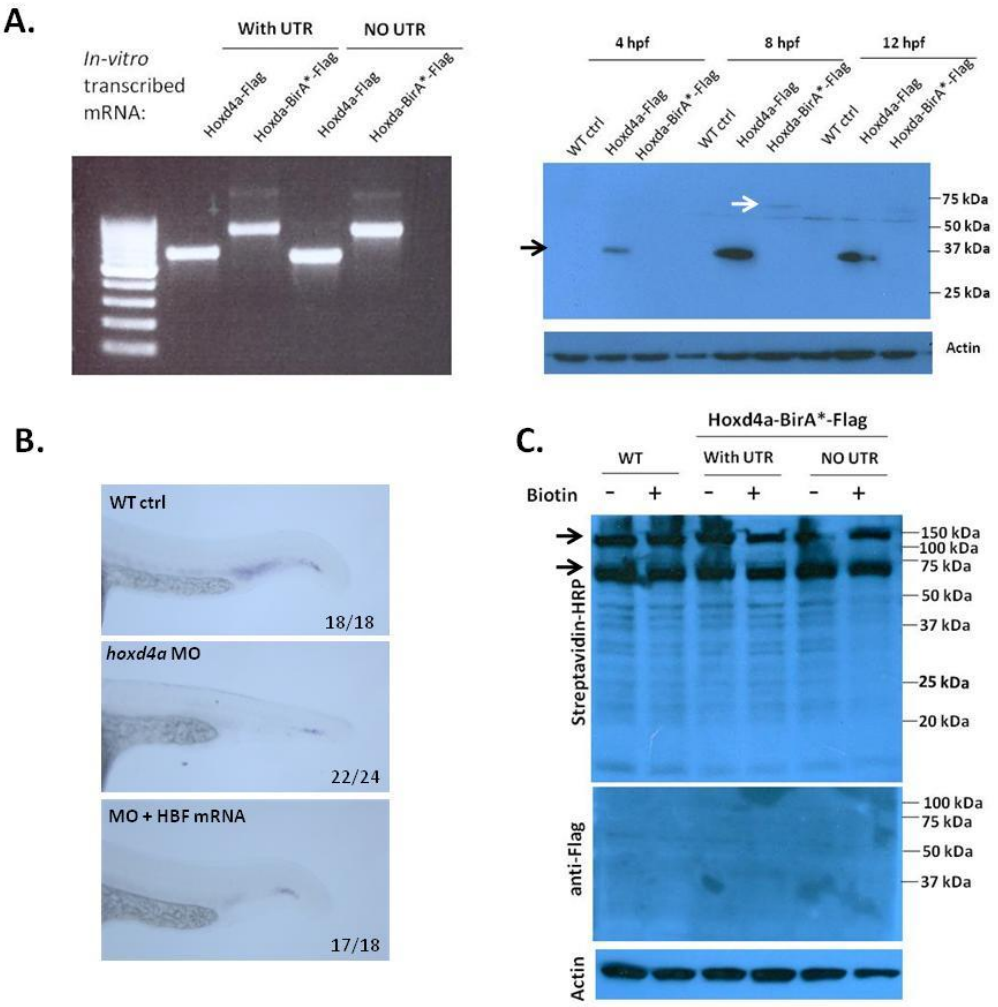

Figure 3.2.10: Application of the BioID system in zebrafish.

(A) Detection of the expression of Hoxd4a-Flag (black arrow) and Hoxd4a-BirA*-Flag (white arrow) in zebrafish with anti-Flag antibody. *In vitro* transcribed mRNAs were checked by 1.5% agarose gel electrophoresis.

(B) The down-regulation of *scl* expression in *hoxd4a* morphants was not rescued by Hoxd4a-BirA*-Flag mRNA injection. Caudal part of 22 hpf embryos is shown in lateral views.

(C) Analysis of the biotinylated proteins in zebrafish by streptavidin-HRP. Endogenous biotinylated proteins are marked by arrows. The level of protein biotinylation was not obviously enhanced by the addition of exogenous biotin.

3.2.3.2. Application of the BioID system in mammalian cells

Next, encouraged by the fact that Hoxd4 orthologs function similarly across large

evolutionary distances (McGinnis et al., 1990), we attempted to apply this system in mammalian cell lines. Human embryonic kidney 293T (HEK293T) cells were transiently transfected with plasmids encoding Hoxd4a-BirA*-Flag. Western blot analysis with anti-Flag antibody was performed to confirm its expression. Intriguingly, the protein was only expressed in the absence of the 5' UTR of *hoxd4a*, implying the presence of negative regulatory elements (Fig 3.2.11, A).

To investigate the ability of Hoxd4a-BirA*-Flag to biotinylate nearby proteins, transfected cells were cultured in the presence of 50 µM biotin. A western blot probed with streptavidin-HRP revealed that addition of exogenous biotin resulted in a massive stimulation of biotinylation in both BirA*-Flag controls and Hoxd4a-BirA*-Flag experimental samples (Fig 3.2.11, B). To determine the efficiency of biotinylation, biotinylated proteins were immunoprecipited by streptavidin agarose beads and subsequently analyzed by immunoblotting probed with an anti-Flag antibody. Hoxd4a-BirA*-Flag protein was not detected in the flow-through fraction, revealing a high efficiency of biotinylation. Next, to assess whether the Hoxd4a-BirA*-Flag fusion protein still retained its activity and function, we checked its ability to interact with known protein partners such as PBX. Co-immunoprecipitation (CO-IP) was performed in cells transfected with PBX and Hoxd4a-BirA*-Flag. Streptavidin beads were used for pull down and the western blot was probed with anti-PBX antibody. PBX protein was found in the elutes fraction (Fig 3.2.11, C), demonstrating Hoxd4a-BirA*-Flag was still able to interact appropriately with PBX. After this, efforts were made to establish stable cell lines using Hygromycin B in HEK293T cells and G418 in Hela cells in conjunction with the respective antibiotic resistance markers.

However, only stable expression of the BirA*-Flag control was successfully achieved in both cell lines (data not shown), suggesting that Hoxd4a-BirA*-Flag may be toxic.

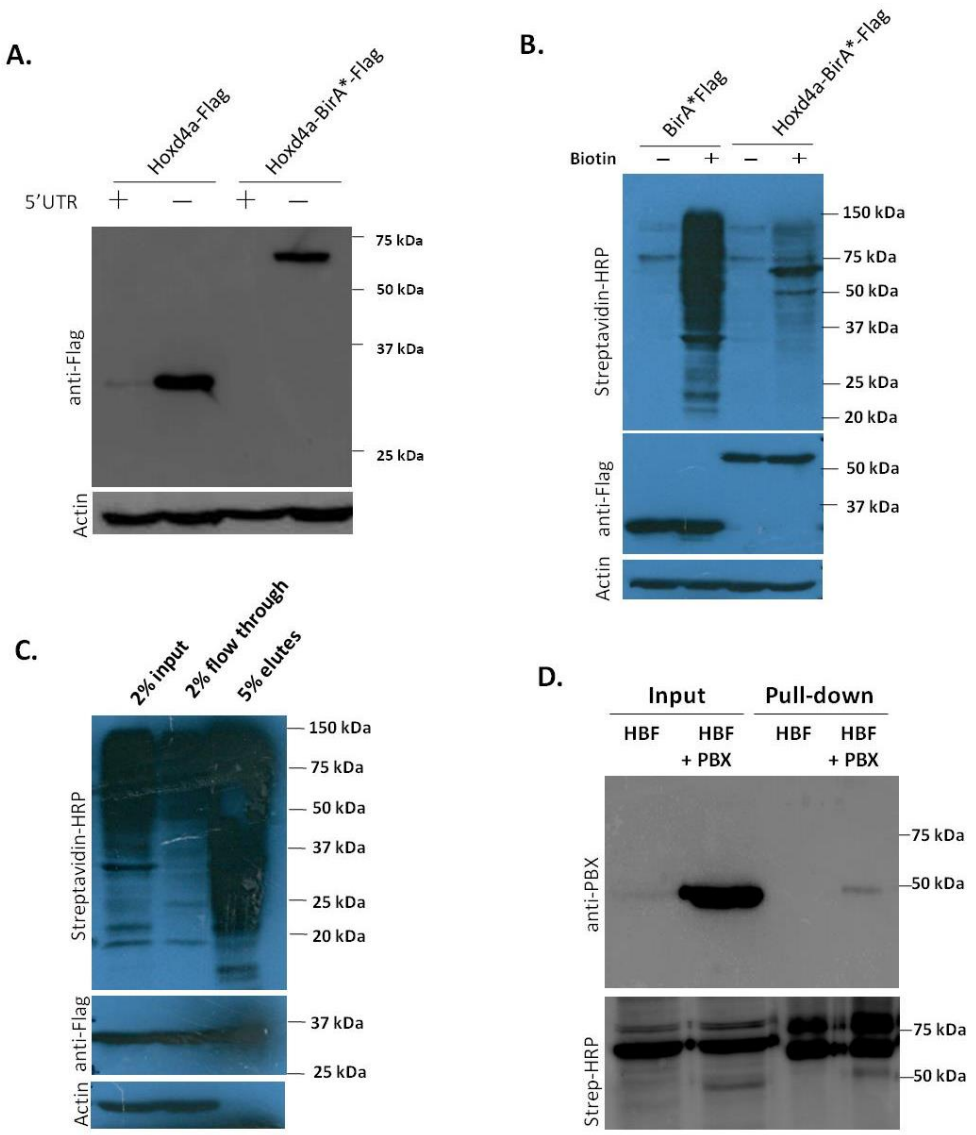

Figure 3.2.11: Application of the BioID system in HEK293T cells.

(A) Expression of Hoxd4a-Flag and Hoxd4a-BirA*-Flag in HEK293T cells.

(B) Analysis of the biotinylated proteins in HEK293T cells by streptavidin-HRP.

(C) Analysis of the efficiency of protein biotinylation. Biotinylated proteins were immunoprecipited by streptavidin agarose beads. The absence of Actin in the elutes indicated the specificity of the binding.

(D) Analysis of the interaction between Hoxd4a and PBX through the BioID system. Streptavidin pull down was performed followed by anti-PBX immunoblotting.

Given the inability to establish cell lines with stable expression of Hoxd4a-BirA*, whole cell protein extracts from transient expression were used for further analysis. Biotinylated proteins from transient overexpression of Hoxd4a-BirA*-Flag were purified by streptavidin agarose beads under stringent conditions and analyzed by LC-MS. Cells transfected with BirA*-Flag were used as controls. In order to reduce false positives, two biological replicates for both control and experimental sample (Hoxd4a-BirA*-Flag) were prepared.

As expected, the most abundant proteins identified in both control and experimental samples were some naturally biotinylated proteins like pyruvate carboxylase, methylcrotonoyl-CoA carboxylase, acetyl-CoA carboxylase and propionyl-CoA carboxylase. These and other proteins identified in control were regarded as background, and were eliminated from the two replicates. Forty-five proteins were finally found to be specifically present in both replicates (Fig. 3.2.12). Gene Ontology (GO) and STRING 10 analysis showed that most of the proteins are related to chromatin remodeling, which includes SWI/SNF remodeling complex (SMARCC2, SMARCE1, ARID1A, ARID3A, ARID4A/RBBP1) and nuclear receptor corepressor 1 (NCOR1) (Fig. 3.2.12). The high-confidence candidates also include regulators involved in mRNA processing, like cleavage stimulation factor 2 (CSTF2), RNA binding motif protein 25 (RBM25) and heterogeneous nuclear ribonucleoprotein C (HNRNPC). Among all of these proteins, XRCC6 (Ku 70) stands out by its known function in DNA repair and also its interactions with many homeodomain proteins (Schild-Poulter et al., 2001). In addition, MGA caught our attention due to its function in DV patterning in cooperation with Smad4 (Sun et al., 2014). Due to time constraints, this work was not further pursued, but could be addressed in future studies.

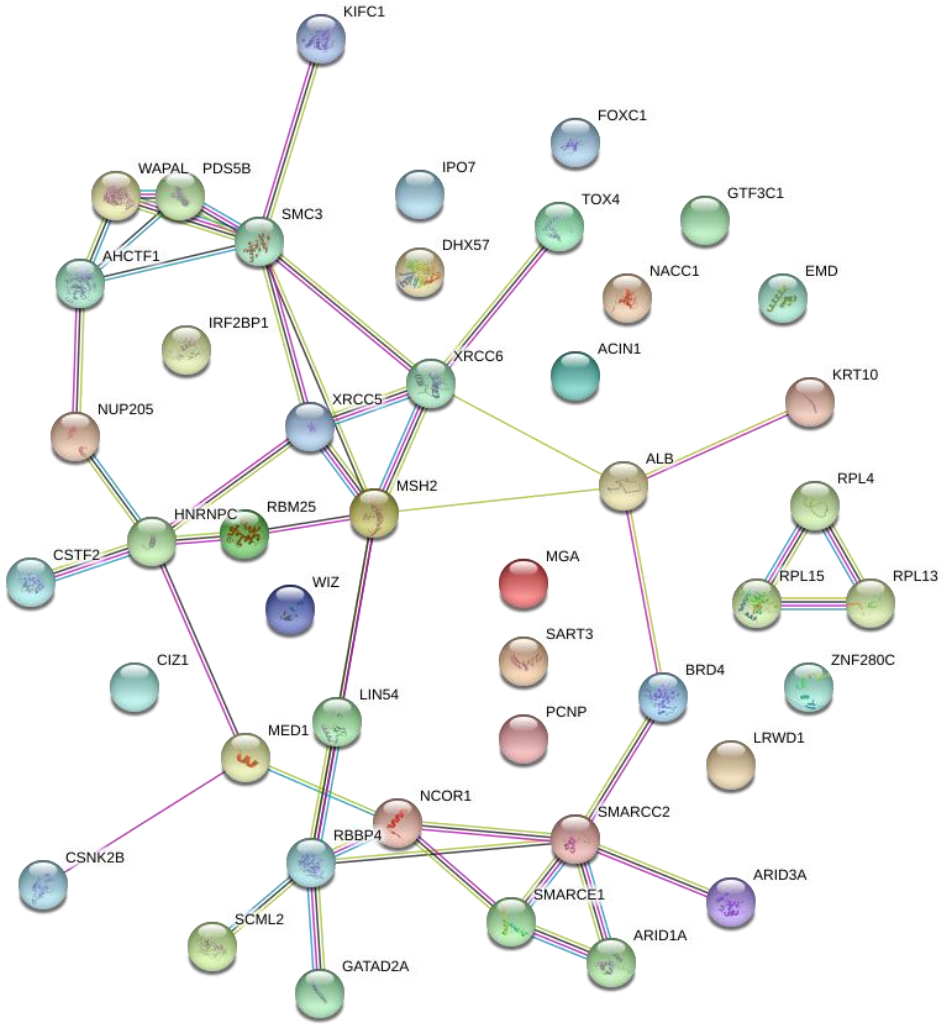

Figure 3.2.12: Protein interaction networks of Hoxd4a interactors identified by the BioID system.

Forty-five proteins were identified by LC-MS specifically present in two biological replicates of Hoxd4a-BirA*-Flag experimental samples, but not in BirA*-Flag control samples. Protein interactions were analyzed by the online software STRING. Network nodes represent different proteins and lines represent protein-protein associations. The color of the lines is based on different sources of information. Blue lines are from curated databases; Pink, experimentally determined; Green, gene neighborhood; Red, gene fusions; Dark blue, gene co-occurrence.

3.2.4. Investigation of interactions between *hoxd4a* and BMP signaling

3.2.3.1. Interactions between *hoxd4a* and BMP signaling

As noted above, we hypothesized that *hoxd4a* could interact with BMP signaling to specify the hemangioblast at an early developmental stage. To test this hypothesis, we adapted a well-established approach - synthetic genetic interaction - that has been used extensively to screen genes that synergistically contribute to a particular phenotype. This method relies on the fact that mutation (or loss-of-function) of two functionally related genes will cause more severe phenotypes than individual mutation under appropriate conditions.

In the context of our hypothesis, we need to establish conditions for comparing the phenotypes resulting from BMP inhibition and *hoxd4a* knockdown alone and in combination. Importantly, the extent of inhibition of each function (BMP signaling vs Hoxd4a function) should be titrated to a level just sufficient to avoid affecting primitive hematopoiesis. For *hoxd4a*, we have found that injection of 3 ng of anti-*hoxd4a* morpholino alone has no obvious effects on *scl* expression. For BMP signaling, LDN193189, a selective inhibitor of BMP type I receptor, was used to inhibit BMP signaling and it has been extensively used to study the requirement of BMP signaling in zebrafish vascular development (Cannon et al., 2010). Its effects on hematopoiesis and embryogenesis were titrated by exposing embryos to different concentrations of the compound from 4 hpf, just before the onset of gastrulation. As reported before, the dorsalization phenotype caused by BMP inhibitors could be divided into five classes (Cannon et al., 2010; Kondo, 2007). Severe dorsalization was observed when embryos were treated with 10 μM LDN193189 (Fig. 3.2.13). In contrast, embryos treated

with 1 μM LDN193189 appeared to develop normally without obvious dorsalization. More importantly, circulating blood cells were affected at this concentration (Fig. 3.2.13).

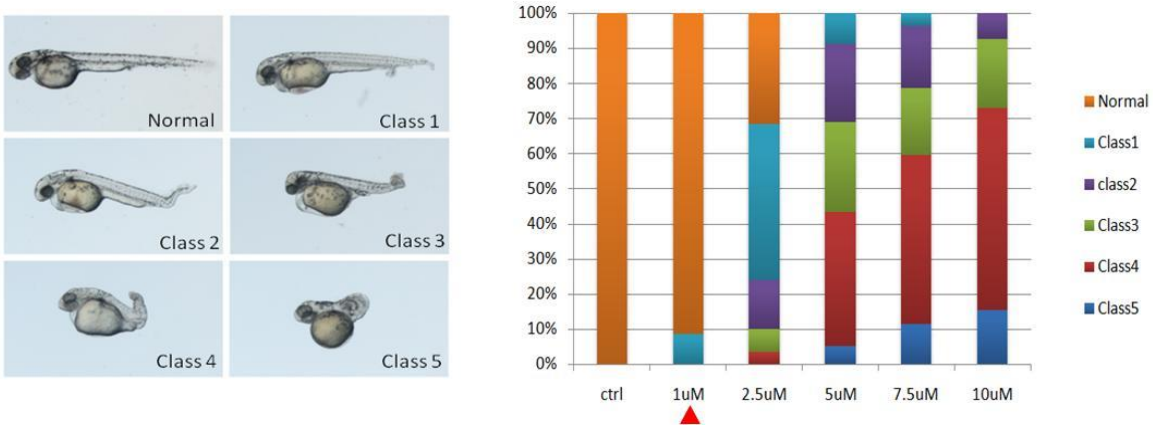

Figure 3.2.13: Summary of dorsalization caused by different concentrations of LDN193189 from 4 hpf. Data are shown as the mean of percentages from two independent experiments.

To investigate if synergy occurs between *hoxd4a* and BMP signaling, embryos injected with 3 ng of anti-*hoxd4a* morpholinos were treated with 1 μM LDN193189 from 4 hpf. The expression of *scl*, *fli1* and *gata1* was assessed at 13 hpf. Surprisingly, the expression of these three markers was quite different (Fig. 3.2.14). For *scl* and *fli1*, signals in embryos either injected with *hoxd4a* morpholino alone or treated with BMP inhibitor alone were comparable to wild type controls. By contrast, marker gene expression was obviously down-regulated when *hoxd4a* and BMP were inhibited together at these same sub-teratogenic doses, suggesting that *hoxd4a* and BMP could function together to regulate the expression of *scl* and *fli1*. By contrast, 3 ng of anti-*hoxd4a* morpholino alone resulted in reduced expression of *gata1* in PLM, suggesting that it is more responsive to the level of *hoxd4a*. Quantitative PCR analysis showed that the reduction of *scl* expression was significant (Fig. 3.2.14).

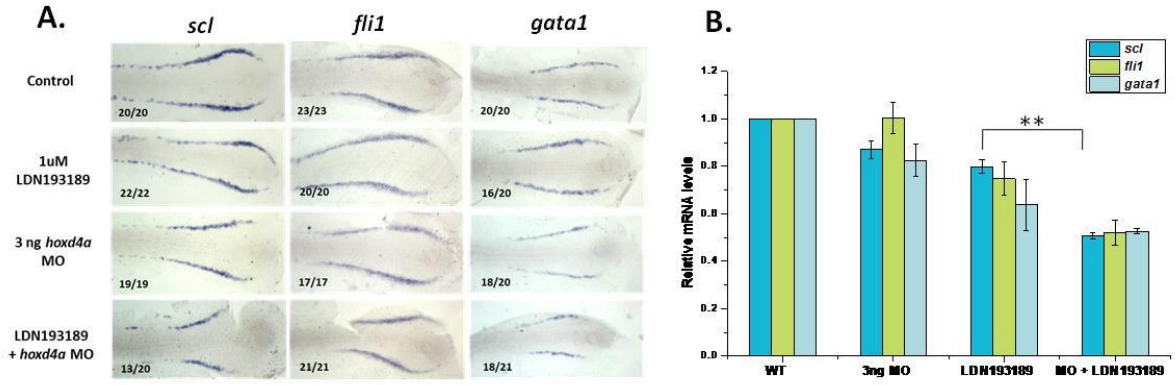

Figure 3.2.14: Expression of *scl, fli1* and *gata1* at 13 hpf under different conditions of *hoxd4a* knockdown and BMP signaling inhibition.

(A) *in situ* hybridization of *scl*, *fli1* and *gata1* in PLM at 13 hpf. Images are shown in dorsal views of flat-mounted embryos, anterior to the left.

(B) qPCR analysis of *scl*, *fli1* and *gata1* expression in 13 hpf embryos. Data are shown as mean of fold change $\pm$ standard error (s.e.m) from three independent experiments (n=3). Samples were normalized to *β-actin*. Error bars indicate standard error. ** denotes p≤value 0.001.

Furthermore, o-dianisidine staining and alkaline phosphatase staining were performed to investigate the effects on hematopoiesis and vasculo/angiogenesis. Consistent with gene expression results, the development of blood cells was obviously disrupted when *hoxd4a* and BMP were slightly reduced concurrently. By contrast, the process of angiogenesis was not much affected as revealed by the formation of intersegmental vessels (ISV), suggesting that these processes could be regulated by different mechanisms.

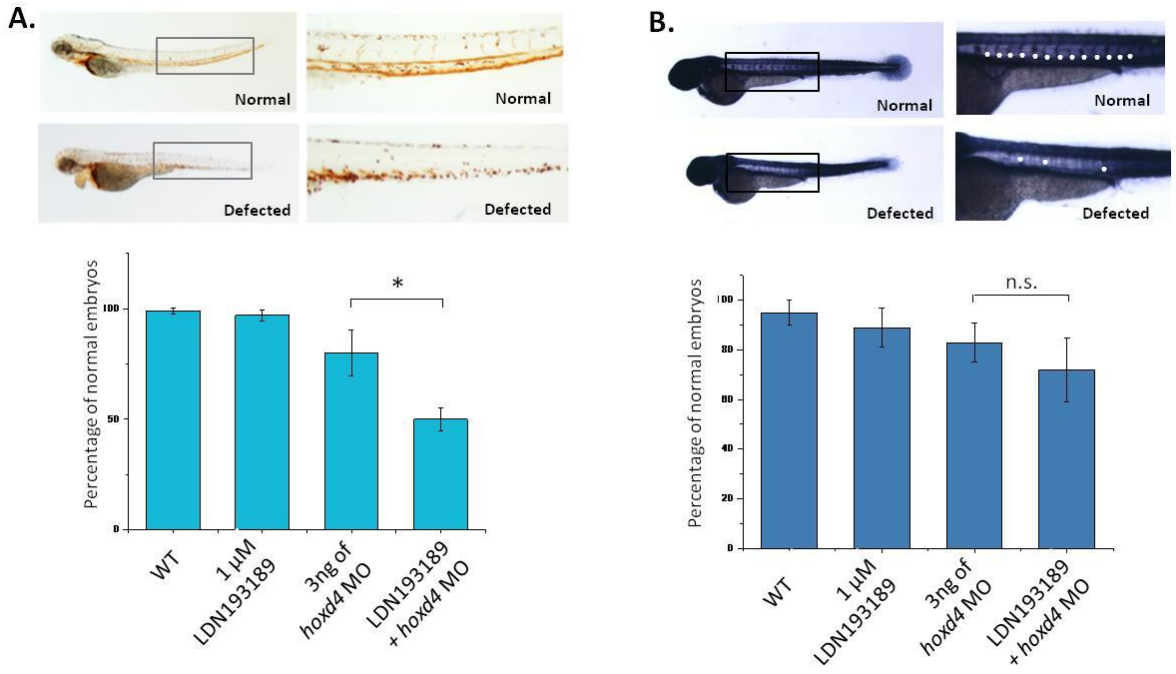

Figure 3.2.15: Analysis of zebrafish hematopoiesis and vasculo/angiogenesis under different conditions of *hoxd4a* knockdown and BMP signaling inhibition. The tail region indicated in the black box is shown on the right in higher magnification. Embryos that developed normally with comparable numbers of red blood cells as wild type (A) or normal vasculature (B) were scored as "normal embryos", while embryos with less red blood cells (A) or intersegmental vessels (B, white dots) are scored as "defected embryos". Data are shown as mean of percentages $\pm$ standard error (s.e.m) from three independent experiments (n=3). * denotes p≤value 0.05.

Most embryos developed normally with comparable numbers of blood cells as wild type controls.

3.2.3.2. Interactions between Hoxd4a and Smad proteins

The presumptive synthetic interaction between *hoxd4a* and BMP signaling pathway could be mediated through the interaction of Hoxd4a and Smad proteins. To test this hypothesis, we first used a specific portion of the amino-terminus of human SMAD4, a part of the MH1 domain (named MH1-c), which has been shown to disrupt the interaction between HOXA9

and SMAD4 in a dominant-negative fashion, without affecting other functions of SMAD4 (Quere et al., 2011). Our reasoning was that SMAD4 might interact with multiple Hox proteins in a similar fashion across species. Therefore, MH1-c would interfere with any Smad4-Hox interactions just as has been shown for SMAD4-HOXA9. To investigate whether the expression of MH1-c has effects on hematopoiesis and vasculogenesis, different amounts of MH1-c mRNA were injected and phenotypes were assessed by o-dianisidine staining and alkaline phosphatase staining at 72 hpf (Fig. 3.2.16, A). Injection of 300 pg of MH1-c mRNA markedly reduced the number of circulating blood cells. Vascular development was also disrupted as no intersegmental vessels or subintestinal vessels were visible. Consistently, the expression of *scl* at 12 hpf was significantly down-regulated when 150 pg mRNA was injected (Fig. 3.2.16).

Next, the same synthetic genetic interaction approach was applied to study the potential interaction between Hoxd4a and Smad proteins. We assumed that if the above impairments of hematopoiesis and vasculogenesis could be due to a disruption of Hoxd4a-Smad interaction, and that simultaneous disruption of *hoxd4a* and *smad* function at a threshold level would result in much more severe phenotypes. As shown above, 150 pg of MH1-c mRNA still caused reduction of *scl* expression, thereby 100 pg of MH1-c mRNA were used as a threshold amount in combination with 3 ng of anti-*hoxd4a* morpholino. The expression of *scl*, *fli1* and *gata1* were checked by *in-situ* hybridization at 13 hpf. To our surprise, none of these three marker gene expression was changed following the injection (3.3.16, B), which could be explained by a dispensable role of MH1 domain in the hypothesized Hoxd4a-Smad interactions in zebrafish.

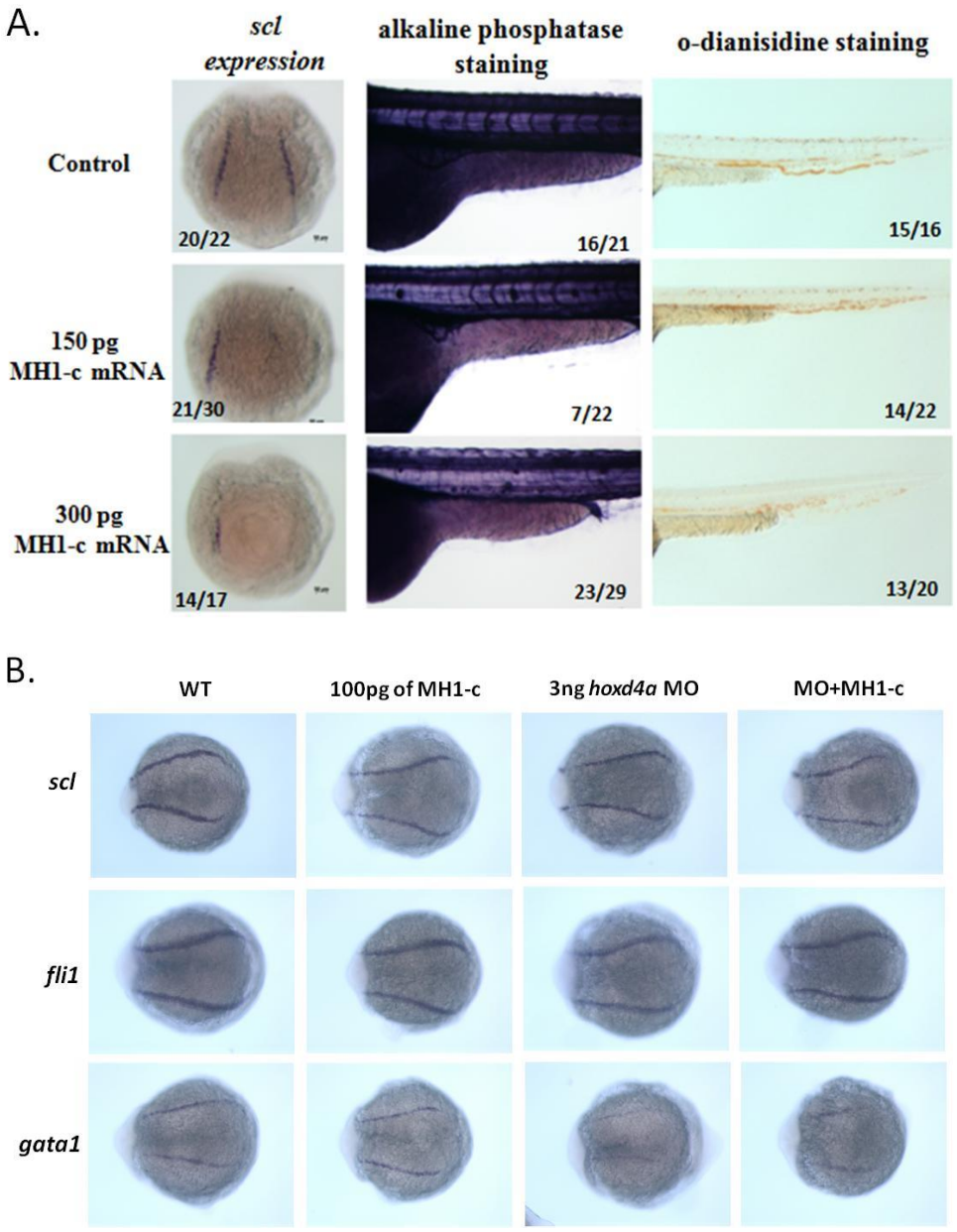

Figure 3.2.16: Analysis of the effect of MH1-c on zebrafish hematopoiesis and vasculogenesis.

(A) Titration of the effect of MH1-c on hematopoiesis, vasculo/angiogenesis. The expression of *scl* in PLM was checked at 12 hpf. For staining, caudal part of 72 hpf embryos were shown in lateral views.

(B) Expression of *scl*, *fli1* and *gata1* expression in the PLM at 13 hpf under different conditions of *hoxd4a* knockdown and MH1-c expression.

To investigate whether Hoxd4a physically interacts with Smad proteins, CO-IP was performed by overexpression of Flag-tagged Hoxd4a and HA-tagged Smad proteins in

HEK293T cells. Strikingly, none of the Smads was found to interact with Hoxd4a (Fig. 3.2.17).

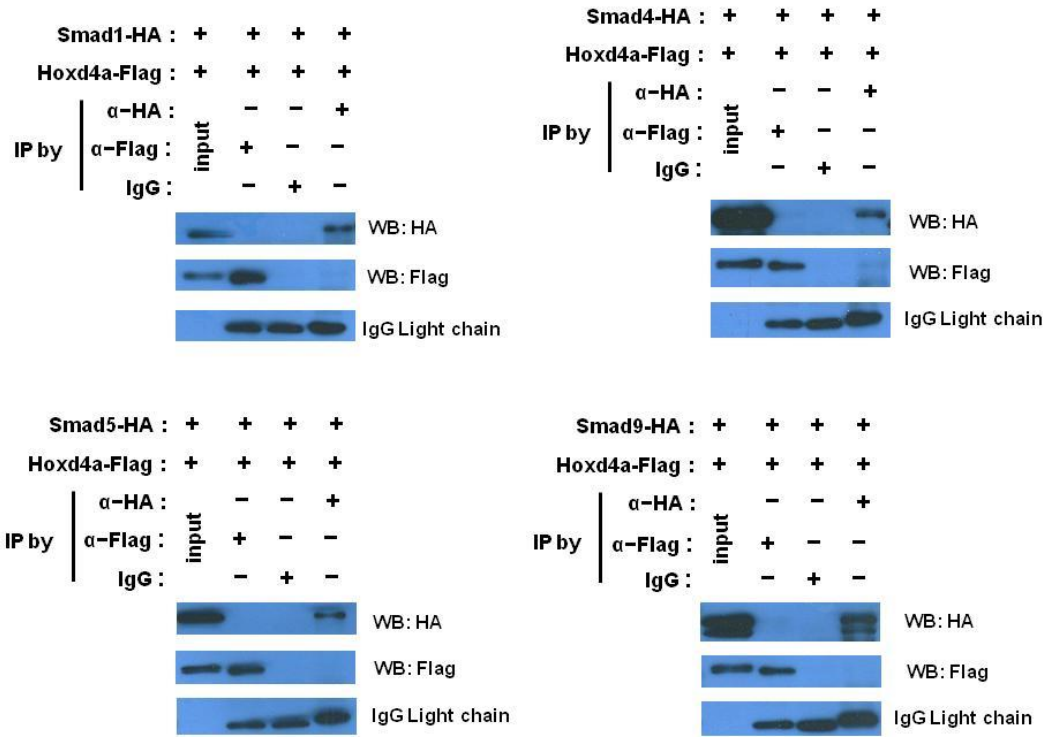

Figure 3.2.17: Co-immunoprecipitation of Hoxd4a-Flag and Smads-HA in HEK293T cells.

Cells were transfected with Flag-tagged Hoxd4a and individual HA-tagged Smad proteins. CO-IP was performed with either anti-Flag antibody or anti-HA antibody and immunoblotting was probed with the other. IgG was used for immunoprecipitation as negative controls.

Taking all above results together, *hoxd4a* was found to synergize with BMP signaling to regulate the hemangioblast formation with slightly different effects on the later erythropoiesis and vasculo/angiogenesis. However, this interaction may not be mediated by physical interactions between Hoxd4a and Smad proteins.

3.2.3. Investigation of interactions between *hoxd4a* and *meis1.1*

Even though previous studies have shown that *meis1.1* is also involved in zebrafish

hematopoiesis (Amali et al., 2013; Cvejic et al., 2011b), whether Hox and Meis act independently or interact with each other to regulate hematopoietic development is still unknown. To answer this question, we used a construct whose engineered product predominantly excludes Meis proteins from the nucleus (Choe et al., 2002). This construct, PCAB, encodes the PBC-A and PBC-B domains of zebrafish Pbx4 protein that are required for the translocation of Meis into the nucleus. By competing with the endogenous Pbx for Meis binding, PCAB acts in a dominant-negative fashion.

First, the effective level of PCAB was titrated by analyzing *scl* expression at 13 hpf. We found that injection of PCAB mRNA decreased the expression of *scl* in a dose-dependent manner (Figure 3.2.18), consistent with the role of *meis* genes in regulating the primitive hematopoiesis (Cvejic et al., 2011b). The threshold amount of PCAB was set at 150 pg as no obvious changes was caused. In addition to the hematopoietic defects, embryos injected with high concentrations of PCAB mRNA seemed to be defective in convergent extension movement, as the expression profile of *scl* in PLM became much shorter and wider when compared with WT controls (Figure 3.2.18), suggesting that *meis* genes could have a role in gastrulation movements.

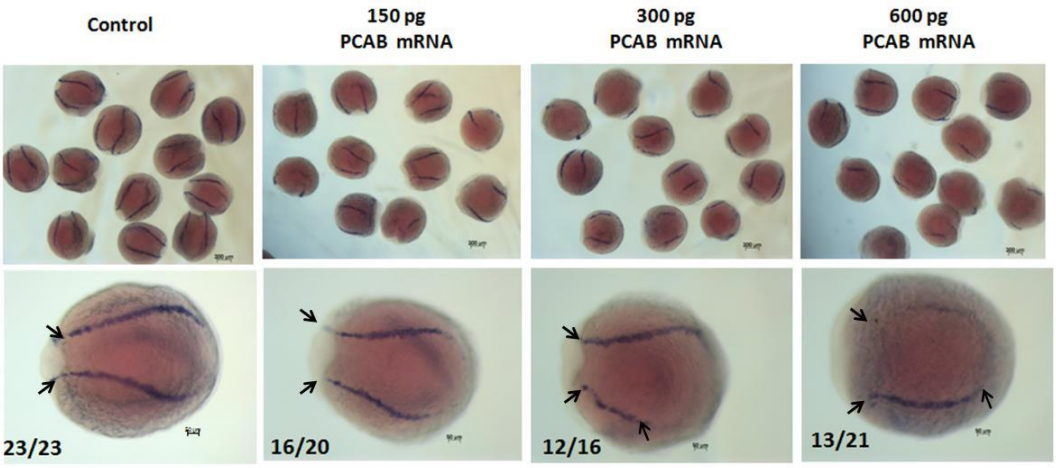

Figure 3.2.18: Titration of the PCAB on *scl* expression at 13 hpf.

Upper panel shows the expression of *scl* in a population of embryos injected with different amounts of PCAB mRNA. Representative embryos from each group are shown in the lower panel in higher magnification. Black arrows indicate the expression of *scl* in the PLM.

Next, the assumed interactions between Hoxd4a and Meis were tested using the synthetic interaction approach described above. As shown in Fig. 3.3.19, the expression of *scl* remained at the same level as controls when either of 3 ng of anti-*hoxd4a* morpholino or 150 pg of PCAB mRNA was injected. But co-injection of the same amounts of anti-*hoxd4a* morpholino and PCAB mRNA resulted in significant reduction of *scl* expression, suggesting that *hoxd4a* and *meis* gene products synergize to regulate hemangioblast formation.

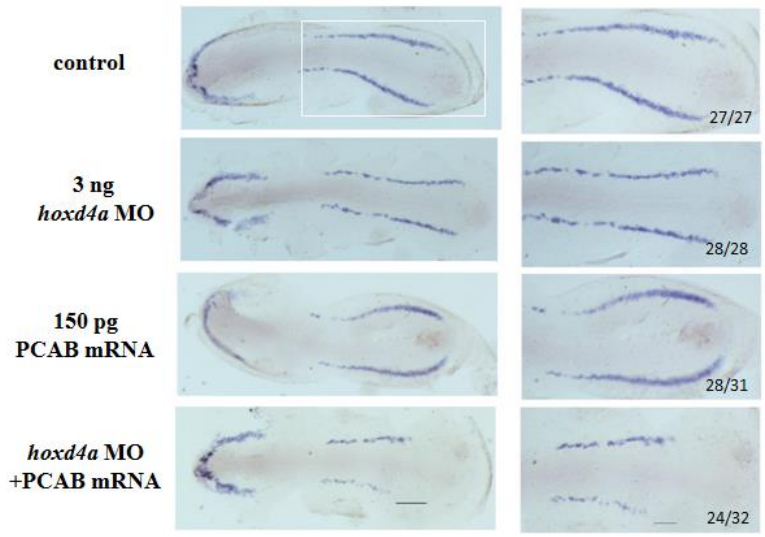

Figure 3.2.19: The expression of *scl* under different conditions of *hoxd4a* knockdown and PCAB expression. Flat-mounted 13 hpf embryos are shown in dorsal views. Higher magnification of the white box area (the PLM) is shown in the right panel.

3.3. Investigation of the specificity of *hoxd4a* morphant phenotypes

While the role of *hoxd4a* in zebrafish hematopoiesis and vasculogenesis has been extensively investigated, our previous findings regarding *hoxd4a* functions are solely based on one morpholino against *hoxd4a*. The specificity of this morpholino induced hematopoietic phenotypes still needs to be addressed despite the fact that it has been validated by the rescue experiment. To this end, we further investigate the specificity of *hoxd4a* knockdown effects by using a second independent morpholino and the corresponding five-nucleotide mismatch morpholinos. Meanwhile, null mutants were generated by CRISPR/Cas9 to characterize the function of *hoxd4a* in zebrafish hematopoiesis.

3.3.1. Mismatch morpholinos

One of the great advantages of morpholinos is the ability to carry out dose-dependent studies

by titration, something which is not feasible using most genetic approaches. To further assess the specificity of the function of *hoxd4a* in zebrafish hematopoiesis, splicing acceptor morpholino (previously referred as anti-*hoxd4a* morpholino, hereafter designated as *hoxd4a*-MO^{SA}) and the corresponding five-nucleotide mismatch morpholino (*hoxd4a*-Mis-MO^{SA}) were injected at different doses. O-dianisidine staining was then performed at 72 hpf to assess the effect on hematopoiesis. As shown in Figure 3.3.1, a dose-dependent reduction of blood cells was observed in embryos injected with increasing amount of *hoxd4a*-MO^{SA}. When embryos were injected with 4 ng of *hoxd4 hoxd4a*-MO^{SA}, blood cells were absent in more than 50% of injected embryos. Some exhibited other mild defects as well, such as short and curly body axis and reduced yolk extension. When 6 ng was injected, most embryos completely lost circulating blood. In contrast, injection of either 3 ng or 4 ng of *hoxd4a*-Mis-MO^{SA} did not cause any morphological abnormalities. Most embryos developed normally with comparable numbers of blood cells as wild type controls. Six nanograms of *hoxd4a*-Mis-MO^{SA} generated a similar phenotype as 4 ng of *hoxd4a*-MO^{SA}, which is expected based on previous publications (Eisen and Smith, 2008).

To investigate the effectiveness of *hoxd4a*-MO^{SA}, RT-PCR was performed at 24 hpf to assess aberrant splicing (Fig. 3.3.1, B). As *hoxd4a* has only two coding exons, a pair of PCR primers designed in exon 1 and exon 2 will be able to distinguish altered splicing transcripts from normal transcripts based on the size of amplified PCR products. Compared with wild type control and *hoxd4a*-Mis-MO^{SA} injected embryos, injection of *hoxd4a*-MO^{SA} resulted in a great reduction of spliced mature mRNA concomitant with an increment of aberrant PCR products which corresponded to unspliced transcripts. It indicates that *hoxd4a*-MO^{SA}

morpholino injection results in intron retention, which could further lead to a truncated and nonfunctional Hoxd4 protein due to premature stop codons.

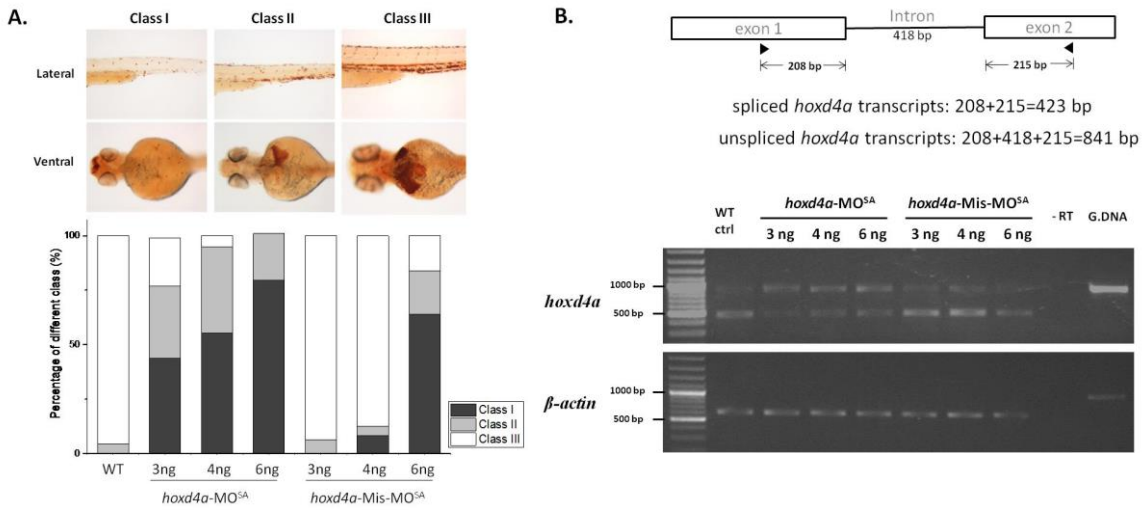

Figure 3.3.1: Effects of *hoxd4a*-MO^{SA} on hematopoiesis and RNA splicing.

(A) Dose response of *hoxd4a*-MO^{SA} in hematopoiesis. O-dianisidine staining was performed at 72 hpf. Lateral views of the tail region (upper panel) and ventral views of the yolk region (lower panel) are shown. The reduction of blood cells can be subdivided into two classes (mild: Class II, severe: Class I) in comparison to wild type level (Class III).

(B) *hoxd4a*-MO^{SA} caused altered splicing in 24 hpf embryos. β-actin is used as controls for PCR amplification. -RT indicates a negative control for reverse transcription reaction without the addition of reverse transcriptase.

Another common used method to address the specificity of MO-induced phenotype is to observe the noted phenotype with a second non-overlapping MO. So the same experiments was carried out with another independent MO targeting the splicing donor site of *hoxd4a* (*hoxd4a*-MO^{SD}) and the corresponding five-nucleotide mismatch morpholino (*hoxd4a*-Mis-MO^{SD}). Consistently, *hoxd4a*-MO^{SD} was also able to inhibit hematopoiesis in a dose-dependent manner with an optimal dose comparable to *hoxd4a*-MO^{SA}. In contrast,

hoxd4a-Mis-MO^{SD} did not cause detectable effects on hematopoiesis at a dose up to 6 ng. In support of this, RT-PCR analysis showed that *hoxd4a*-MO^{SD} injection produced splicing variants as well (Fig. 3.3.2).

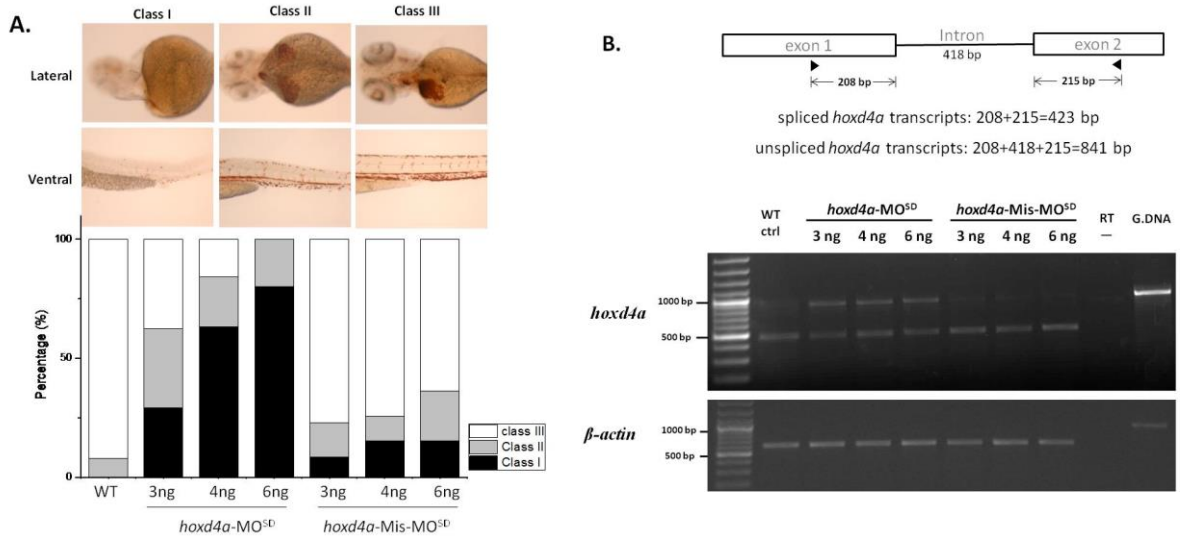

Figure 3.3.2: Effects of *hoxd4a*-MO^{SD} on hematopoiesis and RNA splicing.

(A) Dose response of *hoxd4a*-MO^{SD} in hematopoiesis. O-dianisidine staining was performed in 72 hpf embryos. Lateral views of the tail region and ventral views of the yolk region are shown.

(B) *hoxd4a*-MO^{SD} caused altered splicing in 24 hpf embryos. β-actin is used as controls for PCR amplification.

However, very unexpectedly, many embryos injected with *hoxd4a*-MO^{SD} showed severe body curvature (Fig. 3.3.3, A) and abnormal eye development (Fig. 3.3.3, B), which, in contrast, were not observed in *hoxd4a*-MO^{SA} morphants. To explore the reason behind this discrepancy, we tried to rescue *hoxd4a*-MO^{SD} morphants by co-injecting *hoxd4a* mRNA. Consistent with our previous results, the hematopoietic defects caused by splicing acceptor morpholinos (*hoxd4a*-MO^{SA}) were successfully rescued by *hoxd4a* mRNA. By contrast, for *hoxd4a*-MO^{SD} morphants, the hematopoietic defects and body curvature were partially

restored with injection of *hoxd4a* mRNA, whereas the eye defects was not obviously rescued, which suggests it could be due to some off targeting effects of *hoxd4a*-MO^{SD}.

Meanwhile, we attempted to co-inject these two experimental MOs at a lower dose (2.5 ng of *hoxd4a*-MO^{SA} and 2 ng of *hoxd4a*-MO^{SD}) such that the defect is only slightly apparent with each MO alone. Co-injection of two MOs resulted in much more severe defects than the two individual effects were added together, as shown by an increased number of defected embryos with less circulating blood cells (Fig. 3.3.3, D).

In summary, all above results provide strong evidence for the specificity of the hematopoietic phenotype induced by different MOs against *hoxd4a*.

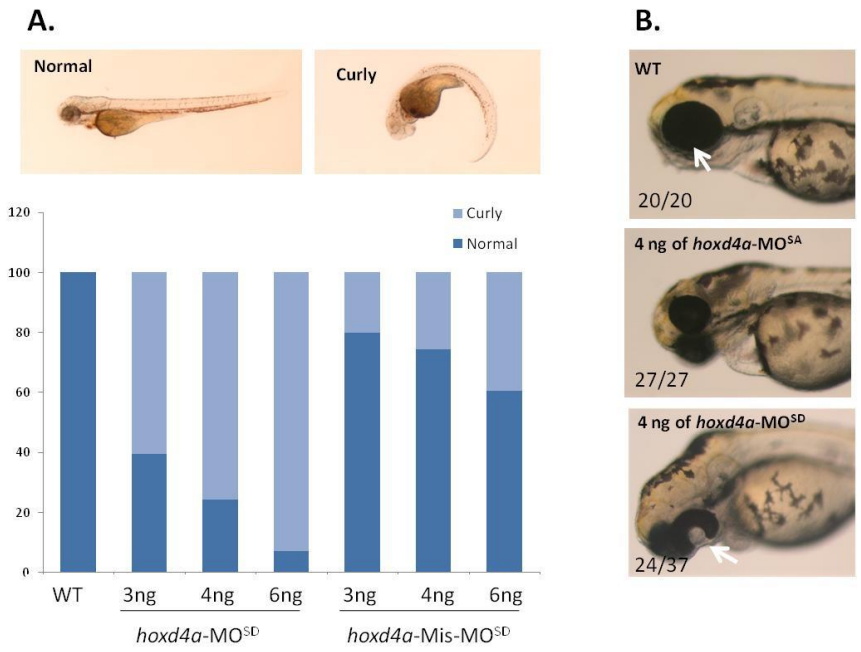

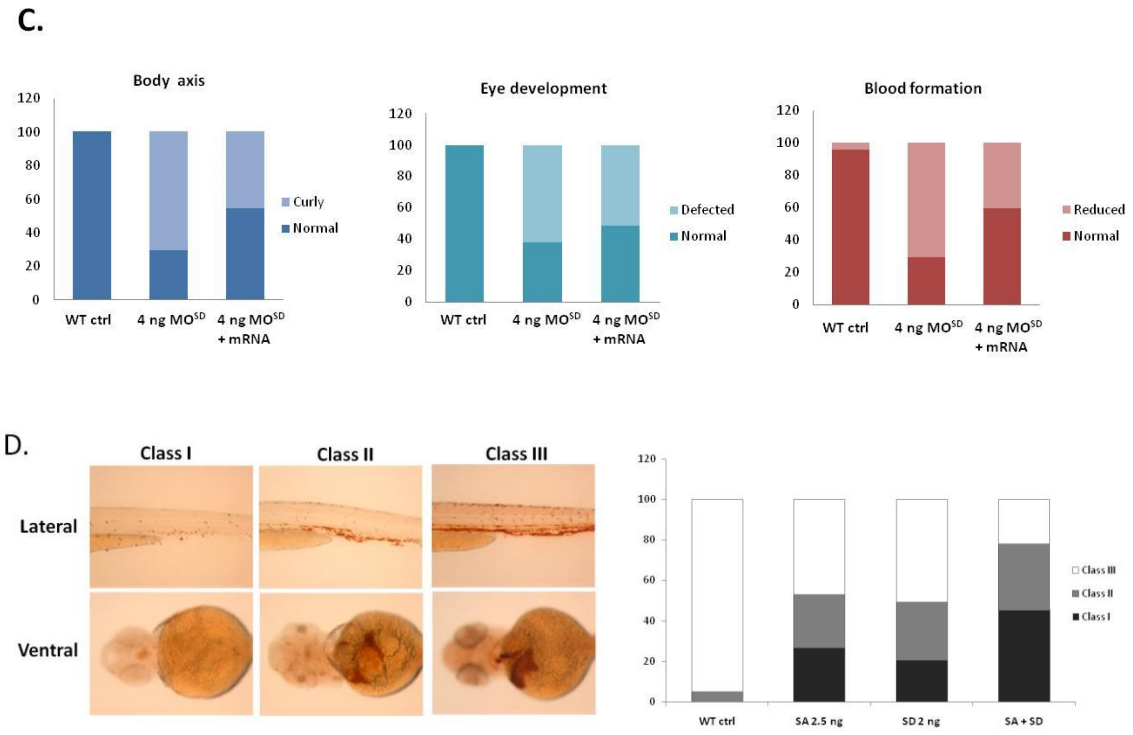

Figure 3.3.3: Phenotypic analysis of *hoxd4a*-MO^{SD} morphants.

(A) *hoxd4a*-MO^{SD} injection caused abnormal body curvature in a dose-dependent fashion.

(B) Images of *hoxd4a*-MO^{SD} injection caused eye defect called coloboma.

(C) Rescue of different phenotypes in *hoxd4a*-MO^{SD} morphants by mRNA injection.

(D) Co-injection of *hoxd4a*-MO^{SA} and *hoxd4a*-MO^{SD}. O-dianisidine staining was performed at 72 hpf. Lateral views of the tail region (upper panel) and ventral views of the yolk region (lower panel) are shown.

3.3.2. CRISPR/Cas9 mutants

As mentioned above, using different splicing morpholinos, our lab found that knocking down of *hoxd4a* results in severe defects in blood and endothelial development (Amali et al., 2013). To further confirm the specificity of these phenotypes, CRISPR/Cas9 was used to generate a knockout mutant of *hoxd4a*.

A CRISPR target in *hoxd4a* was designed using the ZiFiT Targeter program (Morriswood et al., 2013), which provides efficient identification of CRISPR/Cas9 target sites with

predictions about the potential off-targets through direct query of the NCBI BLAST server. Zebrafish *hoxd4a* has only two coding exons with the second exon encoding the homeodomain. The target site was selected in the first exon (Fig. 3.3.4), which is most likely to generate a null mutation by non-homologous end joining (NHEJ) repair. To increase the possibility of null mutations, we used a stop codon cassette which is a single stranded DNA oligonucleotide containing stop codons in all frames (Fig. 3.3.4). Homologous recombination-mediated insertion of the donor cassette would produce a premature stop codon regardless of the INDEL mutations introduced by NHEJ (Gagnon et al., 2014). Instead of Cas9-encoding mRNA, Cas9 protein was used for injection as its immediate action upon injection is expected to be more effective compared to Cas9 mRNA (Gagnon et al., 2014).

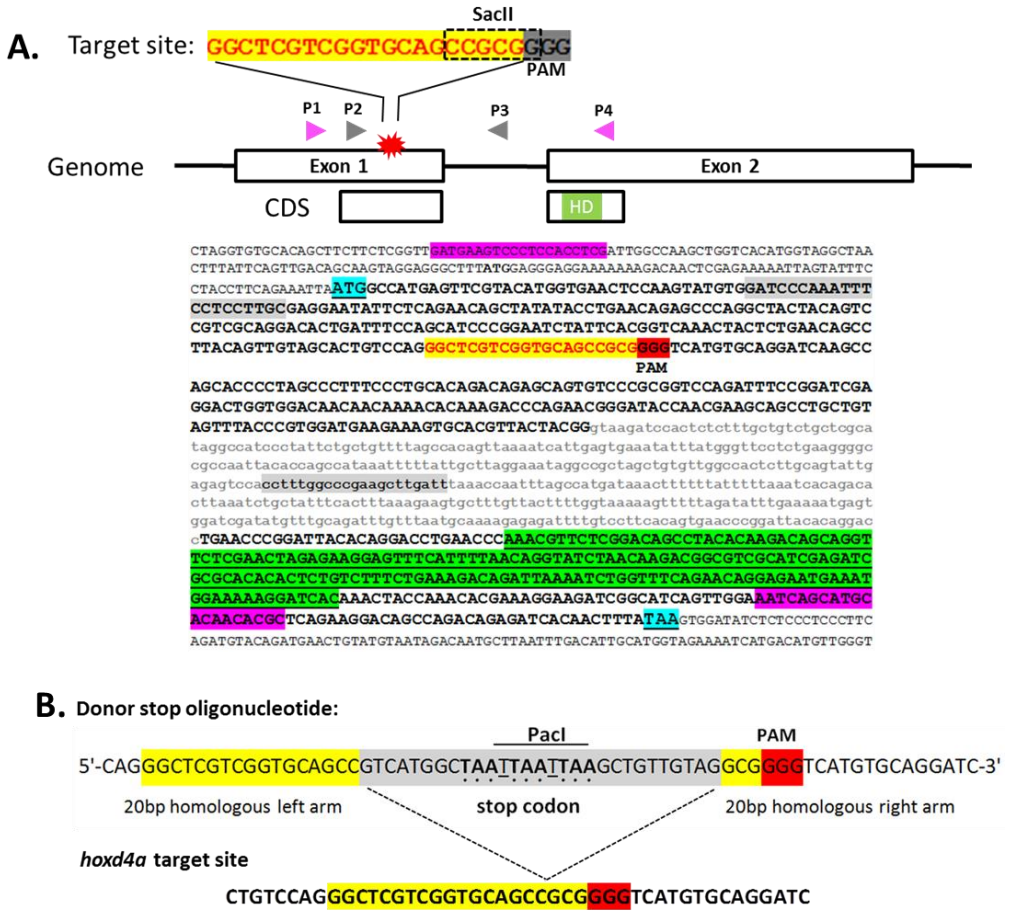

Figure 3.3.4: Schematic representation of *hoxd4a* target site design and the stop codon cassette oligonucleotides.

(A) Design of *hoxd4a* target site. Targeted sequences are shown in red highlighted in yellow and PAM in grey. The homeobox sequences are highlighted in green. Primers used for nested PCR are indicated as triangles.

(B) Design of the stop codon oligonucleotide. The stop codon cassette is highlighted in grey.

Cas9 protein, sgRNA and donor oligonucleotides were co-injected at the one-cell stage. Genomic DNA was extracted at 24 hpf from pooled embryos. PCR products spanning the target site were amplified by nested PCR and analyzed by the T7 endonuclease I (T7EI) assay to evaluate the genome-editing activity. It was shown that the target site was efficiently mutated, especially in the presence of the donor oligonucleotides (Fig. 3.3.5, A). Sequencing of the PCR products confirmed the presence of mutations at the target site of *hoxd4a* by showing highly reduced intensity of multicolored signals after the target locus in sequencing chromatograms (Fig. 3.3.5, B).

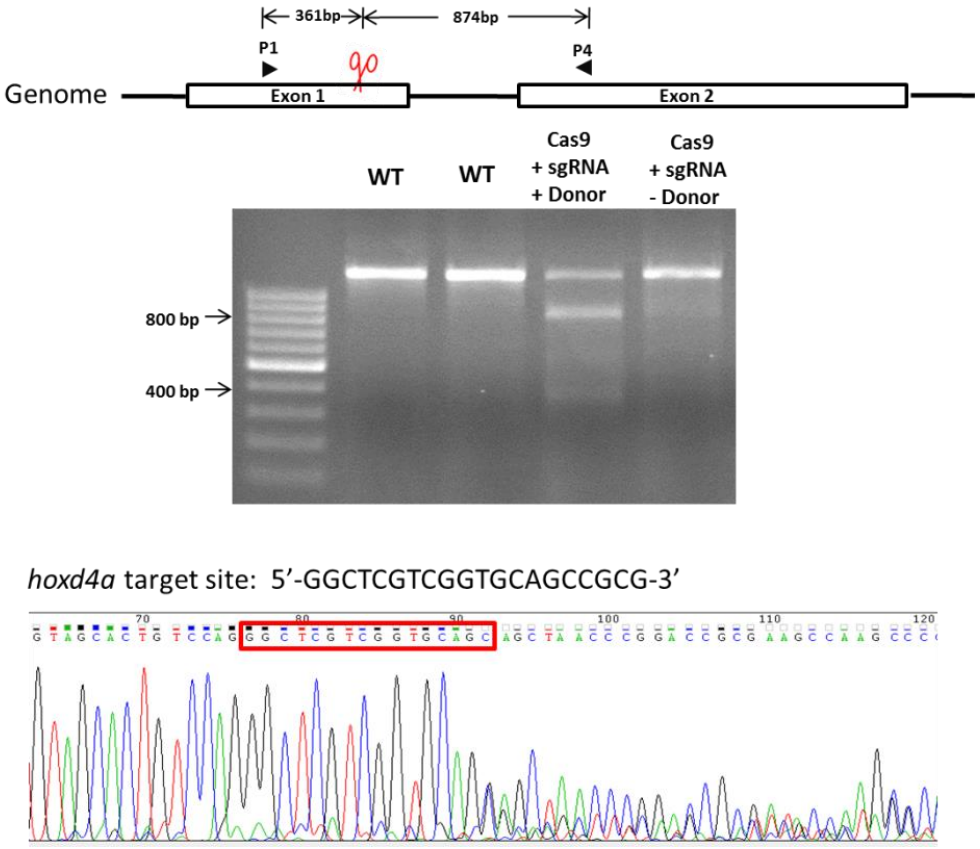

Figure 3.3.5: Mutation analysis of F_0 founder fish by the T7EI assay and sequencing.

PCR products amplified from a pool of 5-10 embryos were analyzed by the T7EI assay. In the sequencing chromatogram, the target site is indicated in red box.

Among the injected F_0 embryos, some displayed severe hematopoietic defects reminiscent of *hoxd4a* morphants, such as pericardial edema and a marked reduction in circulating blood cells. To test if the defects were caused by mutations of *hoxd4a*, we selected 10 such embryos and analyzed their genetic background by the T7EI assay. We found that more than half of the tested embryos contained obvious mutations of *hoxd4a* (Fig. 3.3.6, B). In support of this, some injected embryos showed a reduced expression of *gata1* at 24 hpf (Fig. 3.3.6, C). While these observations were encouraging, F_0 founder fish are still of limited value in establishing a causal link between the phenotype and the gene of interest.

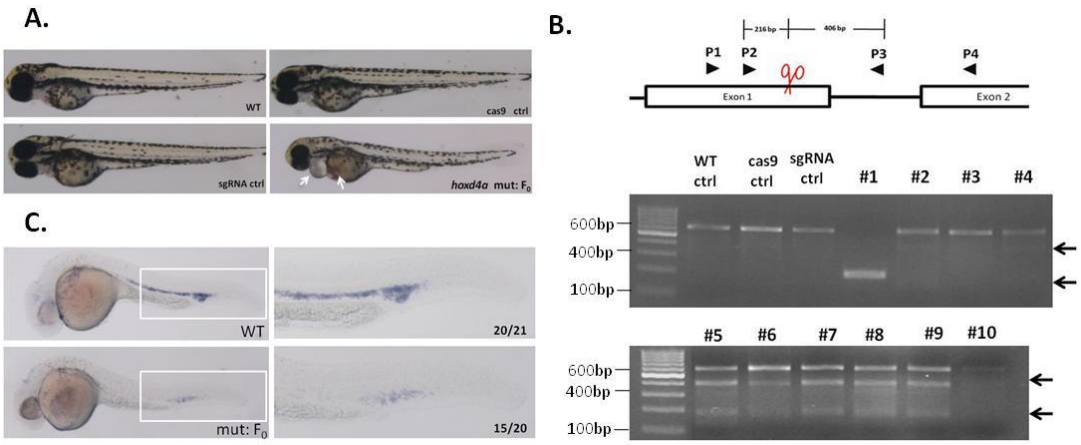

Figure 3.3.6: Analysis of the hematopoiesis in F_0 founder embryos.

(A) Hematopoietic defects in Cas9 protein and *hoxd4a* sgRNA injected embryos. White arrows indicate severe pericardial edema.

(B) Mutation analysis of ten embryos with hematopoietic defects. The T7EI assay was performed using PCR products derived from individual embryos. Black arrows indicates the expected positive bands cleaved by T7 endonuclease I.

(C) *In situ* hybridization of *gata1* in 24 hpf embryos injected with Cas9 protein and *hoxd4a* sgRNA.

F_0 founders were therefore raised to adulthood and mated with wild type zebrafish. Germline transmission was verified by screening individual F_1 offspring. Eleven out of 19 tested F_1 fish were found to be positive for the T7EI assay, revealing a high germline mutagenesis rate in F_0 founder fish. Additionally, we examined the integration of the donor oligonucleotide by PCR amplification with donor cassette specific primers. However, none was positive for successful homologous recombination, indicating the efficiency of ssDNA mediated homologous insertion was very low. To determine the mutations harbored by F_1 carriers, PCR products from individual F_1 heterozygotes were cloned into pCR4-TOPO vector and subjected to direct sequencing. Different INDEL mutations were found at the target locus, including 1-32 bp insertions or 3-8 bp deletions. Out of the eight INDELs, seven are out of frame mutations

resulting in a premature termination codon. Among these F1 fish, #24 carried a 32 bp insertion with point mutations, resulting in a truncated Hoxd4a protein encoding only 90 amino acids and was used for the following studies.

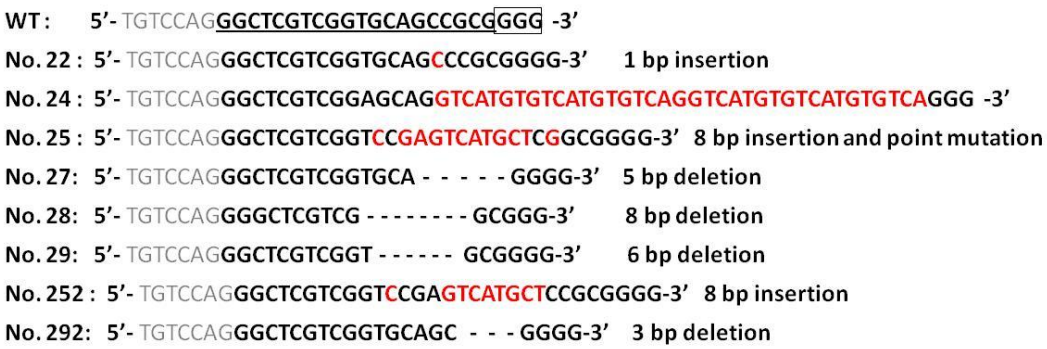

Figure 3.3.7: Representative mutations of F_1 individual embryos.

Target site sequences are underlined. The PAM is shown in the box. Inserted sequences and point mutations are indicated in red. Deletions are shown by a dashed line.

Again, each F_1 fish was outcrossed with wild type in order to generate a family of heterozygous carriers harboring the same mutation. Subsequently, these siblings were intercrossed to generate the F_2 generation in which 25% were expected to be homozygous null. To facilitate the genotyping of the F_2 generation, the restriction site mutation method was first employed. As shown in Figure 3.3.8, a SacII recognition site is located next to the PAM of the *hoxd4a* target site, and is very likely to be disrupted by Cas9-directed DNA cleavage and subsequent INDEL mutations. Sequencing results of F_1 individuals confirmed this by showing seven out of eight identified mutations abolished this SacII site. As expected, loss of the SacII site resulted in an extra band when the PCR products were digested with SacII enzyme, enabling us to discriminate wild type, heterozygotes and homozygotes (Fig. 3.3.8, A). Additionally, we also tested a PCR-based genotyping method which is based on the fact

that stringent binding at the 3' end of a primer is critical for PCR amplification. Mismatch in the 3’ end of PCR primers would result in a reduction or complete loss of PCR products. Consistent with the results of SacII digestion, PCR genotyping was also able to discriminate different genetic backgrounds with respect to *hoxd4a* (Fig. 3.3.8, B). PCR products from putative homozygous mutants were analyzed by direct sequencing, which further confirmed the mutation was present in both alleles by showing evenly spaced single peaks (Fig. 3.3.5, C).

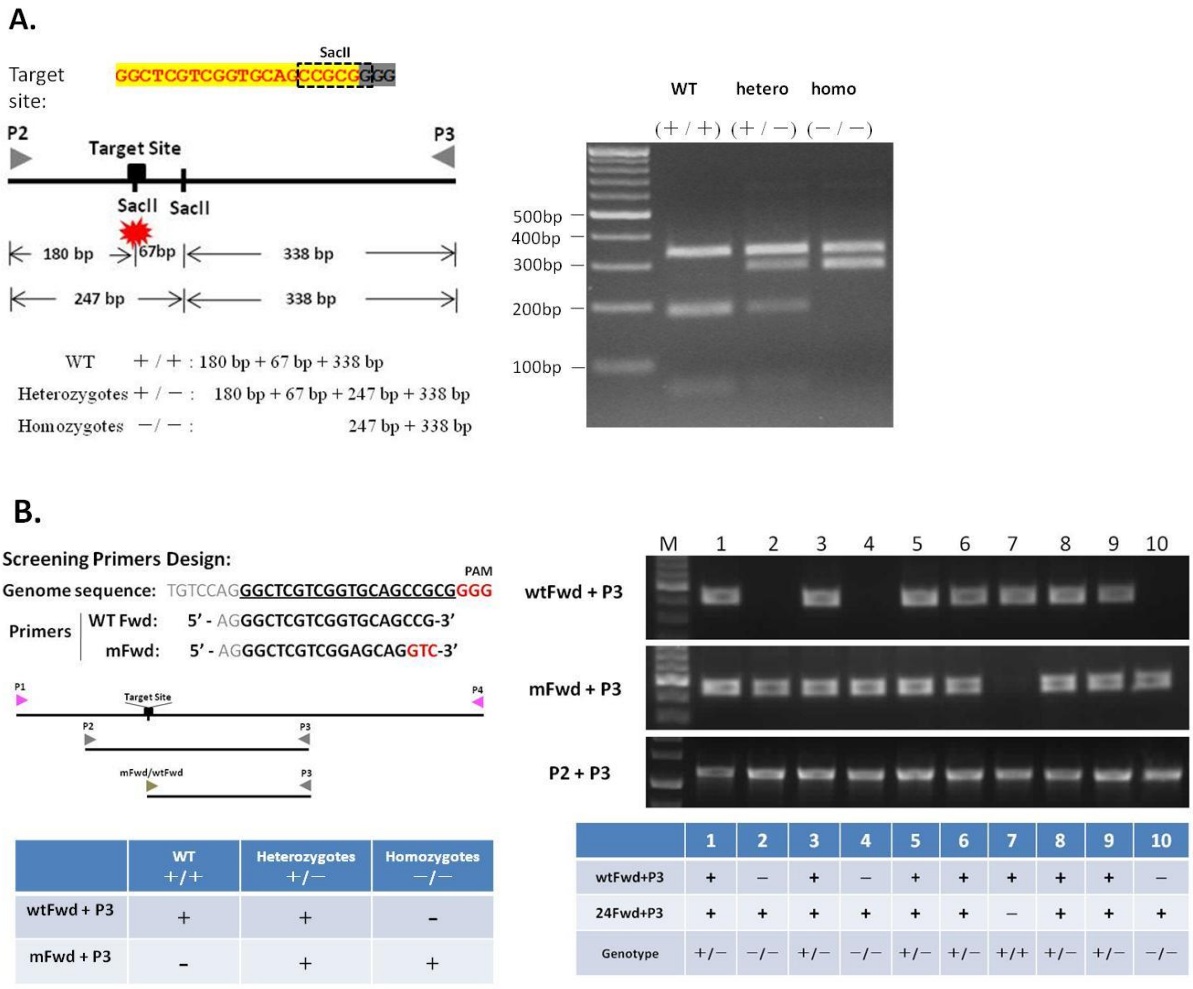

	WT +/+	Heterozygotes +/−	Homozygotes −/−
wtFwd + P3	+	+	-
mFwd + P3	-	+	+

	1	2	3	4	5	6	7	8	9	10
wtFwd+P3	+	–	+	–	+	+	+	+	+	–
24Fwd+P3	+	+	+	+	+	+	–	+	+	+
Genotype	+/−	−/−	+/−	−/−	+/−	+/−	+/+	+/−	+/−	−/−

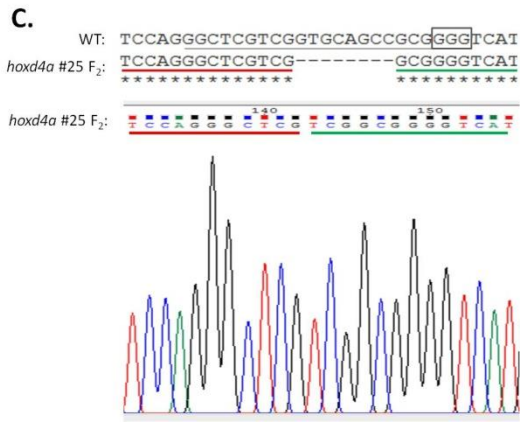

Figure 3.3.8: Different genotyping methods used for *hoxd4a* mutations.

(A) SacII restriction enzyme analysis of embryos with different genetic backgrounds of *hoxd4a* mutations. A SacII enzyme site is adjacent to the PAM sequence, which is most likely to be destroyed by NHEJ-induced mutations. Additionally, there is another SacII site neighboring to the target sequences, which will be not affected by CRISPR/Cas9 editing. As a result, SacII enzyme digestion of wild type PCR products will produce three bands, whereas mutated PCR products will result in two bands as shown in mutants. Heterozygotes have four bands due to the presence of two different alleles.

(B) PCR analysis of embryos with different genetic backgrounds of *hoxd4a* mutations. PCR products amplified with P1 and P4 was used as templates for a second round of nested PCR using locus specific primers. Screening primers (wtFWd and mFwd) were designed on the basis that only wild type or mutated allele is amplified accordingly.

(C) Sanger sequencing of the PCR products amplified from F_2 homozygotes (#25 carrying a 8 bp deletion).

The establishment of reliable genotyping methods enabled us to investigate the phenotype of the identified homozygotes. Unexpectedly, none of the mutants exhibited any defects in hematopoiesis. As the genotype analysis was performed after 7 days post fertilization (dpf), we wanted to know if the mutants developed normally throughout the whole of embryogenesis. To this end, the expression of hematopoietic markers was checked at 12 hpf and 22 hpf using a pool of F_2 embryos. It was assumed that if the gene expression was changed in mutants, 25% of F_2 embryos would be different from the others (50%

heterozygotes and 25% wild type). The difference would be obvious when a large number of F_2 embryos were analyzed. However, all tested embryos seemed to display similar gene expression profiles (Fig. 3.3.9), suggesting that hematopoiesis is normal in homozygous mutants throughout the embryonic development.

The discrepancy between *hoxd4a* morphants and mutants could be due to many reasons. Considering *hoxd4a* has a high maternal expression, the difference could be due to a rescue in F_2 animals by F_1 (heterozygous) maternal transcripts. To test this possibility, we sought to investigate the phenotypes in F_3 homozygous mutants obtained by crossing F_2 homozygotes. Like F_2 homozygotes, F_3 embryos did not show obvious morphological abnormalities during early embryogenesis. O-dianisidine staining also did not reveal any differences between wild type and mutant embryos. In summary, these data indicate that *hoxd4a* null mutants fail to recapitulate the *hoxd4a* morpholino-induced phenotypes.

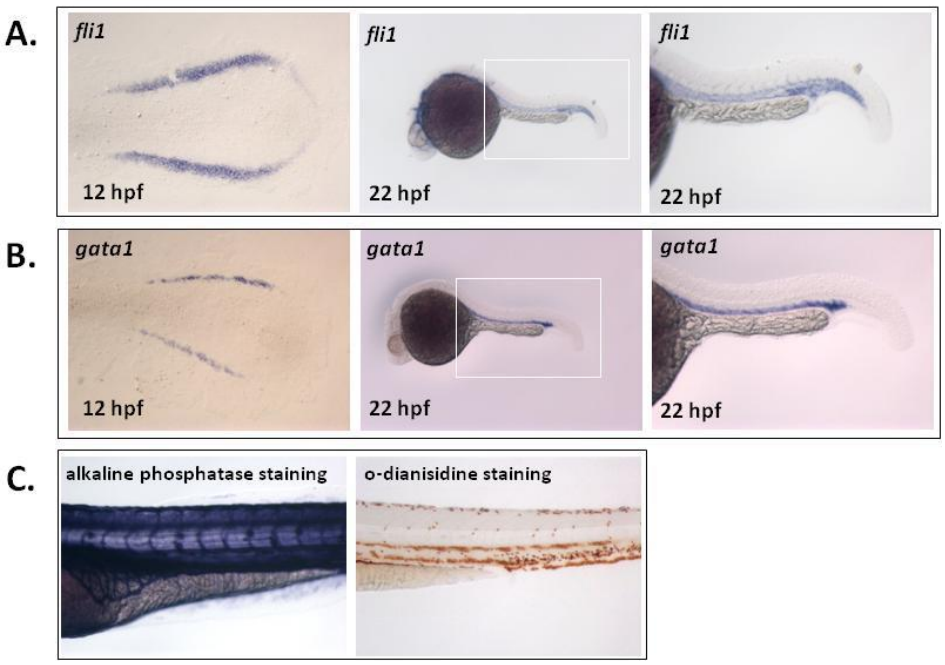

Figure 3.3.9: Gene expression and phenotypic analysis of F_2 offspring.

Whole mount *in situ* hybridization of *fli1* and *gata1* at 12 hpf (flat-mounted in dorsal views) and 22 hpf

(lateral views). Higher magnification of the boxed area is shown on the right. For alkaline phosphatase (AP) staining and o-dianisidine staining, the tail region is shown in lateral views. All embryos exhibited same gene expression as shown above.

We then asked if the phenotype observed in *hoxd4a* morphants was specific. If it was not due to off-target effects of the *hoxd4a* MOs, injection of *hoxd4a* morpholino should not cause any defects in *hoxd4a* null mutants. To test this, we injected F_3 embryos with 4 ng of anti-*hoxd4a* MO (*hoxd4a*-MO^{SA}) at the one-cell stage. O-dianisidine staining showed that injected mutant embryos had much more blood cells than morphants, displaying only mild and incompletely penetrant decreases (Fig. 3.3.10, A-B). Similar results were observed when the experiment was performed in a distinct *hoxd4a* null mutant line (#25) carrying a 8-bp insertion (Fig. 3.3.10, E). Lower doses of morpholino likewise revealed the mutants to be much less sensitive to the effect of *hoxd4a* morpholino than wild type controls (Fig. 3.3.10, D).

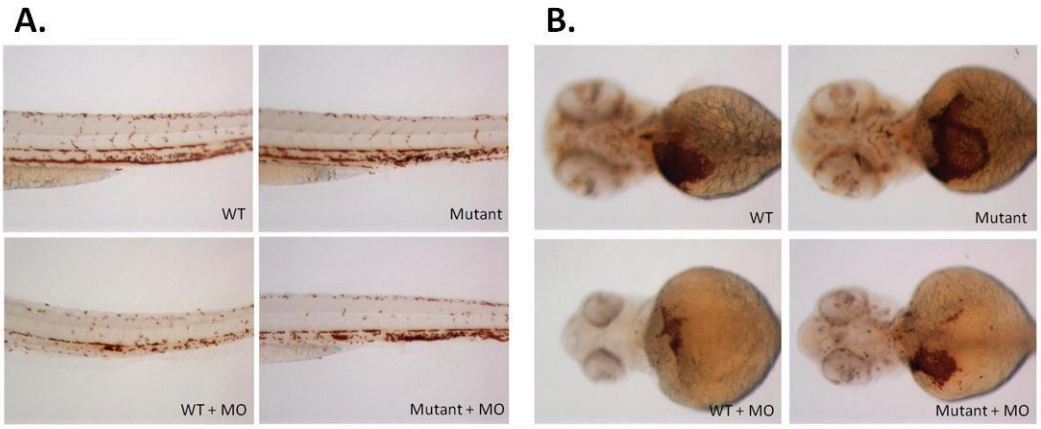

Figure 3.3.10: Mutants injections with anti-*hoxd4a* morpholinos.

(A-B) Representative embryos for each group upon the injection of *hoxd4a*-MO^{SA}. Left panel: caudal part of 72 hpf embryos is shown in lateral views. Right panel: ventral views of the blood cells around the yolk of embryos.

(C) Phenotype distribution of different embryos injection with 4 ng of anti-*hoxd4a* MO. The amount of blood cells can be divided into five classes from the absence (Class I) to the wild type level (Class V).

Three independent experiments were performed.

(D) Phenotype analysis of mutant embryos injection with 3 ng of *hoxd4a* MO.

(E) Phenotype analysis in a different *hoxd4a* mutant line, #25 carrying a 8 bp insertion.

As suggested by a previous study, the phenotypic differences between morphants and mutants could be due to specific genetic compensation that only occurs in mutants but not morphants (Rossi et al., 2015). To test this possibility, we examined the expression of potentially compensating genes by real-time qPCR at 12 hpf (Fig. 3.3.11). First, we found the level of *hoxd4a* expression was not reduced, suggesting the transcripts were not degraded by nonsense-mediated decay. Second, the expression of other three paralog members of group 4 (*hoxa4a*, *hoxb4a* and *hoxc4a*) was not significantly changed as well. Third, of three hematopoietic marker genes (*scl*, *fli1* and *gata1*), the expression of *scl* was significantly decreased in mutants, possibly implying an early perturbation in the initiation of hemangioblast formation. Fourth, we also checked the expression of other *hox* genes known to be important for zebrafish hematopoiesis, such as *hoxb6b*, *hoxb7a* and *hoxa9a*. None of these Hox genes showed a significant change in *hoxd4a* mutants. A similar result was also observed for *meis1.1*.

In conclusion, the expression of all the potentially compensating genes, namely a set of *Hox* genes along with *meis1.1*, retained at the same level as type controls.

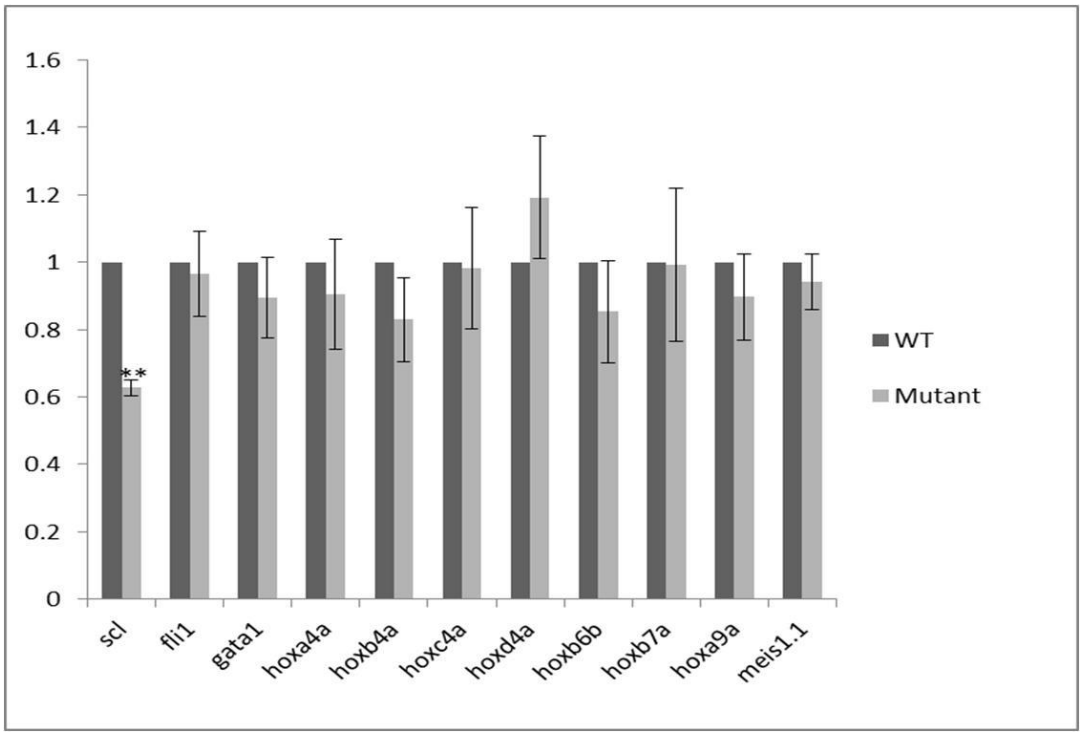

Figure 3.3.11: Gene expression in *hoxd4a* mutants. Data are shown as mean of fold changes ± standard error (s.e.m) from three independent experiments (n=3). ** denotes $p \leq 0.01$.

CHAPTER 4 : DISCUSSION

4.1. Early role of hoxd4a during early development

In contrast to the conventional roles of *Hox* genes in patterning the AP axis, we found that the timing of *hoxd4a* action in hematopoiesis and NPB formation is much earlier. Progenitors for hematopoietic and endothelial lineages, are specified between mid-blastula to gastrula stage (3 to 6 hpf). At shield stage (6 hpf), hemangioblasts, are localized to the ventral-most presumptive mesoderm and interspersed with unipotential progenitors that will give rise to blood and endothelial cells (Vogeli et al., 2006). Like the VMM, the NPB is also specified at the gastrula stage, arising from a region between the prospective neural and ectodermal cells. Our previous studies find that at shield stage, *hoxd4a*, in association with its cofactors like *meis1.1*, is highly co-expressed in the VMM where the hemangioblast originates. Loss of *hoxd4a* results in significant down-regulation of the hemangioblast marker *scl* in the PLM at 12 hpf despite the fact that, at this stage, the expression of *hoxd4a* is almost undetectable in the PLM (Amali et al., 2013). Additionally, simultaneous knocking down of h*oxd4a* and *hoxc4a* leads to decreased expression of the NPB specifier *prdm1* as early as 90% epiboly. All of these findings strongly imply a novel role for *hoxd4a* during the early phase of its expression.

To test this hypothesis, the timing of Hoxd4a action was controlled by fusion to the modified ligand-binding domain of the human estrogen receptor having high affinity for the estrogen antagonist tamoxifen. First, the expression of the hemangioblast marker *scl* was analyzed by *in situ* hybridization at 12 hpf. Strikingly, addition of 4-OHT at 4 and 6 hpf resulted in a full

and partial rescue of *scl* expression, respectively, suggesting that a short window spanning 4 to 6 hpf is critical for *hoxd4a* to serve its function in hemangioblast development. To check if the initiation of primitive hematopoiesis and vasculogenesis was affected, the expression of the erythroid lineage-specific marker *gata1* and the endothelial marker *fli1* were checked at 13 hpf. Likewise, activation of Hoxd4a by 4 hpf was able to rescue the expression of *gata1* and *fli1*, but could not do so by 8 hpf. Unsurprisingly, the circulating blood cells and vasculature development were also rescued by 4 hpf and 6 hpf, but scarcely rescued by 8 hpf, consistent with early defects in hemangioblast specification. Similarly, the expression of *prdm1*, the NCC marker *sox10* and the neuronal marker *islet1* in *hoxd4a*/*hoxc4a* double morphants was also partially rescued by activation of Hoxd4a at 4 hpf. In summary, all these results support a novel role for *hoxd4a* in controlling hematopoiesis, vasculogenesis and NPB formation, which occurs quite early during 4 hpf to 6 hpf.

Pre- or peri-gastrulation roles of *Hox* genes have been documented in different animal models, including fish, amphibians, birds and mammals (Iimura and Pourquie, 2006, 2007; van den Akker et al., 2010). It has been reported that the early activation of *Hox* genes controls gastrulation movements, which could be important for the spatially collinear *Hox* expression at later stages (Iimura and Pourquie, 2006). Another study shows that among the downstream candidates of *hoxb1b* (oe of the first expressed *Hox* gene) in zebrafish and *Xenopus*, genes involved in cell adhesion and movement were over-represented, consistent with a role in cell movement (van den Akker et al., 2010). However, there is no evidence showing that an evolutionarily conserved early phase of *Hox* gene expression plays any role in mammalian development. This suggests that pre-gastrulation function of *Hox* genes could be the ancestral

state in terms of the evolution of *Hox* gene functions. Previous studies suggest that animals first evolved simple patterning mechanisms and only afterwards evolved germ layers and gastrulation (Nakanishi et al., 2014). For example, sponges do not have germ layers and do not undergo gastrulation, whereas Cnidaria and Bilateria do. This may seem obvious, but we can conclude that pre- and post-gastrulation expression windows of *Hox* genes could only evolve after or with gastrulation. Then the question is, along with the evolution of germ layers and gastrulation, which evolved first, pre- or post-gastrulation expression of *Hox* genes? Since the ancestors of sponges that only express *Hox*-like genes are able to pattern their tissues before the evolution of gastrulation, then we might argue that the pre-gastrulation expression of *Hox* genes (or *Hox* gene ancestors) also evolved first. And the post-gastrulation expression period evolved second along with the expansion of true *Hox* genes appearing in Cnidaria and bilateria. Their involvement in post-gastrulation patterning may require the activation of pre-gastrulation expression which could continue to play important roles during gastrulation. It is possible that this function has been lost in mammals, perhaps along with the evolution of the placenta and internal development.

4.2. Functional domains of Hoxd4a in hematopoiesis

In addition to the timing of *hoxd4a* action, the functional domains of Hoxd4a required for hemangioblast specification is another question of interest. Previous studies have identified some functional domains and motifs within HOX proteins. The most remarkable portion could be the invariant asparagine 51 (N51) that is required for DNA binding, and the YPWM motif that is required for the interaction with PBX cofactors. In order to understand the

mechanism of *hoxd4a* in regulating hematopoietic development, we substituted asparagine 51 and the YPWM motif by point mutation. The importance of binding to DNA or PBX was assessed by testing the ability of the mutated mRNAs (*hoxd4a*$^{\triangle N51S}$, *hoxd4a*$^{\triangle YPAA}$, *hoxd4a*$^{\triangle S51+YPAA}$) to rescue the expression of different markers such as *scl, fli1* and *gata1* that have been shown to be rescued by wild-type *hoxd4a* (*hoxd4a* ^{WT}). Of note, previous studies suggest that neither of these mutations affects protein stability or nuclear localization (Rambaldi et al., 1994).

First, we found that all the mutated mRNAs (*hoxd4a*$^{\triangle N51S}$, *hoxd4a*$^{\triangle YPAA}$, *hoxd4a*$^{\triangle S51+YPAA}$) could only partially rescue the reduced expression of *scl* and *fli1*. Compared with Hoxd4a^{WT}, the ability of the non-DNA binding mutant (Hoxd4a$^{\triangle N51S}$) was obviously reduced, suggesting that DNA binding is important for its normal function. But it should be noted that this ability is not completely lost. Instead, the transcripts of *scl* and *fli1* were higher than that of *hoxd4a* morphants, which means that Hoxd4a is still functional without directly binding to DNA when recruited by PBX or other partners. Though there is no evidence supporting this proposal, previous study has shown that their cofactors PBX and MEIS can be recruited as non-DNA binding partners in trimeric complexes with HOX proteins (Shanmugam et al., 1999a; Zandvakili and Gebelein, 2016).

Next, before going on to discuss the results for the YPWM motif mutant, it is necessary to understand previous studies about the effect of YPWM-to-YPAA mutation on *Hox* genes *in vivo* functions, which is quite sophisticated. First, considering that some functions of *Hox* genes are Pbx-independent, it is quite reasonable that this mutation does not affect the ability of *Hox* genes to carry out such functions (Galant et al., 2002). Then, for Pbx-dependent

functions, the final output varies among different *Hox* genes. In most cases, the mutation is likely to abolish the interaction with PBX and therefore impairs their functions, which could be illustrated with an example: the *Drosophila* Hox protein, DFD, fails to carry out its *in vivo* functions with this mutation (Joshi et al., 2010). By contrast, some YPAA mutant HOX proteins like Ubx are still able to bind PBX cooperatively in the presence of DNA due to the presence of independent domains responsible for HOX/PBX interactions (Galant et al., 2002; Merabet and Hudry, 2013). Even for one specific *Hox* gene, the requirement for the YPWM motif could be distinct for different functions. For example, it is strictly required for the eye-to-wing transformation of ANTP, but seems less important for its function in the antenna-to-second leg transformation (Prince et al., 2008).

In this study, the expression of *scl* and *fli1*was only partially rescued by the YPWM motif mutant of *hoxd4a* (*hoxd4a*$^{\triangle YPAA}$), which demonstrated that cooperative DNA binding with PBX is required for Hoxd4a function in this context. However, as this mutation did not completely abrogate the function of Hoxd4a, there could be many possibilities. One explanation could be that other residues of Hoxd4a are involved in interacting with PBX. Another possibility could be due to other potential factors that interact with Hoxd4a through other residues.

More interestingly, we found that none of the mutated mRNAs (*hoxd4a*^{N51S}, *hoxd4a*$^{\triangle YPAA}$, *hoxd4a*$^{\triangle S51+YPAA}$) were able to rescue the expression of *gata1*. This suggests a different mechanism by which *hoxd4a* regulates *gata1* expression in a manner that is strictly dependent on direct cooperative binding of a Hoxd4a-Pbx complex to DNA. Another possibility could be due to the reduced expression of *scl* and *fli1*, a threshold level of which

could be crucial for the initiation of *gata1* expression.

4.3. *Hox* genes and their cofactors in hematopoiesis

Over the past few years, the number of HOX cofactors has grown significantly. Generally, HOX cofactors can be divided into two groups. As most notable HOX cofactors, PBX and MEIS are representative of the first class that is able to bind DNA through the TALE homeodomain. Members of the second group, like CREB-binding protein (CBP), are assembled in HOX transcription complexes without directly binding to DNA, functioning as co-activator or co-repressor for transcription regulation (Ladam and Sagerstrom, 2014).

In this study, we focused on the well-known HOX cofactors PBX and MEIS. As discussed above, substitution of the YPWM motif with YPAA (*hoxd4a*$^{\triangle YPAA}$) significantly impaired its ability to rescue *scl*, *fli1* and *gata1*expression, supporting a model in which the interaction between Hoxd4a and Pbx is important for the expression of *scl*, *fli1*, and especially *gata1*. Co-immunoprecipitation of Hoxd4a and Pbx proteins through the BioID system further confirmed the physical interactions between them.

Consistent with these observations, the requirement for *meis1.1* in hematopoiesis has been demonstrated by previous studies in our lab and others (Amali et al., 2013; Cvejic et al., 2011a; Minehata et al., 2008; Pillay et al., 2010). Here, we corroborated its interaction with *hoxd4a* in hematopoiesis using PCAB, a dominant-negative inhibitor of MEIS protein. By competing with endogenous PBX, it has been shown to be very effective in sequestering MEIS in the cytoplasm and suppressing its function in hindbrain development (Choe, 2002). In this study, injection of PCAB mRNA led to markedly reduced expression of *scl*, consistent

with the role of *Meis* genes in hematopoiesis. Synergistic interactions with *hoxd4a* were confirmed by reduced expression of *scl* when embryos were co-injected with threshold amounts of anti-*hoxd4a* morpholino and PCAB mRNA.

In addition to PBX and MEIS, high throughput proteomic approaches have identified a significant number of interacting partner candidates although many still await further molecular confirmations (Merabet and Dard, 2014). Characterization of context-specific cofactors could enlarge our vision of the molecular mechanism(s) by which Hoxd4a carried out these early functions. To this end, we adopted the BioID system in zebrafish and attempted to identify some functionally relevant interacting partners in the early developmental contexts. Very unexpectedly, while Hoxd4a-Flag was stably expressed from 4 hpf to 12 hpf, the expression of Hoxd4a-BirA*-Flag was not detectable via mRNA injection. This, coupled with the fact that its injection cannot rescue the hematopoietic defects of *hoxd4a* morphants, demonstrates the BioID system does not work for Hoxd4a in zebrafish. This led to find an alternative system to implement the BioID method, namely mammalian cell culture. While such a cross-species approach may raise concerns, the molecular functions of Hox proteins are highly conserved across evolution. For example, human HOXD4 can substitute for the specific regulatory functions of its *Drosophila* ortholog, *Deformed* (*Dfd*) in transgenic flies (McGinnis et al., 1990). When HOXD4 was introduced into the *Drosophila* genome under the control of a heat-shock promoter, it was able to specifically activate ectopic expression of *Dfd* in developing embryos and recapitulate the head phenotype of a dominant mutant allele of *Dfd*. Therefore, we assume that identification of the interacting proteins of zebrafish Hoxd4a can be implemented in mammalian cells and could give some

clues about its functions in vertebrates generally.

The BioID system turns out to be very specific and efficient in cultured HEK293T cells. Forty-five proteins were finally found to be present in two replicates of Hoxd4a-BirA* experimental samples, but not in BirA* negative controls. Gene Ontology and STRING 10 analysis show that most of the proteins are related to chromatin remodeling and mRNA processing, which is in consistent with other studies using high-throughput approaches. Since Hoxd4a itself is a transcription factor, the identification of proteins involved in transcriptional machinery further validates our approach. However, as suggested by previous studies, Hox interacting partners are not restricted to transcription factors, and even not obligatory nuclear components (Merabet and Dard, 2014). In particular, a signification number of cytoplasmic proteins have been identified as Hox candidate cofactors, which are involved in cell regulatory processes such as signal transduction, mRNA stability, post-translational modifications (Merabet and Dard, 2014). This implies that the activity of Hox proteins could not be limited to gene regulation.

Among the candidates, we are especially interested into MGA due to its function in dorsoventral patterning in the cooperation with Smad4 (Sun et al., 2014). In zebrafish, MGA is maternally and zygotically expressed in all cells until 90% epiboly. MGA participates in BMP signaling within the YSL and is required to establish the BMP gradient in the latter stages. And injection of *mga* morpholino into YLS results in changes of *gata1* expression, implying that *mga* could regulate hematopoiesis indirectly through its action on the DV axis patterning. Consistent with this, we have confirmed that the optimal time for Hoxd4a-ERT2 to exert its function is 4 hpf, a timing that could also be important for *mga* function in

establishing dorsoventral axis. Based on these findings, we assume that *hoxd4a*, *mga* and BMP signaling could interact synergistically at early developmental stage.

4.4. The interaction between *hoxd4a* and BMP signaling pathway in hematopoiesis

As mentioned above, *Hox* genes and BMPs are closely related in many common developmental processes. In our context, loss of *hoxd4a* and *hoxc4a* specifically causes defects of the NPB and decreased expression of genes that specify the NPB and its derivatives. Moreover, a high level of BMP signaling is known to be required to specify the VMM from where the hemangioblast and unipotential progenitors arise. These along with the early expression of *hoxd4a* strongly suggest an interaction between *Hox* genes and BMP signaling during early embryonic development. To test this hypothesis, we adopted the synthetic genetic interaction method which requires simultaneous inhibition of BMP signaling and *hoxd4a* function at a threshold level that is just sufficient to avoid affecting primitive hematopoiesis. A threshold concentration of LDN193189 was first established. Then the potential Hox-BMP interaction was checked by comparing the expression of *scl*, *fli1* and *gata1* under conditions of *hoxd4a* knockdown and BMP inhibition at the threshold level.

Strikingly, the expression of these three markers differed from each other under different conditions. Firstly, the expression of *scl* was only reduced in embryos with simultaneous loss of *hoxd4a* and BMP, suggesting that, as hypothesized, *hoxd4a* synergizes with BMP signaling to regulate *scl* expression. For *fli1*, the expression was also decreased but only to a milder extent, leading us to conclude that it is less sensitive to reductions in *hoxd4a* and BMP

signaling than *scl*. Last, we found *gata1* expression was down-regulated when embryos were only injected with 3 ng of anti-*hoxd4a* morpholino. Consistently, our previous results show that 4 ng anti-*hoxd4a* morpholino resulted in total absence of *gata1* signal, while it only reduced *scl* and *fli1* expression significantly, suggesting that compared with *scl* and *fli1*, *gata1* could be more responsive to subtle changes in the level of *hoxd4a* function. In support of this, the significant reduction of blood cells, coupled with the fact that most embryos develop the vasculature normally, further confirms that the hematopoietic pathway is more affected than the vasculogenic pathway.

As suggested by our previous results, the function of *hoxd4a* in hematopoiesis is required by 4 hpf. In combination of the fact that high BMP signaling is also required at early gastrula stage in directing hematopoiesis, it strongly suggests the interaction of *hoxd4a* and BMP signaling occurs at pre-gastrulation. This hypothesis was evidenced by reduced expression of *scl* in situations where the embryos injected with 3 ng of anti-*hoxd4a* morpholino were treated with LDN193189 during 4-8 hpf (data not shown). However, the function of BMP signaling in patterning ventral mesoderm has been shown to be stage-specific (Pyati et al., 2005). As opposed to its function during gastrulation, BMP signaling restricts the hematopoietic and vascular development during the segmentation stages. This makes it more complicated to analyze their effects when the phenotype was checked at 72 hpf under a condition that the BMP signaling is inhibited throughout the embryonic development.

Encouraged by numerous studies showing that Hox proteins can physically associate with Smad proteins, we assumed the synergistic effect of *hoxd4a* and BMP signaling could be mediated by interactions between Hoxd4a and Smad proteins. *Hox* gene products have been

shown to be involved in the downstream events of BMP signaling (Shi et al., 1999b). SMAD1 and SMAD4 have been reported to directly interact with HOX proteins, inhibiting their abilities of binding to DNA and suppressing their regulation of downstream targets (Wang et al., 2006). Physical interaction occurs through the homeodomain of HOX and the MH1 domain of SMADs (Shi et al., 1999b). MH1-c, a truncated MH1 domain, was able to disrupt interactions between endogenous SMAD4 and HOXA9 and thus block the malignant transformation of primitive hematopoietic cells caused by NUP98-HOXA9 (Quere et al., 2011). In this study, the effect of MH1-c on hematopoiesis was investigated in zebrafish following mRNA injection. MH1-c was shown to reduce *scl* expression and blood cell formation in a dose-dependent manner, which supports the role of Smads in hematopoietic development. However, when embryos were injected with threshold amounts of anti-*hoxd4a* morpholino and MH1-c mRNA, the expression of different hematopoietic markers was not changed, which suggests the hypothesized Hoxd4a-Smad interaction could be independent of the MH1 domain of Smads. To test this possibility, CO-IP was performed by transient overexpression of Hoxd4a and different Smad proteins in cultured cells. However, no physical interactions were detected, suggesting that the interaction between *hoxd4a* and BMP signaling could be mediated by other mechanisms.

4.5. The specificity of *hoxd4a* morphant phenotypes

Though the specificity of the anti-*hoxd4a* morpholino-induced phenotype was validated by rescue experiments, our initial work was based on a single such morpholino (*hoxd4a*-MO^{SA}) paired with a scrambled negative control morpholino. To increase confidence in the

specificity of our findings, the function of *hoxd4a* in hematopoiesis was further characterized with an expanded complement of morpholinos. Whereas *hoxd4a*-MO^{SA} targeted the splice acceptor, we designed a second non-overlapping morpholino that targeted the splice donor (*hoxd4a*-MO^{SD}). In addition, we designed two negative-control morpholinos bearing five-nucleotide mismatches to either *hoxd4a*-MO^{SA} or *hoxd4a*-MO^{SD}, respectively, as such mismatch MOs are considered to provide greater stringency than scrambled MOs. As summarized below, the results with these additional reagents strongly supported the conclusion that the hematopoietic phenotypes are specific to *hoxd4a*.

First, two independent morpholinos against *hoxd4a* (*hoxd4a*-MO^{SA} and *hoxd4a*-MO^{SD}) caused the same defects in hematopoiesis, including less circulating blood cells and severe pericardial edema. A dose-dependent reduction of blood cells was observed in embryos injected with increasing amounts of either morpholino. In contrast, the corresponding five-nucleotide mismatch morpholinos (*hoxd4a*-Mis-MO^{SA} and *hoxd4a*-Mis-MO^{SD}) did not produce any morphological abnormalities when injected at the same or even higher doses. Most embryos injected with the mismatch morpholinos developed normally with comparable numbers of blood cells as wild type controls. This demonstrates that the phenotype is not due to off-target effects. Consistently, *hoxd4a*-MO^{SA} and *hoxd4a*-MO^{SD} both worked efficiently by showing a great reduction of spliced mature mRNA coupled with an increase in aberrant transcripts, while this was not observed in embryos injected with either mismatch morpholino. Furthermore, co-injection of the two specific morpholinos at lower doses produced synergistic effects.

Additionally, the specificity is also revealed by different rescue experiments. As mentioned

above, the hematopoietic and vasculogenic defects caused by *hoxd4a*-MO^{SA} are rescued by *hoxd4a* mRNA injection. However, this rescue ability was diminished when either the homeodomain or the YPWM motif was mutated so as to impair DNA binding or interaction with Pbx respectively. This directly demonstrates the importance of these two domains in the function of Hoxd4a. Beyond this, the action of *hoxd4a* in hematopoiesis was shown to be required by 4 hpf, consistent with a specific function during a narrow window. In support of this, the hematopoietic defects caused by another independent morpholino against h*oxd4a* (*hoxd4a*-MO^{SD}) was also rescued by *hoxd4a* mRNA despite the fact that this morpholino caused other abnormalities like coloboma which was not rescued. On the other hand, this enables us to distinguish the specific phenotype from non-specific effects. In this case, it implies that the eye malformation caused by *hoxd4a*-MO^{SD} could largely be due to off-target effects.

However, despite all above evidence proving the specificity of *hoxd4a* morpholinos, the *hoxd4a* null mutants fail to recapitulate the phenotype of *hoxd4a* morphants. The reason behind this discrepancy could be due to compensation by other genes, especially *Hox* genes that are known to have a role in hematopoiesis. However, such *Hox* genes, like *hoxb6b*, *hoxb7a* and *hoxa9a* as well as the other three members of group 4 (*hoxa4a*, *hoxb4a* and *hoxc4a*) were found to be expressed at a level comparable to wild type controls at 12 hpf. In contrast, most of these *Hox* genes were highly down-regulated in *hoxd4a* morphants (Amali et al., 2013). The question then becomes why the overall down-regulation of *Hox* genes only occurs in *hoxd4a* morphants but not in the mutants? With limited studies about such specific responses in morphants, this question still needs further investigations. Meanwhile, another

question arises regarding the proposed compensation effect, that is, do compensating genes have to be up-regulated in order to compensate for the lack of another gene's function? In other words, could wild type expression levels of some *Hox* genes compensate for the loss of *hoxd4a* in hematopoiesis? It could be true as wild type mRNA levels could still result in significant differences in protein expression. In addition to other *Hox* genes, their cofactors, like Meis and Pbx, could also compensate the loss of *hoxd4a* as they were also shown to be conserved in the role of regulating hematopoiesis (Azcoitia et al., 2005; Cvejic et al., 2011b; DiMartino et al., 2001; Pillay et al., 2010).

Further, the question becomes more complicated when it comes to the time window of the proposed compensation effects. Though we have shown that the function of *hoxd4a* in hematopoiesis is required by 4 hpf, it does not necessarily mean that the action of compensation has to be fully restricted to the same time window. Despite all these questions, the fact that the null mutants are largely resistant to anti-*hoxd4a* morpholino injections is still strong evidence for the specificity of the phenotype.

In conclusion, though the *hoxd4a* mutants fail to phenocopy the morphants, we have enough evidence to prove the hematopoietic defects induced by *hoxd4a* morpholinos are specific phenotypes.

CHAPTER 5 : CONCLUSIONS

The major findings of this study are summarized below:

First, in contrast to the late phase function of *Hox* genes in regulating body axis, the role of *hoxd4a* in zebrafish hematopoiesis, vasculogenesis and NPB formation is much earlier at approximately 4 hpf, a point preceding gastrulation.

Second, both of the homeodomain and the YPWM motif are important for Hoxd4a in directing hematopoiesis and vasculogenesis, suggesting cooperative binding to DNA with PBX cofactors is required for Hoxd4a in this process. Differences in the extent of rescue by different mutated mRNA may suggest different mechanisms by which *hoxd4a* regulates its downstream targets.

Third, the BMP signaling pathway synergizes with *hoxd4a* to regulate hematopoiesis, but this may not be mediated by physical interactions between Hoxd4a and Smad proteins.

Fourth, while *hoxd4a* mutants fail to recapitulate the phenotype of *hoxd4a* morphants, such mutants are resistant to the effects of anti-*hoxd4a* morpholinos, confirming that the phenotype is specific to *hoxd4a* and strongly suggesting that compensatory pathways are deployed in the mutant embryos.

CHAPTER 6 : FUTURE DIECTIONS

In this study, *hoxd4a* and its cofactors are found to act together at an early stage of embryonic development to regulate hematopoiesis, a novel function that is totally different from the expected role of *Hox* genes in patterning the AP axis. However, there are still many questions requiring further investigations.

First, given the fact that zebrafish retains the early phase expression of many *Hox* genes, it would be very interesting to study whether other *Hox* genes also play roles during pre-gastrulation stages of zebrafish development. In *Xenopus* and chick, the early phase of *Hox* expression is linked to the establishment of the later collinear initiation of *Hox* gene expression (Iimura and Pourquie, 2006; Wacker et al., 2004a). By contrast, there is no evidence showing that early *Hox* expression contributes to mammalian development. This makes it very interesting to study the extent to which the functions of early-phase *Hox* gene expression are conserved in evolution. Consistent with conserved functions, zebrafish *hoxb1a* was found to be specifically expressed in the mesoderm except for the shield region (Kudoh et al., 2001), which is very similar to the expression of its paralog *hoxd1* in *Xenopus* (Wacker et al., 2004a). Furthermore, the interaction between *Hox*-expressing non-organizer mesoderm and the Spemann organizer was found to be very important to the establishment of the *Hox* code in *Xenopus*, which suggests a similar role for zebrafish *hoxb1a*. Apart from the inducible method based on fusion to the ligand-binding domain (LBD) of a human estrogen receptor variant (ERT2), embryonic gene expression can be spatiotemporally controlled by caged morpholino (cMO) oligonucleotides that are activated by 360-nm light at different time

points to knockdown gene expression (Shestopalov and Chen, 2011).

The interaction between *hoxd4a* and BMP signaling in directing hematopoiesis also requires further studies. Considering that the roles of BMP signaling on hematopoiesis are stage-specific, it would be very interesting to conditionally disrupt the function of *hoxd4a* or BMP signaling during different phases, which could be achieved by cMOs and inducible expression of a dominant-negative BMP receptor, respectively. Contrary to our hypothesis, CO-IP did not reveal evidence for Hoxd4a-Smad interaction in cultured cells. To exclude the possibility of post-translational modification, pull-down experiments could be performed in shield-stage embryos overexpressing Hoxd4a-Flag and individual HA tagged Smads by mRNA injection at the one-cell stage. Meanwhile, Bimolecular Fluorescence Complementation (BiFC) method could be used to visualize Hoxd4a-Smad interactions. This could be implemented by fusing the two halves of the Venus fluorescent protein to Hoxd4a and individual Smads. At the one-cell stage, embryos would be injected with mRNAs encoding the Hoxd4a-Venus and Smad-Venus fusion proteins and fluorescent signals can be scanned during gastrula stage. Furthermore, Hoxd4a could also be recruited by Smad proteins to the regulatory elements of BMP target genes that are required for the formation of the hemangioblast and NPB. This could be reflected by a co-occupancy of Hoxd4a and Smad in the regulatory region of the targets. To test this hypothesis, ChIP-seq could be performed to assess the genome-wide binding sites of Hoxd4a and Smad protein at shield stage. While an antibody against zebrafish Smad4 is available for ChIP assay, we failed to generate a good monoclonal antibody against Hoxd4a. In this case, the experiment can be completed by injection of mRNA encoding Hoxd4a-Flag which has been shown to be stably expressed

from 4 hpf to 12 hpf. A minimum amount of mRNA required for a rescue of the hematopoietic defects would be used to minimize the non-specific bindings. Individual sites co-bound by Hoxd4a and Smad4 should represent a responsive regulatory element of Hoxd4a and BMP signaling, which would need to be confirmed by examining their expressions when the function of *hoxd4a* or BMP signaling is inhibited.

The reason behind the phenotypic discrepancy between *hoxd4a* mutants and morphants is also very interesting. To identify the possible compensation molecules, RNA-seq and mass spectrometry could be performed in WT, *hoxd4a* morphant and null mutant embryos. Above experiments could be done at 12 hpf, a time point when hematopoietic makers just start to express. Assessment of the RNA profiling and proteomes would allow us to identify genes that are up-regulated in mutants compared to WT and morphants. Their compensation role can be further assessed by overexpression of individual compensating genes in *hoxd4a* morphants to check if they can functionally replace *hoxd4a*.

To further confirm the reliability of the BioID system, direct interaction between Hoxd4a and the novel partner candidates needs to be validated in mammalian cells first and then in zebrafish embryos. The next logical step would be to study the functional importance of the interaction in zebrafish embryonic development. To test our hypothesis for Hoxd4a and MGA, the expression of *hoxd4a* and other hematopoietic markers can be checked in *mga* morphants to determine the possible function of MGA in hematopoiesis and also the genetic hierarchy. Besides, as we were able to detect the expression of Hoxd4a-Flag in zebrafish by mRNA injection, interacting partners can also be identified by affinity purification coupled with mass spectrometry (AP-MS) at shield stage. This would allow us to make a comparison of the

BioID results that is performed in mammalian cells with the AP-MS results performed in zebrafish, which would be interesting to find any differences.

To better understand how *hoxd4a* regulates hematopoiesis, it would be useful to identify the downstream targets that are directly bound and regulated by Hoxd4a. Genetic targets must meet two requirements: first, their expression must be regulated by Hoxd4a, which could be reflected by altered expression of targets when the level of *hoxd4a* is changed. More importantly, direct binding of Hoxd4a at a presumptive enhancer region must be present. To this end, RNA-seq would need to be conducted first using embryos injected with anti-*hoxd4a* morpholinos. To determine the binding sites of Hoxd4a across the zebrafish genome, ChIP-seq will be performed using epitope-tagged Hoxd4a, for example, Hoxd4a-Flag by mRNA injection. These would find numerous potential gene targets of Hoxd4a, but only those that are known for a role in hematopoiesis would be further investigated. Such genes could be identified by searching the consensus Hox binding site, TAAT, in their regulatory region and their binding to Hoxd4a could be confirmed by electrophoretic mobility shift assay (EMSA) coupled with point mutations of these sites. Identified candidates could be further confirmed by studying their functions in controlling zebrafish hematopoiesis.

REFERENCES

Abramovich, C., Shen, W.F., Pineault, N., Imren, S., Montpetit, B., Largman, C., Humphries, R.K., 2000. Functional cloning and characterization of a novel nonhomeodomain protein that inhibits the binding of PBX1-HOX complexes to DNA. J Biol Chem. 275, 26172-26177.

Abu-Shaar, M., Ryoo, H.D., Mann, R.S., 1999. Control of the nuclear localization of Extradenticle by competing nuclear import and export signals. Genes Dev. 13, 935-945.

Alexandre, D., Clarke, J.D., Oxtoby, E., Yan, Y.L., Jowett, T., Holder, N., 1996. Ectopic expression of Hoxa-1 in the zebrafish alters the fate of the mandibular arch neural crest and phenocopies a retinoic acid-induced phenotype. Development 122, 735-746.

Alharbi, R.A., Pettengell, R., Pandha, H.S., Morgan, R., 2013. The role of HOX genes in normal hematopoiesis and acute leukemia. Leukemia 27, 1000-1008.

Amali, A.A., Sie, L., Winkler, C., Featherstone, M., 2013. Zebrafish hoxd4a acts upstream of meis1.1 to direct vasculogenesis, angiogenesis and hematopoiesis. PLoS One 8, e58857. doi: 58810.51371/journal.pone.0058857. Epub 0052013 Mar 0058815.

Antonchuk, J., Sauvageau, G., Humphries, R.K., 2001. HOXB4 overexpression mediates very rapid stem cell regeneration and competitive hematopoietic repopulation. Exp Hematol 29, 1125-1134.

Azcoitia, V., Aracil, M., Martinez, A.C., Torres, M., 2005. The homeodomain protein Meis1 is essential for definitive hematopoiesis and vascular patterning in the mouse embryo. Developmental biology 280, 307-320.

Bai, S., Shi, X., Yang, X., Cao, X., 2000. Smad6 as a transcriptional corepressor. J Biol Chem 275, 8267-8270.

Berthelsen, J., Zappavigna, V., Ferretti, E., Mavilio, F., Blasi, F., 1998. The novel homeoprotein Prep1 modulates Pbx-Hox protein cooperativity. EMBO J. 17, 1434-1445.

Bill, B.R., Petzold, A.M., Clark, K.J., Schimmenti, L.A., Ekker, S.C., 2009. A primer for morpholino use in zebrafish. Zebrafish 6, 69-77.

Blin, K., Pedersen, L.E., Weber, T., Lee, S.Y., 2016. CRISPy-web: an online resource to design sgRNAs for CRISPR applications. Synthetic and Systems Biotechnology 1, 118-121.

Brun, A.C., Bjornsson, J.M., Magnusson, M., Larsson, N., Leveen, P., Ehinger, M., Nilsson, E., Karlsson, S., 2004. Hoxb4-deficient mice undergo normal hematopoietic development but exhibit a mild proliferation defect in hematopoietic stem cells. Blood 103, 4126-4133.

Cannon, J.E., Upton, P.D., Smith, J.C., Morrell, N.W., 2010. Intersegmental vessel formation in zebrafish: requirement for VEGF but not BMP signalling revealed by selective and non-selective BMP antagonists. British journal of pharmacology 161, 140-149.

Casanova, J., Sanchez-Herrero, E., Morata, G., 1985. Prothoracic transformation and functional structure of the Ultrabithorax gene of Drosophila. Cell 42, 663-669.

Chang, C.P., Brocchieri, L., Shen, W.F., Largman, C., Cleary, M.L., 1996a. Pbx modulation of Hox homeodomain amino-terminal arms establishes different DNA-binding specificities across the Hox locus. Mol Cell Biol. 16, 1734-1745.

Chang, C.P., Brocchieri, L., Shen, W.F., Largman, C., Cleary, M.L., 1996b. Pbx modulation of Hox homeodomain amino-terminal arms establishes different DNA-binding specificities across the Hox locus. Mol Cell Biol 16, 1734-1745.

Chen, A.T., Zon, L.I., 2009. Zebrafish blood stem cells. Journal of cellular biochemistry 108, 35-42.

Choe, S.K., 2002. <Meis family proteins are required for hindbrain development in the zebrafish.pdf>.

Choe, S.K., Vlachakis, N., Sagerstrom, C.G., 2002. Meis family proteins are required for hindbrain development in the zebrafish. Development 129, 585-595.

Ciau-Uitz, A., Liu, F., Patient, R., 2010. Genetic control of hematopoietic development in Xenopus and zebrafish. Int J Dev Biol 54, 1139-1149. doi: 1110.1387/ijdb.093055ac.

Comartin, D., Gupta, G.D., Fussner, E., Coyaud, E., Hasegan, M., Archinti, M., Cheung, S.W., Pinchev, D., Lawo, S., Raught, B., Bazett-Jones, D.P., Luders, J., Pelletier, L., 2013. CEP120 and SPICE1 cooperate with CPAP in centriole elongation. Current biology : CB 23, 1360-1366.

Cong, L., Ran, F.A., Cox, D., Lin, S., Barretto, R., Habib, N., Hsu, P.D., Wu, X., Jiang, W., Marraffini, L.A., Zhang, F., 2013. Multiplex genome engineering using CRISPR/Cas systems. Science 339, 819-823.

Conlon, R.A., Rossant, J., 1992. Exogenous retinoic acid rapidly induces anterior ectopic expression of murine Hox-2 genes in vivo. Development 116, 357-368.

Crocker, J., Abe, N., Rinaldi, L., McGregor, A.P., Frankel, N., Wang, S., Alsawadi, A., Valenti, P., Plaza, S., Payre, F., Mann, R.S., Stern, D.L., 2014. Low Affinity Binding Site Clusters Confer Hox Specificity and Regulatory Robustness. Cell 30, 01518-01519.

Cvejic, A., Serbanovic-Canic, J., Stemple, D.L., Ouwehand, W.H., 2011a. The role of meis1 in primitive and definitive hematopoiesis during zebrafish development. Haematologica 96, 190-198.

Cvejic, A., Serbanovic-Canic, J., Stemple, D.L., Ouwehand, W.H., 2011b. The role of meis1 in primitive and definitive hematopoiesis during zebrafish development. Haematologica. 96, 190-198. doi: 110.3324/haematol.2010.027698. Epub 022010 Nov 027693.

Dale, L., Howes, G., Price, B.M., Smith, J.C., 1992. Bone morphogenetic protein 4: a ventralizing factor in early Xenopus development. Development 115, 573-585.

Davidson, A.J., Zon, L.I., 2004. The 'definitive' (and 'primitive') guide to zebrafish hematopoiesis. Oncogene 23, 7233-7246.

Davidson, A.J., Ernst, P., Wang, Y., Dekens, M.P., Kingsley, P.D., Palis, J., Korsmeyer, S.J., Daley, G.Q., Zon, L.I., 2003. cdx4 mutants fail to specify blood progenitors and can be rescued by multiple hox genes. Nature. 425, 300-306.

Davis, A.P., Witte, D.P., Hsieh-Li, H.M., Potter, S.S., Capecchi, M.R., 1995. Absence of radius and ulna in mice lacking hoxa-11 and hoxd-11. Nature 375, 791-795.

de la Cruz, C.C., Der-Avakian, A., Spyropoulos, D.D., Tieu, D.D., Carpenter, E.M., 1999. Targeted disruption of Hoxd9 and Hoxd10 alters locomotor behavior, vertebral identity, and peripheral nervous system development. Developmental biology 216, 595-610.

De Robertis, E.M., Larrain, J., Oelgeschlager, M., Wessely, O., 2000. The establishment of Spemann's organizer and patterning of the vertebrate embryo. Nat Rev Genet 1, 171-181.

Detrich, H.W., 3rd, Kieran, M.W., Chan, F.Y., Barone, L.M., Yee, K., Rundstadler, J.A., Pratt, S., Ransom, D., Zon, L.I., 1995. Intraembryonic hematopoietic cell migration during vertebrate development. Proc Natl Acad Sci U S A. 92, 10713-10717.

Dick, A., Hild, M., Bauer, H., Imai, Y., Maifeld, H., Schier, A.F., Talbot, W.S., Bouwmeester, T., Hammerschmidt, M., 2000. Essential role of Bmp7 (snailhouse) and its prodomain in dorsoventral patterning of the zebrafish embryo. Development 127, 343-354.

DiMartino, J.F., Selleri, L., Traver, D., Firpo, M.T., Rhee, J., Warnke, R., O'Gorman, S., Weissman, I.L.,

Cleary, M.L., 2001. The Hox cofactor and proto-oncogene Pbx1 is required for maintenance of definitive hematopoiesis in the fetal liver. Blood 98, 618-626.

Dingar, D., Kalkat, M., Chan, P.K., Srikumar, T., Bailey, S.D., Tu, W.B., Coyaud, E., Ponzielli, R., Kolyar, M., Jurisica, I., Huang, A., Lupien, M., Penn, L.Z., Raught, B., 2015. BioID identifies novel c-MYC interacting partners in cultured cells and xenograft tumors. Journal of proteomics 118, 95-111.

Dooley, K.A., Davidson, A.J., Zon, L.I., 2005. Zebrafish scl functions independently in hematopoietic and endothelial development. Developmental biology 277, 522-536.

Duboule, D., Morata, G., 1994. Colinearity and functional hierarchy among genes of the homeotic complexes. Trends Genet 10, 358-364.

Dupe, V., Davenne, M., Brocard, J., Dolle, P., Mark, M., Dierich, A., Chambon, P., Rijli, F.M., 1997. In vivo functional analysis of the Hoxa-1 3' retinoic acid response element (3'RARE). Development 124, 399-410.

Duprez, D.M., Kostakopoulou, K., Francis-West, P.H., Tickle, C., Brickell, P.M., 1996. Activation of Fgf-4 and HoxD gene expression by BMP-2 expressing cells in the developing chick limb. Development 122, 1821-1828.

Eisen, J.S., Smith, J.C., 2008. Controlling morpholino experiments: don't stop making antisense. Development 135, 1735-1743.

Feldman, B., Dougan, S.T., Schier, A.F., Talbot, W.S., 2000. Nodal-related signals establish mesendodermal fate and trunk neural identity in zebrafish. Current biology : CB 10, 531-534.

Feldman, B., Gates, M.A., Egan, E.S., Dougan, S.T., Rennebeck, G., Sirotkin, H.I., Schier, A.F., Talbot, W.S., 1998. Zebrafish organizer development and germ-layer formation require nodal-related signals. Nature 395, 181-185.

Fischbach, N.A., Rozenfeld, S., Shen, W., Fong, S., Chrobak, D., Ginzinger, D., Kogan, S.C., Radhakrishnan, A., Le Beau, M.M., Largman, C., Lawrence, H.J., 2005. HOXB6 overexpression in murine bone marrow immortalizes a myelomonocytic precursor in vitro and causes hematopoietic stem cell expansion and acute myeloid leukemia in vivo. Blood 105, 1456-1466.

Forlani, S., Lawson, K.A., Deschamps, J., 2003. Acquisition of Hox codes during gastrulation and axial elongation in the mouse embryo. Development 130, 3807-3819.

Fromental-Ramain, C., Warot, X., Messadecq, N., LeMeur, M., Dolle, P., Chambon, P., 1996. Hoxa-13 and Hoxd-13 play a crucial role in the patterning of the limb autopod. Development 122, 2997-3011.

Fu, Y., Sander, J.D., Reyon, D., Cascio, V.M., Joung, J.K., 2014. Improving CRISPR-Cas nuclease specificity using truncated guide RNAs. Nature biotechnology 32, 279-284.

Gagnon, J.A., Valen, E., Thyme, S.B., Huang, P., Akhmetova, L., Pauli, A., Montague, T.G., Zimmerman, S., Richter, C., Schier, A.F., 2014. Efficient mutagenesis by Cas9 protein-mediated oligonucleotide insertion and large-scale assessment of single-guide RNAs. PLoS One 9, e98186.

Galant, R., Walsh, C.M., Carroll, S.B., 2002. Hox repression of a target gene: extradenticle-independent, additive action through multiple monomer binding sites. Development. 129, 3115-3126.

Greer, J.M., Puetz, J., Thomas, K.R., Capecchi, M.R., 2000. Maintenance of functional equivalence during paralogous Hox gene evolution. Nature 403, 661-665.

Gupta, S., Zhu, H., Zon, L.I., Evans, T., 2006. BMP signaling restricts hemato-vascular development from lateral mesoderm during somitogenesis. Development 133, 2177-2187.

Hammerschmidt, M., Serbedzija, G.N., McMahon, A.P., 1996. Genetic analysis of dorsoventral

pattern formation in the zebrafish: requirement of a BMP-like ventralizing activity and its dorsal repressor. Genes Dev 10, 2452-2461.

Harlow, E., Lane, D., 1988. A laboratory manual. New York: Cold Spring Harbor Laboratory 579.

Hild, M., Dick, A., Rauch, G.J., Meier, A., Bouwmeester, T., Haffter, P., Hammerschmidt, M., 1999. The smad5 mutation somitabun blocks Bmp2b signaling during early dorsoventral patterning of the zebrafish embryo. Development 126, 2149-2159.

Hilton, I.B., D'Ippolito, A.M., Vockley, C.M., Thakore, P.I., Crawford, G.E., Reddy, T.E., Gersbach, C.A., 2015. Epigenome editing by a CRISPR-Cas9-based acetyltransferase activates genes from promoters and enhancers. Nature biotechnology 33, 510-517.

Hisa, T., Spence, S.E., Rachel, R.A., Fujita, M., Nakamura, T., Ward, J.M., Devor-Henneman, D.E., Saiki, Y., Kutsuna, H., Tessarollo, L., Jenkins, N.A., Copeland, N.G., 2004. Hematopoietic, angiogenic and eye defects in Meis1 mutant animals. The EMBO journal 23, 450-459.

Horan, G.S., Ramirez-Solis, R., Featherstone, M.S., Wolgemuth, D.J., Bradley, A., Behringer, R.R., 1995. Compound mutants for the paralogous hoxa-4, hoxb-4, and hoxd-4 genes show more complete homeotic transformations and a dose-dependent increase in the number of vertebrae transformed. Genes Dev 9, 1667-1677.

Housley, M.P., Reischauer, S., Dieu, M., Raes, M., Stainier, D.Y., Vanhollebeke, B., 2014. Translational profiling through biotinylation of tagged ribosomes in zebrafish. Development 141, 3988-3993.

Hsu, P.D., Scott, D.A., Weinstein, J.A., Ran, F.A., Konermann, S., Agarwala, V., Li, Y., Fine, E.J., Wu, X., Shalem, O., Cradick, T.J., Marraffini, L.A., Bao, G., Zhang, F., 2013. DNA targeting specificity of RNA-guided Cas9 nucleases. Nature biotechnology 31, 827-832.

Iacovino, M., Hernandez, C., Xu, Z., Bajwa, G., Prather, M., Kyba, M., 2009. A conserved role for Hox paralog group 4 in regulation of hematopoietic progenitors. Stem Cells Dev. 18, 783-792. doi: 710.1089/scd.2008.0227.

Iimura, T., Pourquie, O., 2006. Collinear activation of Hoxb genes during gastrulation is linked to mesoderm cell ingression. Nature. 442, 568-571. Epub 2006 Jun 2007.

Iimura, T., Pourquie, O., 2007. Hox genes in time and space during vertebrate body formation. Dev Growth Differ. 49, 265-275.

Ikeya, M., Takada, S., 2001. Wnt-3a is required for somite specification along the anteroposterior axis of the mouse embryo and for regulation of cdx-1 expression. Mech Dev 103, 27-33.

Jinek, M., Chylinski, K., Fonfara, I., Hauer, M., Doudna, J.A., Charpentier, E., 2012. A programmable dual-RNA-guided DNA endonuclease in adaptive bacterial immunity. Science 337, 816-821.

Joshi, R., Sun, L., Mann, R., 2010. Dissecting the functional specificities of two Hox proteins. Genes Dev. 24, 1533-1545. doi: 1510.1101/gad.1936910.

Kappen, C., 2000. Disruption of the homeobox gene Hoxb-6 in mice results in increased numbers of early erythrocyte progenitors. Am J Hematol 65, 111-118.

Kim, D.I., Birendra, K.C., Zhu, W., Motamedchaboki, K., Doye, V., Roux, K.J., 2014. Probing nuclear pore complex architecture with proximity-dependent biotinylation. Proceedings of the National Academy of Sciences of the United States of America 111, E2453-2461.

Kimelman, D., 2006. Mesoderm induction: from caps to chips. Nat Rev Genet 7, 360-372.

Kimelman, D., Schier, A.F., 2002. Mesoderm induction and patterning. Results Probl Cell Differ 40, 15-27.

Kimmel, C.B., Warga, R.M., Schilling, T.F., 1990. Origin and organization of the zebrafish fate map. Development 108, 581-594.

Kimmel, C.B., Ballard, W.W., Kimmel, S.R., Ullmann, B., Schilling, T.F., 1995. Stages of embryonic development of the zebrafish. Developmental dynamics : an official publication of the American Association of Anatomists 203, 253-310.

Kishimoto, Y., Lee, K.H., Zon, L., Hammerschmidt, M., Schulte-Merker, S., 1997. The molecular nature of zebrafish swirl: BMP2 function is essential during early dorsoventral patterning. Development 124, 4457-4466.

Kissinger, C.R., Liu, B.S., Martin-Blanco, E., Kornberg, T.B., Pabo, C.O., 1990. Crystal structure of an engrailed homeodomain-DNA complex at 2.8 A resolution: a framework for understanding homeodomain-DNA interactions. Cell. 63, 579-590.

Kmita, M., Tarchini, B., Zakany, J., Logan, M., Tabin, C.J., Duboule, D., 2005. Early developmental arrest of mammalian limbs lacking HoxA/HoxD gene function. Nature 435, 1113-1116.

Knoepfler, P.S., Lu, Q., Kamps, M.P., 1996. Pbx-1 Hox heterodimers bind DNA on inseparable half-sites that permit intrinsic DNA binding specificity of the Hox partner at nucleotides 3' to a TAAT motif. Nucleic Acids Res. 24, 2288-2294.

Koh, E.G., Lam, K., Christoffels, A., Erdmann, M.V., Brenner, S., Venkatesh, B., 2003. Hox gene clusters in the Indonesian coelacanth, Latimeria menadoensis. Proc Natl Acad Sci U S A. 100, 1084-1088. Epub 2003 Jan 1023.

Kok, F.O., Shin, M., Ni, C.W., Gupta, A., Grosse, A.S., van Impel, A., Kirchmaier, B.C., Peterson-Maduro, J., Kourkoulis, G., Male, I., DeSantis, D.F., Sheppard-Tindell, S., Ebarasi, L., Betsholtz, C., Schulte-Merker, S., Wolfe, S.A., Lawson, N.D., 2015. Reverse genetic screening reveals poor correlation between morpholino-induced and mutant phenotypes in zebrafish. Developmental cell 32, 97-108.

Kondo, M., 2007. Bone morphogenetic proteins in the early development of zebrafish. FEBS J. 274, 2960-2967. Epub 2007 May 2922.

Krumlauf, R., 1994. Hox genes in vertebrate development. Cell. 78, 191-201.

Kudoh, T., Tsang, M., Hukriede, N.A., Chen, X., Dedekian, M., Clarke, C.J., Kiang, A., Schultz, S., Epstein, J.A., Toyama, R., Dawid, I.B., 2001. A gene expression screen in zebrafish embryogenesis. Genome research 11, 1979-1987.

Ladam, F., Sagerstrom, C.G., 2014. Hox regulation of transcription: more complex(es). Developmental dynamics : an official publication of the American Association of Anatomists 243, 4-15.

Lengerke, C., Daley, G.Q., 2012. Caudal genes in blood development and leukemia. Ann N Y Acad Sci 1266, 47-54.

Lengerke, C., Schmitt, S., Bowman, T.V., Jang, I.H., Maouche-Chretien, L., McKinney-Freeman, S., Davidson, A.J., Hammerschmidt, M., Rentzsch, F., Green, J.B., Zon, L.I., Daley, G.Q., 2008. BMP and Wnt specify hematopoietic fate by activation of the Cdx-Hox pathway. Cell Stem Cell. 2, 72-82. doi: 10.1016/j.stem.2007.1010.1022.

Lewis, E.B., 1978. A gene complex controlling segmentation in Drosophila. Nature 276, 565-570.

Li, J., Zhang, B.B., Ren, Y.G., Gu, S.Y., Xiang, Y.H., Du, J.L., 2015. Intron targeting-mediated and endogenous gene integrity-maintaining knockin in zebrafish using the CRISPR/Cas9 system. Cell research 25, 634-637.

Li, X., Nie, S., Chang, C., Qiu, T., Cao, X., 2006a. Smads oppose Hox transcriptional activities. Experimental cell research 312, 854-864.

Li, X., Nie, S., Chang, C., Qiu, T., Cao, X., 2006b. Smads oppose Hox transcriptional activities. Exp Cell

Res. 312, 854-864. Epub 2006 Jan 2010.
Liu, F., Walmsley, M., Rodaway, A., Patient, R., 2008. Fli1 acts at the top of the transcriptional network driving blood and endothelial development. Current biology : CB 18, 1234-1240.
Liu, J., Zhou, Y., Qi, X., Chen, J., Chen, W., Qiu, G., Wu, Z., Wu, N., 2017. CRISPR/Cas9 in zebrafish: an efficient combination for human genetic diseases modeling. Human genetics 136, 1-12.
Liu, P., Wakamiya, M., Shea, M.J., Albrecht, U., Behringer, R.R., Bradley, A., 1999. Requirement for Wnt3 in vertebrate axis formation. Nat Genet 22, 361-365.
Lu, Q., Kamps, M.P., 1996. Structural determinants within Pbx1 that mediate cooperative DNA binding with pentapeptide-containing Hox proteins: proposal for a model of a Pbx1-Hox-DNA complex. Mol Cell Biol. 16, 1632-1640.
Lyons, S.E., Lawson, N.D., Lei, L., Bennett, P.E., Weinstein, B.M., Liu, P.P., 2002. A nonsense mutation in zebrafish gata1 causes the bloodless phenotype in vlad tepes. Proceedings of the National Academy of Sciences of the United States of America 99, 5454-5459.
Mallo, M., Alonso, C.R., 2013. The regulation of Hox gene expression during animal development. Development 140, 3951-3963.
Mallo, M., Wellik, D.M., Deschamps, J., 2010. Hox genes and regional patterning of the vertebrate body plan. Developmental biology 344, 7-15.
Mangelsdorf, D.J., Evans, R.M., 1995. The RXR heterodimers and orphan receptors. Cell 83, 841-850.
Manzanares, M., Cordes, S., Ariza-McNaughton, L., Sadl, V., Maruthainar, K., Barsh, G., Krumlauf, R., 1999. Conserved and distinct roles of kreisler in regulation of the paralogous Hoxa3 and Hoxb3 genes. Development 126, 759-769.
Marshall, H., Nonchev, S., Sham, M.H., Muchamore, I., Lumsden, A., Krumlauf, R., 1992. Retinoic acid alters hindbrain Hox code and induces transformation of rhombomeres 2/3 into a 4/5 identity. Nature 360, 737-741.
McGinnis, N., Kuziora, M.A., McGinnis, W., 1990. Human Hox-4.2 and Drosophila deformed encode similar regulatory specificities in Drosophila embryos and larvae. Cell 63, 969-976.
McReynolds, L.J., Gupta, S., Figueroa, M.E., Mullins, M.C., Evans, T., 2007. Smad1 and Smad5 differentially regulate embryonic hematopoiesis. Blood. 110, 3881-3890. Epub 2007 Aug 3829.
Medina-Martinez, O., Bradley, A., Ramirez-Solis, R., 2000. A large targeted deletion of Hoxb1-Hoxb9 produces a series of single-segment anterior homeotic transformations. Developmental biology 222, 71-83.
Merabet, S., Hudry, B., 2013. Hox transcriptional specificity despite a single class of cofactors: are flexible interaction modes the key? Plasticity in Hox/PBC interaction modes as a common molecular strategy for shaping Hox transcriptional activities. Bioessays. 35, 88-92. doi: 10.1002/bies.201200146. Epub 201202012 Dec 201200119.
Merabet, S., Dard, A., 2014. Tracking context-specific transcription factors regulating hox activity. Developmental dynamics : an official publication of the American Association of Anatomists 243, 16-23.
Minehata, K., Kawahara, A., Suzuki, T., 2008. meis1 regulates the development of endothelial cells in zebrafish. Biochem Biophys Res Commun. 374, 647-652. doi: 610.1016/j.bbrc.2008.1007.1075. Epub 2008 Jul 1024.
Mizuno, T., Yamaha, E., Kuroiwa, A., Takeda, H., 1999. Removal of vegetal yolk causes dorsal deficencies and impairs dorsal-inducing ability of the yolk cell in zebrafish. Mech Dev 81, 51-63.
Moens, C.B., Selleri, L., 2006. Hox cofactors in vertebrate development. Dev Biol. 291, 193-206. Epub

2006 Mar 2003.

Moreno-Mateos, M.A., Vejnar, C.E., Beaudoin, J.D., Fernandez, J.P., Mis, E.K., Khokha, M.K., Giraldez, A.J., 2015. CRISPRscan: designing highly efficient sgRNAs for CRISPR-Cas9 targeting in vivo. Nature methods 12, 982-988.

Morriswood, B., Havlicek, K., Demmel, L., Yavuz, S., Sealey-Cardona, M., Vidilaseris, K., Anrather, D., Kostan, J., Djinovic-Carugo, K., Roux, K.J., Warren, G., 2013. Novel bilobe components in Trypanosoma brucei identified using proximity-dependent biotinylation. Eukaryot Cell 12, 356-367.

Murayama, E., Kissa, K., Zapata, A., Mordelet, E., Briolat, V., Lin, H.F., Handin, R.I., Herbomel, P., 2006. Tracing hematopoietic precursor migration to successive hematopoietic organs during zebrafish development. Immunity. 25, 963-975. Epub 2006 Dec 2007.

Naito, Y., Hino, K., Bono, H., Ui-Tei, K., 2015. CRISPRdirect: software for designing CRISPR/Cas guide RNA with reduced off-target sites. Bioinformatics 31, 1120-1123.

Nakanishi, N., Sogabe, S., Degnan, B.M., 2014. Evolutionary origin of gastrulation: insights from sponge development. BMC biology 12, 26.

Nelson, C.E., Morgan, B.A., Burke, A.C., Laufer, E., DiMambro, E., Murtaugh, L.C., Gonzales, E., Tessarollo, L., Parada, L.F., Tabin, C., 1996. Analysis of Hox gene expression in the chick limb bud. Development 122, 1449-1466.

Nolte, C., Krumlauf, R., 2007. Expression of Hox genes in the nervous system of vertebrates, HOX gene expression. Springer, pp. 14-41.

Nonchev, S., Maconochie, M., Vesque, C., Aparicio, S., Ariza-McNaughton, L., Manzanares, M., Maruthainar, K., Kuroiwa, A., Brenner, S., Charnay, P., Krumlauf, R., 1996. The conserved role of Krox-20 in directing Hox gene expression during vertebrate hindbrain segmentation. Proceedings of the National Academy of Sciences of the United States of America 93, 9339-9345.

Paik, E.J., Zon, L.I., 2010. Hematopoietic development in the zebrafish. Int J Dev Biol 54, 1127-1137.

Paik, E.J., Mahony, S., White, R.M., Price, E.N., Dibiase, A., Dorjsuren, B., Mosimann, C., Davidson, A.J., Gifford, D., Zon, L.I., 2013. A Cdx4-Sall4 regulatory module controls the transition from mesoderm formation to embryonic hematopoiesis. Stem cell reports 1, 425-436.

Papageorgiou, S., 2007. HOX gene expression. Springer.

Partanen, J., Schwartz, L., Rossant, J., 1998. Opposite phenotypes of hypomorphic and Y766 phosphorylation site mutations reveal a function for Fgfr1 in anteroposterior patterning of mouse embryos. Genes Dev 12, 2332-2344.

Passner, J.M., Ryoo, H.D., Shen, L., Mann, R.S., Aggarwal, A.K., 1999. Structure of a DNA-bound Ultrabithorax-Extradenticle homeodomain complex. Nature. 397, 714-719.

Pillay, L.M., Forrester, A.M., Erickson, T., Berman, J.N., Waskiewicz, A.J., 2010. The Hox cofactors Meis1 and Pbx act upstream of gata1 to regulate primitive hematopoiesis. Dev Biol. 340, 306-317. doi: 310.1016/j.ydbio.2010.1001.1033. Epub 2010 Feb 1011.

Piper, D.E., Batchelor, A.H., Chang, C.P., Cleary, M.L., Wolberger, C., 1999. Structure of a HoxB1-Pbx1 heterodimer bound to DNA: role of the hexapeptide and a fourth homeodomain helix in complex formation. Cell. 96, 587-597.

Porcher, C., Swat, W., Rockwell, K., Fujiwara, Y., Alt, F.W., Orkin, S.H., 1996. The T cell leukemia oncoprotein SCL/tal-1 is essential for development of all hematopoietic lineages. Cell. 86, 47-57.

Pownall, M.E., Tucker, A.S., Slack, J.M., Isaacs, H.V., 1996. eFGF, Xcad3 and Hox genes form a

molecular pathway that establishes the anteroposterior axis in Xenopus. Development 122, 3881-3892.

Prince, F., Katsuyama, T., Oshima, Y., Plaza, S., Resendez-Perez, D., Berry, M., Kurata, S., Gehring, W.J., 2008. The YPWM motif links Antennapedia to the basal transcriptional machinery. Development. 135, 1669-1679. doi: 1610.1242/dev.018028. Epub 012008 Mar 018026.

Pyati, U.J., Webb, A.E., Kimelman, D., 2005. Transgenic zebrafish reveal stage-specific roles for Bmp signaling in ventral and posterior mesoderm development. Development 132, 2333-2343.

Qi, L.S., Larson, M.H., Gilbert, L.A., Doudna, J.A., Weissman, J.S., Arkin, A.P., Lim, W.A., 2013. Repurposing CRISPR as an RNA-guided platform for sequence-specific control of gene expression. Cell 152, 1173-1183.

Quere, R., Karlsson, G., Hertwig, F., Rissler, M., Lindqvist, B., Fioretos, T., Vandenberghe, P., Slovak, M.L., Cammenga, J., Karlsson, S., 2011. Smad4 binds Hoxa9 in the cytoplasm and protects primitive hematopoietic cells against nuclear activation by Hoxa9 and leukemia transformation. Blood 117, 5918-5930.

Rambaldi, I., Kovacs, E.N., Featherstone, M.S., 1994. A proline-rich transcriptional activation domain in murine HOXD-4 (HOX-4.2). Nucleic acids research 22, 376-382.

Rancourt, D.E., Tsuzuki, T., Capecchi, M.R., 1995. Genetic interaction between hoxb-5 and hoxb-6 is revealed by nonallelic noncomplementation. Genes Dev 9, 108-122.

Remacle, S., Abbas, L., De Backer, O., Pacico, N., Gavalas, A., Gofflot, F., Picard, J.J., Rezsohazy, R., 2004. Loss of function but no gain of function caused by amino acid substitutions in the hexapeptide of Hoxa1 in vivo. Mol Cell Biol 24, 8567-8575.

Robu, M.E., Larson, J.D., Nasevicius, A., Beiraghi, S., Brenner, C., Farber, S.A., Ekker, S.C., 2007. p53 activation by knockdown technologies. PLoS genetics 3, e78.

Rossi, A., Kontarakis, Z., Gerri, C., Nolte, H., Holper, S., Kruger, M., Stainier, D.Y., 2015. Genetic compensation induced by deleterious mutations but not gene knockdowns. Nature 524, 230-233.

Rossi, C.C., Kaji, T., Artinger, K.B., 2009. Transcriptional control of Rohon-Beard sensory neuron development at the neural plate border. Developmental dynamics : an official publication of the American Association of Anatomists 238, 931-943.

Roux, K.J., Kim, D.I., Burke, B., 2013. BioID: a screen for protein-protein interactions. Current protocols in protein science / editorial board, John E. Coligan ... [et al.] 74, Unit 19 23.

Roux, K.J., Kim, D.I., Raida, M., Burke, B., 2012. A promiscuous biotin ligase fusion protein identifies proximal and interacting proteins in mammalian cells. The Journal of cell biology 196, 801-810.

Saleh, M., Rambaldi, I., Yang, X.J., Featherstone, M.S., 2000. Cell signaling switches HOX-PBX complexes from repressors to activators of transcription mediated by histone deacetylases and histone acetyltransferases. Mol Cell Biol. 20, 8623-8633.

Saude, L., Woolley, K., Martin, P., Driever, W., Stemple, D.L., 2000. Axis-inducing activities and cell fates of the zebrafish organizer. Development 127, 3407-3417.

Sauvageau, G., Thorsteinsdottir, U., Eaves, C.J., Lawrence, H.J., Largman, C., Lansdorp, P.M., Humphries, R.K., 1995. Overexpression of HOXB4 in hematopoietic cells causes the selective expansion of more primitive populations in vitro and in vivo. Genes Dev 9, 1753-1765.

Sauvageau, G., Lansdorp, P.M., Eaves, C.J., Hogge, D.E., Dragowska, W.H., Reid, D.S., Largman, C., Lawrence, H.J., Humphries, R.K., 1994. Differential expression of homeobox genes in functionally distinct CD34+ subpopulations of human bone marrow cells. Proceedings of the

National Academy of Sciences of the United States of America 91, 12223-12227.
Schaefer, K.A., Wu, W.H., Colgan, D.F., Tsang, S.H., Bassuk, A.G., Mahajan, V.B., 2017. Unexpected mutations after CRISPR-Cas9 editing in vivo. Nature methods 14, 547-548.
Schier, A.F., 2003. Nodal signaling in vertebrate development. Annu Rev Cell Dev Biol 19, 589-621.
Schier, A.F., Talbot, W.S., 2005. Molecular genetics of axis formation in zebrafish. Annual review of genetics 39, 561-613.
Schild-Poulter, C., Pope, L., Giffin, W., Kochan, J.C., Ngsee, J.K., Traykova-Andonova, M., Hache, R.J., 2001. The binding of Ku antigen to homeodomain proteins promotes their phosphorylation by DNA-dependent protein kinase. The Journal of biological chemistry 276, 16848-16856.
Schmerer, M., Evans, T., 2003. Primitive erythropoiesis is regulated by Smad-dependent signaling in postgastrulation mesoderm. Blood 102, 3196-3205.
Schmid, B., Furthauer, M., Connors, S.A., Trout, J., Thisse, B., Thisse, C., Mullins, M.C., 2000. Equivalent genetic roles for bmp7/snailhouse and bmp2b/swirl in dorsoventral pattern formation. Development 127, 957-967.
Schneider, S., Steinbeisser, H., Warga, R.M., Hausen, P., 1996. Beta-catenin translocation into nuclei demarcates the dorsalizing centers in frog and fish embryos. Mech Dev 57, 191-198.
Sham, M.H., Vesque, C., Nonchev, S., Marshall, H., Frain, M., Gupta, R.D., Whiting, J., Wilkinson, D., Charnay, P., Krumlauf, R., 1993. The zinc finger gene Krox20 regulates HoxB2 (Hox2.8) during hindbrain segmentation. Cell 72, 183-196.
Shanmugam, K., Green, N.C., Rambaldi, I., Saragovi, H.U., Featherstone, M.S., 1999a. PBX and MEIS as non-DNA-binding partners in trimeric complexes with HOX proteins. Mol Cell Biol 19, 7577-7588.
Shanmugam, K., Green, N.C., Rambaldi, I., Saragovi, H.U., Featherstone, M.S., 1999b. PBX and MEIS as non-DNA-binding partners in trimeric complexes with HOX proteins. Mol Cell Biol. 19, 7577-7588.
Shen, W.F., Montgomery, J.C., Rozenfeld, S., Moskow, J.J., Lawrence, H.J., Buchberg, A.M., Largman, C., 1997. AbdB-like Hox proteins stabilize DNA binding by the Meis1 homeodomain proteins. Mol Cell Biol. 17, 6448-6458.
Shestopalov, I.A., Chen, J.K., 2011. Spatiotemporal control of embryonic gene expression using caged morpholinos. Methods in cell biology 104, 151-172.
Shi, X., Yang, X., Chen, D., Chang, Z., Cao, X., 1999a. Smad1 interacts with homeobox DNA-binding proteins in bone morphogenetic protein signaling. J Biol Chem 274, 13711-13717.
Shi, X., Yang, X., Chen, D., Chang, Z., Cao, X., 1999b. Smad1 interacts with homeobox DNA-binding proteins in bone morphogenetic protein signaling. J Biol Chem. 274, 13711-13717.
Shu, L.P., Zhou, Z.W., Zhou, T., Deng, M., Dong, M., Chen, Y., Fu, Y.F., Jin, Y., Zhou, S.F., He, Z.X., 2015. Ectopic expression of Hoxb4a in hemangioblasts promotes hematopoietic development in early embryogenesis of zebrafish. Clin Exp Pharmacol Physiol 42, 1275-1286.
Simeone, A., Acampora, D., Arcioni, L., Andrews, P.W., Boncinelli, E., Mavilio, F., 1990. Sequential activation of HOX2 homeobox genes by retinoic acid in human embryonal carcinoma cells. Nature 346, 763-766.
Soshnikova, N., Dewaele, R., Janvier, P., Krumlauf, R., Duboule, D., 2013. Duplications of hox gene clusters and the emergence of vertebrates. Developmental biology 378, 194-199.
Subramanian, V., Meyer, B.I., Gruss, P., 1995. Disruption of the murine homeobox gene Cdx1 affects axial skeletal identities by altering the mesodermal expression domains of Hox genes. Cell 83,

641-653.
Suemori, H., Noguchi, S., 2000. Hox C cluster genes are dispensable for overall body plan of mouse embryonic development. Developmental biology 220, 333-342.
Sun, Y., Tseng, W.C., Fan, X., Ball, R., Dougan, S.T., 2014. Extraembryonic signals under the control of MGA, Max, and Smad4 are required for dorsoventral patterning. Developmental cell 28, 322-334.
Tarchini, B., Duboule, D., 2006. Control of Hoxd genes' collinearity during early limb development. Developmental cell 10, 93-103.
Thisse, C., Thisse, B., 2008. High-resolution in situ hybridization to whole-mount zebrafish embryos. Nat Protoc 3, 59-69. doi: 10.1038/nprot.2007.1514.
Thorsteinsdottir, U., Sauvageau, G., Humphries, R.K., 1999. Enhanced in vivo regenerative potential of HOXB4-transduced hematopoietic stem cells with regulation of their pool size. Blood 94, 2605-2612.
Thorsteinsdottir, U., Sauvageau, G., Hough, M.R., Dragowska, W., Lansdorp, P.M., Lawrence, H.J., Largman, C., Humphries, R.K., 1997. Overexpression of HOXA10 in murine hematopoietic cells perturbs both myeloid and lymphoid differentiation and leads to acute myeloid leukemia. Mol Cell Biol. 17, 495-505.
Thorsteinsdottir, U., Mamo, A., Kroon, E., Jerome, L., Bijl, J., Lawrence, H.J., Humphries, K., Sauvageau, G., 2002. Overexpression of the myeloid leukemia-associated Hoxa9 gene in bone marrow cells induces stem cell expansion. Blood. 99, 121-129.
Treisman, J., Gonczy, P., Vashishtha, M., Harris, E., Desplan, C., 1989. A single amino acid can determine the DNA binding specificity of homeodomain proteins. Cell. 59, 553-562.
Tvrdik, P., Capecchi, M.R., 2006. Reversal of Hox1 gene subfunctionalization in the mouse. Developmental cell 11, 239-250.
van den Akker, E., Forlani, S., Chawengsaksophak, K., de Graaff, W., Beck, F., Meyer, B.I., Deschamps, J., 2002. Cdx1 and Cdx2 have overlapping functions in anteroposterior patterning and posterior axis elongation. Development 129, 2181-2193.
van den Akker, W.M., Durston, A.J., Spaink, H.P., 2010. Identification of hoxb1b downstream genes: hoxb1b as a regulatory factor controlling transcriptional networks and cell movement during zebrafish gastrulation. Int J Dev Biol 54, 55-62. doi: 10.1387/ijdb.082678wv.
Van Itallie, C.M., Aponte, A., Tietgens, A.J., Gucek, M., Fredriksson, K., Anderson, J.M., 2013. The N and C termini of ZO-1 are surrounded by distinct proteins and functional protein networks. J Biol Chem 288, 13775-13788.
Veres, A., Gosis, B.S., Ding, Q., Collins, R., Ragavendran, A., Brand, H., Erdin, S., Cowan, C.A., Talkowski, M.E., Musunuru, K., 2014. Low incidence of off-target mutations in individual CRISPR-Cas9 and TALEN targeted human stem cell clones detected by whole-genome sequencing. Cell stem cell 15, 27-30.
Vershon, A.K., Jin, Y., Johnson, A.D., 1995. A homeo domain protein lacking specific side chains of helix 3 can still bind DNA and direct transcriptional repression. Genes Dev. 9, 182-192.
Vidal, L., Blagden, S., Attard, G., de Bono, J., 2005. Making sense of antisense. European journal of cancer 41, 2812-2818.
Wacker, S.A., McNulty, C.L., Durston, A.J., 2004a. The initiation of Hox gene expression in Xenopus laevis is controlled by Brachyury and BMP-4. Dev Biol. 266, 123-137.
Wacker, S.A., Jansen, H.J., McNulty, C.L., Houtzager, E., Durston, A.J., 2004b. Timed interactions

between the Hox expressing non-organiser mesoderm and the Spemann organiser generate positional information during vertebrate gastrulation. Dev Biol. 268, 207-219.

Wang, N., Kim, H.G., Cotta, C.V., Wan, M., Tang, Y., Klug, C.A., Cao, X., 2006. TGFbeta/BMP inhibits the bone marrow transformation capability of Hoxa9 by repressing its DNA-binding ability. EMBO J. 25, 1469-1480. Epub 2006 Mar 1469.

Warga, R.M., Nusslein-Volhard, C., 1999. Origin and development of the zebrafish endoderm. Development 126, 827-838.

Waskiewicz, A.J., Rikhof, H.A., Hernandez, R.E., Moens, C.B., 2001. Zebrafish Meis functions to stabilize Pbx proteins and regulate hindbrain patterning. Development. 128, 4139-4151.

Wei, C.Y., Wang, H.P., Zhu, Z.Y., Sun, Y.H., 2014. Transcriptional factors smad1 and smad9 act redundantly to mediate zebrafish ventral specification downstream of smad5. J Biol Chem 289, 6604-6618.

Weinstein, B.M., Schier, A.F., Abdelilah, S., Malicki, J., Solnica-Krezel, L., Stemple, D.L., Stainier, D.Y., Zwartkruis, F., Driever, W., Fishman, M.C., 1996. Hematopoietic mutations in the zebrafish. Development 123, 303-309.

Westerfield, M., 2000. The zebrafish book. A guide for the laboratory use of zebrafish (Danio rerio). 2000, Eugene. Univ. of Oregon Press.

Wilkinson, R.N., Elworthy, S., Ingham, P.W., van Eeden, F.J., 2013. A method for high-throughput PCR-based genotyping of larval zebrafish tail biopsies. BioTechniques 55, 314-316.

Williams, T.M., Williams, M.E., Heaton, J.H., Gelehrter, T.D., Innis, J.W., 2005a. Group 13 HOX proteins interact with the MH2 domain of R-Smads and modulate Smad transcriptional activation functions independent of HOX DNA-binding capability. Nucleic acids research 33, 4475-4484.

Williams, T.M., Williams, M.E., Heaton, J.H., Gelehrter, T.D., Innis, J.W., 2005b. Group 13 HOX proteins interact with the MH2 domain of R-Smads and modulate Smad transcriptional activation functions independent of HOX DNA-binding capability. Nucleic Acids Res. 33, 4475-4484. Print 2005.

Xie, S., Shen, B., Zhang, C., Huang, X., Zhang, Y., 2014. sgRNAcas9: a software package for designing CRISPR sgRNA and evaluating potential off-target cleavage sites. PLoS One 9, e100448.

Yamanaka, Y., Mizuno, T., Sasai, Y., Kishi, M., Takeda, H., Kim, C.H., Hibi, M., Hirano, T., 1998. A novel homeobox gene, dharma, can induce the organizer in a non-cell-autonomous manner. Genes Dev 12, 2345-2353.

Yang, X., Ji, X., Shi, X., Cao, X., 2000. Smad1 domains interacting with Hoxc-8 induce osteoblast differentiation. J Biol Chem 275, 1065-1072.

Zakany, J., Duboule, D., 2007. The role of Hox genes during vertebrate limb development. Curr Opin Genet Dev 17, 359-366.

Zandvakili, A., Gebelein, B., 2016. Mechanisms of Specificity for Hox Factor Activity. Journal of developmental biology 4.

Zhou, B., Chen, L., Wu, X., Wang, J., Yin, Y., Zhu, G., 2008. MH1 domain of SMAD4 binds N-terminal residues of the homeodomain of Hoxc9. Biochim Biophys Acta. 1784, 747-752. doi: 710.1016/j.bbapap.2008.1001.1021. Epub 2008 Feb 1020.